UNIVERSITY OF CALIFORNIA SAN DIEGO

Regulation of Enhancer Elements by *p53* in Human Cancer

A dissertation submitted in partial satisfaction of the
requirements for the degree
Doctor of Philosophy

in

Biology

by

Homa Rahnamoun

Committee in charge:

Professor Shannon Lauberth, Chair
Professor James Kadonaga
Professor Lorraine Pillus
Professor Dong Wang
Professor James Wilhelm

2020

The Dissertation of Homa Rahnamoun is approved, and it is acceptable in quality and form for publication on microfilm and electronically:

_____

_____

_____

_____

_____

Chair

University of California San Diego

2020

DEDICATION

To my parents, the two most gracious souls I have ever met,
for all your sacrifices and all your support,
for all that you have done and continue to do,
I become more grateful, every day.

And to my sister,
for inspiring me every day.

EPIGRAPH

The garden of the world has no limits, except in your mind.

- *Rumi*

TABLE OF CONTENTS

LIST OF FIGURES

LIST OF TABLES

ACKNOWLEDGEMENTS

I would like to express my deepest gratitude to Dr. Shannon Lauberth for being my graduate mentor. Her unwavering guidance has shaped me into the scientist I am today. It has been a privilege to learn from her both technically and academically and I am forever grateful for the opportunity of a lifetime. I also thank my thesis committee members, Dr. Jim Kadonaga, Dr. Lorraine Pillus, Dr. Dong Wang, and Dr. Jim Wilhelm for their continuous support. I also would like to express my profound appreciation for Dr. Don Helinski who inspires me every day, not only with his vast knowledge and wit but also with his kindness and compassion.

I also thank the many friends and colleagues who have contributed their ideas, time, and support that has helped with the completion of this dissertation. I must particularly thank Isaac for his friendship throughout the years that has inspired countless hours of discussing epigenetic related papers over dinner, as well as Paola and Lidija for being affable labmates and extraordinary friends in every regard. Lastly, I would like to thank my sister for being my best friend and my parents for all their sacrifices and willingness to go through distressing obstacles and hardships in order to provide me with the opportunity of pursuing my dreams.

Chapter 2, in full, is a reprint of the material as it occurs in *Nature Communications*, Rahnamoun, H.; Lu, H.; Duttke, S. H.; Benner, C.; Glass, C. K.; Lauberth, S. M.; Nature Research, 2017. I was the primary author.

Chapter 3, in part, is unpublished material coauthored with Orozco, P. and Vukovic, L. I was the primary author of this chapter.

VITA

Education

2014 Bachelor of Science, Bioengineering: Biotechnology, UC San Diego, CA

2020 Doctor of Philosophy, Biology, UC San Diego, CA

Academic Employment

2014 – 2016 Research assistant in Lauberth laboratory, UC San Diego, CA

2016 – 2020 Graduate research assistant, UC San Diego, CA

Publications

Rahnamoun, H.; Orozco, P.; Lauberth, S. M., The role of enhancer RNAs in epigenetic regulation of gene expression. *Transcription* 2019, 1-7.

Rahnamoun, H.; Lee, J.; Sun, Z.; Lu, H.; Ramsey, K. M.; Komives, E. A.; Lauberth, S. M., RNAs interact with BRD4 to promote enhanced chromatin engagement and transcription activation. *Nature Structural & Molecular Biology* 2018, 25 (8), 687-697.

Rahnamoun, H.; Hong, J.; Sun, Z.; Lee, J.; Lu, H.; Lauberth, S. M., Mutant p53 regulates enhancer-associated H3K4 monomethylation through interactions with the methyltransferase MLL4. *Journal of Biological Chemistry* 2018.

Rahnamoun, H.; Lu, H.; Duttke, S. H.; Benner, C.; Glass, C. K.; Lauberth, S. M., Mutant p53 shapes the enhancer landscape of cancer cells in response to chronic immune signaling. *Nature Communications* 2017, 8 (1), 754.

Stijf-Bultsma, Y.; Sommer, L.; Tauber, M.; Baalbaki, M.; Giardoglou, P.; Jones, D. R.; Gelato, K. A.; van Pelt, J.; Shah, Z.; **Rahnamoun, H.**; Toma, C.; Anderson, K. E.; Hawkins, P.; Lauberth, S. M.; Haramis, A. P.; Hart, D.; Fischle, W.; Divecha, N., The basal transcription complex component TAF3 transduces changes in nuclear phosphoinositides into transcriptional output. *Molecular Cell* 2015, 58 (3), 453-67.

Pollard DA.; Asamoto CK.; **Rahnamoun H.**; Abendroth AS.; Lee SR.; and Rifkin SA. Natural genetic variation modifies gene expression dynamics at the protein level during pheromone response in Saccharomyces cerevisiae. *BioRxiv* preprint 2016.

Academic Awards

2018 – 2021 National Science Foundation Graduate Research Fellowship Program

2018 – 2020 Achievement Rewards for College Scientists (ARCS) Scholar

2018 UC San Diego Biology Founding Faculty Award for Graduate Excellence

2017 – 2018 National Institute of Health Cellular and Molecular Genetics Training Grant

2013 Provost's Honors, UC San Diego

2012 San Diego Center for Systems Biology (SDCSB) Summer Fellowship

2012 Winifred and Harry Galles Chemistry Scholarship (Golden West College)

ABSTRACT OF THE DISSERTATION

Regulation of Enhancer Elements by *p53* in Human Cancer

by

Homa Rahnamoun

Doctor of Philosophy in Biology

University of California San Diego, 2020

Professor Shannon Lauberth, Chair

While the dynamic crosstalk between cancer and immune cells within the tumor microenvironment have been extensively investigated, the mechanisms by which immune signaling drives alterations in the cancer cell transcriptome remain to be fully examined. Notably, cytokines such as TNF-α that are released by immune cells can serve as tumor promoting signals to trigger activation of pro-oncogenic networks by the master inflammatory regulator, NFκB. Importantly, tumor promoting properties of inflammation are further regulated by various genetic aberrations in cancer cells. Of special interest are gain-of-function (GOF) mutations in the tumor suppressor gene, *p53* which occur in approximately 50% of all human cancers and have been established to promote inflammation-induced oncogenesis.

in this dissertation, I provide mechanistic insights into the various modes by which mutant p53 fuels proinflammatory gene expression programs in colon cancer cells. First, I

established that mutant p53 and NFκB redirect each other's binding to distinct subsets of distal regulatory elements, commonly referred to as enhancers in response to chronic TNF signaling. Notably, this co-occupancy by mutant p53 and NFκB results in activation of such pro-tumorigenic enhancers. I also found that mutant p53 regulates the enhancer occupancy of the RNA polymerase II machinery and supports the biogenesis of nascent transcripts known as enhancer RNAs (eRNAs). Importantly, this pro-inflammatory eRNA signature was dependent on mutant p53 and not detected in cancer cell lines or human nonneoplastic tissues that expressed wild type p53.

Our group has since revealed the consequences of mutant p53-dependent eRNAs in gene regulation by establishing that these transcripts form complexes with the bromodomain and extra-terminal motif (BET) protein, BRD4 which often occupies active enhancers and regulates inflammatory and oncogenic programs. In this dissertation, I further explore the significance of transcriptional cofactors also functioning as noncanonical RNA binding proteins by establishing DNA topoisomerase 1 (TOP1) as an RNA interacting factor and demonstrating TOP1's dependency on RNA associations to maintain its native protein interactome. Collectively, these findings define previously unrecognized mechanisms by which mutant p53 promotes inflammation-induced tumorigenesis through modulation of enhancer activity and underscore critical consequences of RNA-protein complexes.

Chapter 1

Introduction

1.1 *p53* and its gain-of-function mutations in cancer

The p53 protein is a sequence-specific transcription factor (TF) that acts as an essential tumor suppressor to protect cells from diverse insults by regulating cell cycle arrest, DNA repair, and apoptosis. Mutations that cause loss of wild type (WT) p53 functions are frequently detected in many different cancer types. Indeed, *TP53* is the most frequently mutated gene in all human cancers (Kandoth et al. 2013). Notably, perturbations in p53 regulatory pathways are thought to be the underlying requirement for development of most cancers, further supporting the notion that reactivation of p53 activities has significant therapeutic benefits. While genetic alterations have been identified essentially along the entire length of p53, over 80% of the cancer-associating missense mutations are found within the DNA binding domain (DBD) of the protein and are classified as either contact or conformational mutants (Olivier et al. 2002, Leroy et al. 2013). Contact mutations of p53 affect the amino acids that make direct connections to DNA, thus disrupting the protein's ability to recognize and bind to its consensus DNA elements while conformational p53 mutants are structurally distorted. These mutations typically result in loss or attenuation of WT p53 activities and given that p53 functions as a tetramer, the mutant proteins may also exhibit dominant negative behavior (Wang et al. 2011c). Notably however, convincing evidence accumulated over the past two decades has established that a number of p53 mutants confer aggressive tumorigenic behaviors which are indicative of new oncogenic functions exerted by these oncoproteins.

The gain of function (GOF) paradigm for mutant p53 was first established when the introduction of mutant p53 proteins in p53-null cells resulted in new phenotypes and enhanced tumorigenic potential (Dittmer et al. 1993). The GOF activity of mutant p53 is further consistent with patients who harbor a germline missense *TP53* mutation exhibiting a notably earlier cancer onset than those with mutations that result in loss of the p53 protein (Bougeard et al. 2008, Zerdoumi et al. 2013). Extensive in vivo analyses have further validated that mice expressing mutant forms of p53 develop more aggressive and metastatic forms tumors that WT or null p53 mice (Doyle et al. 2010, Olive et al. 2004, Lang et al. 2004).

While mutant forms of p53 generally lose their ability to bind WT p53's response elements (REs), they still modulate gene expression (Weisz, Oren and Rotter 2007b). A well-established mechanism by which mutant p53 controls gene regulation is through its ability to interact with binding factors. For example, a number of studies have revealed that the p53 family protein and antimetastatic factor p63 interacts with mutant but not WT p53 which results in p63 inhibition and subsequent regulation of invasive transcription networks by mutant p53 (Gaiddon et al. 2001, Strano et al. 2002, Adorno et al. 2009, Girardini et al. 2011). Besides p63, mutant p53 also interacts with the nuclease MRE11 and inhibits the MRE11-Rad50-NBS1 complex that ultimately leads to genomic instability (Song, Hollstein and Xu 2007). Moreover, mutant p53 can promote functions of other TFs such as ETS2 (Do et al. 2012) and NRF2 (Kalo et al. 2012) to promote etoposide resistance and accumulate reactive oxygen species, respectively.

1.2 The crosstalk between inflammation and tumorigenesis

Inflammation is fundamentally a protective cellular response that can become a major contributor to pathogenesis once it goes awry (Ben-Neriah and Karin 2011, Schetter, Heegaard and Harris 2010, Demaria et al. 2010, Hanahan and Weinberg 2011). Over the past decade, the

functional importance of immune cells in promoting neoplastic progression has been extensively examined. Importantly, inflammatory cells release various bioactive molecules that include growth factors, extracellular matrix-modifying enzymes, cytokines, and chemokines which contribute to the promotion of multiple cancer hallmarks such as angiogenesis, invasion, and metastasis (Grivennikov, Greten and Karin 2010, DeNardo, Andreu and Coussens 2010, Qian and Pollard 2010, Karnoub and Weinberg 2006). Tumor-associating immune cells can also release chemicals such as reactive oxygen species, which act as mutagenic agents on the nearby cancer cells and further promote their genetic evolution towards a more enhanced state of malignancy (Grivennikov et al. 2010).

A key mediator of inflammation-induced carcinogenesis is the TF, NFκB that is commonly thought of as the key regulator of inflammation response (Barnes and Karin 1997). Under normal conditions, cytoplasmic NFκB is negatively regulated by IκB. Following inflammation induction, IκB is phosphorylated and subsequently degraded, which allows the now(subsequently)-activated NFκB to translated (transport) to the nucleus (Gilmore and Herscovitch 2006). Notably, NFκB can bind to its REs at the promoter regions of most genes that encode cytokines and chemokines, and this NFκB-mediated activation is essential for induction of these signaling proteins in response to immune challenges (Bonizzi and Karin 2004). Activated NFκB also promotes the expression of several cell cycle regulating genes which ultimately lead to augmented cell proliferation. NFκB stimulation also promotes angiogenesis by activating vascular endothelial growth factor and desensitizes cells to apoptosis through direct and indirect regulation of numerous targets that include, inhibitor of apoptosis proteins (IAPs) (Silke and Meier 2013), TNF receptor-associated factors (TRAFs) (Rothe et al. 1995), and p53 (Ryan et al. 2000).

Given the deregulation of NFκB and p53 pathways in many cancer types, the extensive crosstalk between both pathways is not surprising (Perkins 2007). For example, p53 protein stability is attenuated by NFκB through the induction of E3 ubiquitin ligase MDM2 (Kashatus, Cogswell and Baldwin 2006, Tergaonkar et al. 2002). Furthermore, NFκB and p53 compete for transcriptional co-activators such as the histone acetyltransferases CBP and p300 (Ravi et al. 1998, Wadgaonkar et al. 1999, Webster and Perkins 1999, Huang et al. 2007). Importantly, it has been reported that mutant p53 augments the activation of NFκB in cultured cells through direct protein-protein interactions (Schneider et al. 2010, Scian et al. 2005, Weisz et al. 2007a).

1.3 Mutant p53-mediated modulation of the tumor microenvironment

Recent analyses have also started to identify the roles of GOF p53 mutants in modulating the tumor stroma. It has been well recognized that tumor cells do not act in isolation. Rather, they live and, in many cases, thrive in a diverse microenvironment that consists of extracellular matrix, fibroblasts, endothelial, and immune cells. Growing evidence has established that the tumor stroma plays an integral role in cancer initiation, expansion, and advancement (Pietras and Ostman 2010). Notably, cancer-associating fibroblasts which are the most abundant cell type found in the tumor stroma secrete cytokines, hormones, and growth factors such as HGF and TGF-β, both of which have been shown to mediate cell invasion and metastasis that is dependent on mutant p53 (Adorno et al. 2009, Muller et al. 2013). Moreover, mutant p53 has also been linked to promoting inflammation-associated colorectal cancer by prolonging the cytokine-induced NFκB activation (Cooks et al. 2013) and reprogramming TNF signaling through its interactions with the tumor suppressor DAB2IP (Di Minin et al. 2014). More recently it was shown that mutant p53 expressing cancer cells instigate neighboring macrophages to display anti-inflammatory behavior by releasing miR-1246-containing

exosomes that upon uptake by the immune cells, trigger their miR-1246-dependent reprogramming into a tumor-promoting state (Cooks et al. 2018).

1.4 Deregulation of the epigenetic landscape and chromatin structure in cancer

The classic view on cancer has defined this disease as the result of accumulating genetic alterations in oncogenes and tumor-suppressor genes that ultimately lead to aberrant cell growth. It is now well-appreciated that changes to the epigenetic landscape also contribute to oncogenesis. Indeed, understanding how DNA methylation, nucleosome remodeling, histone modifications, and noncoding RNAs (ncRNAs) mediate gene regulation has been intensely studied for many years.

In eukaryotic cells, genomic DNA is wrapped around histone proteins to form the macromolecule chromatin, with its basic functional unit that contains 147 base pairs of DNA and two of each of histones H2A, H2B, H3, and H4 known as the nucleosome (Luger et al. 1997). Efforts towards understanding the coordinated mechanisms that regulate the nucleosome has revealed that it is subjected to covalent posttranslational modifications (PTMs) which fundamentally change the configuration and functions of chromatin (Goldberg, Allis and Bernstein 2007). Indeed, the diverse range of histone PTMs underscores the complex and combinatorial ways by which they can regulate the chromatin structure. These covalent modifications that include acetylation, methylation, phosphorylation, ubiquitination, and sumoylation are deposited to the flexible and charged N-terminus domain of histone proteins, commonly referred to as the histone tails which protrude out of the nucleosome. Notably, histone modifications are reversible and dynamically deposited and/or removed by chromatin regulatory enzymes that include histone acetyltransferases (HATs), deacetylates (HDACs), methyltransferases (HMTs), demethylases (HDMs), various kinases, and phosphatases (reviewed in (Dawson and Kouzarides 2012, Kouzarides 2007)). Histone PTMs can also serve

as docking sites for unique domains within specific proteins that recognize them. These chromatin readers can subsequently recruit other effector proteins such as chromatin modifying and remodeling enzymes.

Importantly, many chromatin modifying and binding factors are deregulated in cancer. For example, the HMT, *MLL2* is recurrently mutated in approximately 90% of follicular lymphoma cases (Morin et al. 2011) and *UTX* which functions as a HDM was identified to be mutated in numerous cancer types (van Haaften et al. 2009). Additionally, expression of *EZH2* which is the enzymatically functional component of the Polycomb Repressive Complex 2 (PRC2) was shown to be directly linked to increased cell proliferation rate in at least four cancer types (Bachmann et al. 2006). Moreover, chromatin reader domains have been utilized as targetable regions for the development of small molecule inhibitors. Namely, highly specific and potent molecules against the bromodomains (BDs) of BET family proteins (BRD2, BRD3, BRD4, and BRDT) efficiently abrogate the binding of these factors to acetylated chromatin (Filippakopoulos et al. 2010). Targeting of BET BDs has demonstrated high efficacy in various carcinomas and hematological malignancies primarily through downregulation of *MYC* oncogene transcription (Dawson et al. 2011, Delmore et al. 2011, Zuber et al. 2011).

Extensive analysis of various histone marks has established that accumulation of specific histone modifications is associated with activation while presence of some histone marks is indicative of transcriptional repression. Notably however, such histone modification patterns are not static and can dynamically evolve in a context- and cell type-dependent manner. Active and repressive histone marks are also not always mutually exclusive and there has been evidence that one or more histone modifications can influence the deposition, erasure, or the interpretation of other histone marks (Lee, Smith and Shilatifard 2010).

1.5 Mechanisms of enhancer malfunction in tumorigenesis

Cis-acting DNA elements known as enhancers serve as regulatory hubs for sequence specific TFs that upon binding can recruit chromatin-modifying co-factors and regulate gene expression in a spatial and temporal manner. Such enhancer-mediated regulatory events shape gene expression programs that specify cellular identity and function and their deregulation is implicated in multiple human diseases. Notably, the challenging task of Identifying enhancer elements was transformed with the explosion of genome-wide studies which have uncovered various enhancer "signatures" that are now used as hallmarks of defining active, *cis*-regulatory regions. Most enhancers contain specific DNA motifs that are recognized by tissue-specific and signal-dependent TFs that often promote the activation of target genes (Spitz and Furlong 2012). This is well-corelated with depletion of nucleosomes at active enhancer sites that provides further accessibility for the recruitment of TFs (Song et al. 2011, Li et al. 2011). Many enhancers also display a high density of other regulatory factors including the mediator, cohesin complex, and various cofactors (Hnisz et al. 2013, Whyte et al. 2013).

Among co-activators and co-repressors that are found at enhancers, many are chromatin modifying enzymes such as the MLL3/MLL4 HMT complexes and CBP/p300 HATs that deposit various PTMs on histones. Thereby unsurprisingly, a number of histone modifications have been ascribed as being predominantly accumulated at enhancer elements. Namely, histone H3 lysine 4 monomethylation (H3K4me1) is a prominent histone PTM at active enhancers but has also been found to demarcate poised enhancers (Heintzman et al. 2007). Moreover, histone H3 lysine 27 acetylation (H3K27ac) and histone H3 lysine 27 trimethylation (H3K27me3) were also demonstrated to be differentially enriched at active and inactive enhancers, respectively (Creyghton et al. 2010, Heintzman et al. 2009, Rada-Iglesias et al. 2011, Zentner, Tesar and Scacheri 2011). Importantly, accumulation of such histone

modifications holds the potential to recruit specific chromatin reader factors. Among such effector proteins that occupy enhancer regions are TIP60 which is a H3K4me1-binder (Jeong et al. 2011) as well as BRD4 (Hnisz et al. 2013) and other BD-containing proteins such as a subunit of chromatin remodeling complexes, BRG1 (Shi et al. 2013, De et al. 2011) which recognize acetylated histones.

Based on the established enhancer “signatures”, a number of studies have started to examine the hypothesis that alterations in the enhancer landscape may correlate with oncogenesis. Several reports have established such links between changes in DNA methylation patterns at enhancers and disease progression in various cancer types (Aran, Sabato and Hellman 2013, Aran and Hellman 2013, Taberlay et al. 2014). Similarly, increases and losses in H3K4me1 accumulation levels at many enhancer elements have been identified in colon cancer (Akhtar-Zaidi et al. 2012). Interestingly, it has also been demonstrated that changes in the chromatin landscape at enhancers underlie resistance to therapies in breast cancer and acute lymphoblastic leukemia (Magnani et al. 2013, Knoechel et al. 2014).

In addition to alterations in the landscape of histone modifications at enhancers that have been implicated in modulating tumorigenesis, many enhancer-associating chromatin modifiers and mediators of enhancer-promoter interactions are frequently mutated and/or mis-regulated in various cancers. Namely, somatic mutations in HMT complexes MLL3 and MLL4, HATs CBP and p300, H3K27 demethylase UTX, the insulator protein CTCF, and various subunits of the cohesin complex are often found in various cancer cell types (reviewed in (Herz 2016)). Plausible mechanisms that may explain how mis-regulation of enhancer-bound chromatin regulators drive oncogenesis include aberrant activation of pro-tumorigenic enhancers and/or deactivation of enhancers that regulate tumor suppressor genes.

Specific alterations in the DNA sequence of various enhancers have also been linked to tumorigenesis (Yeager et al. 2007, Huang et al. 2014, Oldridge et al. 2015). For example, a

number of genome-wide association studies (GWAS) have cataloged numerous single nucleotide polymorphisms (SNPs) within the gene-free region upstream of the *MYC* locus that are associated with increased risk of acquiring certain cancer types (summarized in (Grisanzio and Freedman 2010)).

1.6 Functions of noncoding RNAs as epigenetic regulators of gene expression

The advancements in high-throughput sequencing platforms and techniques have established that only about 2% of our transcriptome is translated to protein-coding genes (Amaral et al. 2008). The remaining ncRNAs are generally categorized into those that are less than 200 nucleotides in length and include microRNAs (miRNAs), small nucleolar RNAs (snoRNAs), and PIWI-interacting RNAs (piRNAs) and those that can be kilo base pairs long, commonly referred to as long noncoding RNAs (lncRNAs).

Unlike most small ncRNAs which are highly conserved across species and play critical roles in transcriptional regulation through well-preserved modes of action, most lncRNAs do not exhibit high levels of sequence conservation and exert their roles through variable mechanisms. Namely, lncRNAs execute their molecular functions by acting as signals, guides, scaffolds, and decoys and have been shown to control chromosomal dynamics, long-range interactions, and epigenetic gene regulation in normal development as well as disease initiation and progression (Wang and Chang 2011, Ponting, Oliver and Reik 2009, Bernstein and Allis 2005). It is also well-established that many lncRNAs associate with the chromatin structure and nucleosome modifying factors to help with the formation and regulation of active versus inactive chromatin states (Bernstein and Allis 2005, Tsai et al. 2010a). One such lncRNA is the *trans*-acting HOTAIR transcript. This lncRNA is overexpressed in colorectal and breast cancer cells and has been shown to serve as a scaffold for the PRC2 complex (Wang and Chang 2011, Kogo et al. 2011, Rinn et al. 2007). LncRNAs can also function in *cis*, as best exemplified by the HOTTIP

transcript that is expressed from the mammalian *HOXA* cluster and acts to promote transcriptional activation. Notably, this lncRNA is brought to close proximity of the 5' *HOXA* genes through looping and subsequently recruits the MLL1 complex to deposit the histone H3 lysine 4 trimethylation (H3K4me3) mark and promote transcription (Wang and Chang 2011).

About a decade ago, it was identified that many enhancers support the biogenesis of nascent transcripts derived from these regions that are commonly referred to as enhancer RNAs (eRNAs) (Djebali et al. 2012, Li, Notani and Rosenfeld 2016, Andersson et al. 2014, Arner et al. 2015). Indeed, it is estimated that human cells express approximately 40,000-65,000 eRNAs (Andersson et al. 2014, Arner et al. 2015), which accounts for a notable portion of the cell's transcriptome. Given the pervasiveness of eRNA synthesis, critical questions regarding the significance of enhancer transcription and functionality of the resulting nascent transcripts have arose. One initial hypothesis regarding eRNAs which does hold true in some cases (Kaikkonen et al. 2013, Ho et al. 2006, Ling et al. 2004, Mikhaylichenko et al. 2018) is that these noncoding transcripts are simply transcriptional noise, produced by nonspecific RNA polymerase II (RNAPII) activity that occurs at open chromatin regions. However, the robust and regulated biogenesis of eRNAs argue for likely functional roles. In support of this, a number of studies (Bonn et al. 2012, Wang et al. 2011a, Kaikkonen et al. 2013, Bose et al. 2017, Schaukowitch et al. 2014, Mousavi et al. 2013) have shown that the synthesis of specific eRNAs is required to support higher expression levels of their protein coding genes which underscore the functional implications of these transcripts.

More recently, a number of studies have started to uncover functional roles of eRNAs by connecting them to signal-dependent looping complexes that strengthen enhancer-promoter interactions in prostate and breast cancer (Hsieh et al. 2014, Li et al. 2013), increasing chromatin accessibility during myogenesis (Mousavi et al. 2013), and facilitating the release of paused RNAPII by acting as a decoy for the negative elongation factor (NELF) upon induction of

immediate early genes in neurons (Schaukowitch et al. 2014). In addition, eRNAs have been shown to contribute to gene control through formation of functional associations with several regulatory factors such CBP that ultimately leads to stimulation of its HAT activity (Bose et al. 2017).

In summary, the epigenetic landscape and regulation of histone modifications play essential roles in conveying information related to the precise control of DNA-based processes that include, transcription, replication, and DNA repair. Therefore, aberrant expression or deregulation of chromatin modifying factors can have detrimental consequences in initiating and promoting tumorigenesis. Furthermore, it has become increasingly evident that oncogenesis is often associated with changes to the epigenetic landscape at enhancers and that mis-regulation of chromatin modifying enzymes at such *cis*-regulatory elements can have profound effects on enhancer activity. Moreover, association of chromatin-regulating factors with ncRNAs adds further complexity to the epigenetic mechanisms that drive disease progression. Thus, understanding the key regulators and fundamental mechanisms that converge to perversely regulate the activity state of enhancer elements is of great significance.

Chapter 2

Mutant p53 shapes the enhancer landscape of cancer cells in response to chronic immune signaling

2.1 Abstract

Inflammation influences cancer development, progression, and the efficacy of cancer treatments, yet the mechanisms by which immune signaling drives alterations in the cancer cell transcriptome remain unclear. Using ChIP-seq, RNA-seq, and GRO-seq, here we demonstrate a global overlap in the binding of tumor-promoting p53 mutants and the master proinflammatory regulator NFκB that drives alterations in enhancer and gene activation in response to chronic TNF-α signaling. We show that p53 mutants directly interact with NFκB and that both factors impact the other's binding at diverse sets of active enhancers. In turn, the simultaneous and cooperative binding of these factors is required to regulate RNAPII recruitment, the synthesis of enhancer RNAs, and the activation of tumor-promoting genes. Collectively, these findings establish a mechanism by which chronic TNF-α signaling orchestrates a functional interplay between mutant p53 and NFκB that underlies altered patterns of cancer-promoting gene expression.

2.2 Introduction

Despite intensive investigation of the crosstalk between tumor and immune cells of the adjacent microenvironment, the mechanisms by which immune signaling drives alterations in the cancer cell transcriptome remain poorly understood. Diffusible immune cell mediators that include chemokines and cytokines function in tumor-promoting inflammation by converging on the activation of transcription factors such as NFκB, which drives altered gene expression programs in cancer cells (Ben-Neriah and Karin 2011, Natoli 2012). Also, the cancer-promoting effects of inflammation vary based on regulatory factors that are linked to genetic aberrations in cancer cells (Grivennikov et al. 2010). Of special interest here are p53 gene mutations, which are the most frequent alterations in human cancer that give rise to mutant proteins that exhibit a loss of their tumor suppressor activities or a gain in their oncogenic (GOF) functions that promote tumorigenesis (Beckerman and Prives 2010).

In recent support of the p53 GOF paradigm is the finding that mutant p53 (mutp53) augments NFκB activation and results in chronic but not acute inflammation-induced tumor initiation in a mouse model of inflammatory bowel disease (Cooks et al. 2013). Another seminal study revealed that mutp53 prolongs NFκB activation by inhibiting apoptosis-stimulated kinase (ASK1)-JNK pathways in response to chronic tumor necrosis factor alpha (TNF-α) signaling (Di Minin et al. 2014). These studies underscore the significance of investigating the mechanisms underlying the interactions between mutp53 and NFκB to advance our understanding of the protumorigenic roles for immune signaling.

Growing evidence supports mutp53 GOF activities that are connected to gene regulation (Muller and Vousden 2014, Di Agostino et al. 2006). However, the mechanisms controlling mutp53 DNA binding and transcriptional functions are not well understood. Following our global profiling analyses of mutp53 and NFκB in response to chronic TNF-α signaling, we focus on the

possibility of a functional cooperativity between these factors at distinct subsets of enhancers. Enhancers are DNA elements that are activated by transcriptional regulators to orchestrate cell and signal-specific gene expression programs (Barish et al. 2010, Biddie et al. 2011, Heinz et al. 2010, Lefterova et al. 2010, Mullen et al. 2011, Nielsen et al. 2008, Trompouki et al. 2011). Enhancer activity is often correlated with an enrichment of the histone mark, histone H3 lysine 27 acetylation (H3K27ac) (Chepelev et al. 2012, Heintzman et al. 2009, Heintzman et al. 2007) and RNA polymerase II (RNAPII) recruitment that drives the production of bidirectional transcripts known as enhancer RNAs (eRNAs) (De Santa et al. 2010, Hah et al. 2011, Kim et al. 2010b, Wang et al. 2011b). Despite remarkable progress in understanding the pathways that control enhancer priming and activation, relatively little is understood about the mechanisms that promote enhancer activation for the regulation of oncogenic gene expression programs.

In this study, we uncover enhancers that become active in response to chronic TNF-α signaling as revealed by the global accumulation of the chromatin modifications, histone 3 lysine 4 monomethylation (H3K4me1) and H3K27ac that are hallmarks of active enhancers. In addition, we find that these enhancers integrate mutual mutp53 and NFκB regulation of RNAPII recruitment, the synthesis of eRNAs, and the activation of tumor-promoting genes. Collectively, our findings uncover an enhancer transcription “signature” that is linked to alterations in tumor-promoting gene expression and enhanced cancer cell growth.

2.3 Results

2.3.1 Alterations in gene expression by TNF signaling and mutp53

To investigate the mechanisms underlying the roles of mutp53 in promoting chronic inflammation-induced tumorigenesis, we performed mRNA sequencing (mRNA-seq) in human SW480 colon cancer cells expressing doxycycline-inducible short hairpin RNAs (shRNAs) against mutp53 before and following TNF-α treatment for 16 h. Relative to a non-targeting

shRNA against LacZ (control), p53 shRNA markedly reduced mutp53 R273H mRNA and protein levels before and after TNF-α treatment (+/–TNF-α) (Fig. 2.1a). By comparing the transcriptomes of control and mutp53-depleted cells (+/–TNF-α), we found that mutp53 alters (≥2-fold, false discovery rate (FDR) < 0.05) a comparable number of genes before (n = 2360, 51%) and following (n = 2264, 49%) TNF-α treatment (Fig. 2.1b), which is consistent with a broad role for mutp53 in regulating gene expression. Notably, the colon cancer cell transcriptome regulated by mutp53 is also extensively altered by chronic immune signaling as revealed by the identification of a subset of gained mutp53-regulated genes (n = 772) that are upregulated or downregulated in response to TNF-α (Fig. 2.1b). Analysis of this gained subset of TNF-α-responsive genes revealed 303 (39%) mutp53-repressed genes that include key regulators of organ morphogenesis, development, and hypoxia as revealed by gene ontology (GO) enrichment analysis (Fig. 2.1c). Conversely, GO categories corresponding to the 469 (61%) mutp53-activated genes are largely related to immunogenic and tumor-promoting processes that include cytokine – cytokine receptor interaction, hallmark TNF signaling via NFκB, and regulation of locomotion (Fig. 2.1c). Next, we investigated a role for mutp53 in regulating TNF-α-inducible gene expression. As revealed in Fig. 2.1d, we identified 482 RefSeq genes that are induced (≥2-fold, FDR< 0.05) by TNF-α in the control knockdown cells. Among the TNF-α-induced genes, we identified a number of genes (n = 187, 39%) that are induced in a mutp53-dependent manner (≥2-fold) as revealed by the significant decrease in inducible gene expression following mutp53 depletion (Fig. 2.1d). Conversely, a much smaller subset (n = 9, 2%) of TNF-α-inducible genes are repressed by mutp53 (Fig. 2.1d). Overall, our mRNA-seq data indicate the role of mutp53 in potent gene activation in response to chronic TNF signaling.

Consistent with our RNA-seq data, quantitative polymerase chain reaction with reverse transcription (qRT-PCR) revealed that mutp53 is required for the induction of a subset of TNF-α-

induced genes. Specifically, mutp53 knockdown revealed significant downregulation of the TNF-α-induced expression of *MMP9*, *CCL2*, *UBD*, and *LTB* (Fig. 2.1e), which are among the top ten most highly induced mutp53-dependent genes identified in our mRNA-seq data (Fig. 2.1d). In comparison, mutp53 had little to no effect on the expression of wild-type p53 target genes (Fig. 2.1e). The TNF-α-inducible gene-selective effects of mutp53 were also identified when using an siRNA oligonucleotide that is directed against a different region of p53 mRNA in SW480 cells (Fig. 2.7a) and in breast cancer MDA-MB-231 cells that express mutp53 R280K (Fig. 2.7b).

Cell invasion assays were performed to investigate whether TNF-α and mutp53-dependent alterations in the transcriptome are associated with changes in cancer cell growth. As revealed in Fig. 2.1f, chronic TNF-α results in an approximately sevenfold increase in the number of control cells that pass through the Matrigel. Under uninduced conditions, mutp53 depletion had little to no effect on the number of cells that invade. Notably, however, mutp53 depletion significantly reduced the number of cells that invade following TNF-α signaling for 16 h to a level that is comparable to the number of control cells that invade prior to TNF-α signaling (Fig. 2.1f). These findings reveal that mutp53 modulates chronic TNF-α-dependent alterations in the cancer cell transcriptome that enhance cancer cell invasion.

2.3.2 TNF signaling uncovers enhancers occupied by mutp53 and NFκB

To further explore the interplay between mutp53 and chronic TNF-α signaling at the genomic level, we performed chromatin immunoprecipitation followed by deep sequencing (ChIP-seq) for mutp53 R273H and NFκB/p65 in SW480 cells (+/–TNF-α). Following TNF-α signaling, stringent p65 peaks (n = 24,965; FDR< 0.001) were identified that showed a striking colocalization with unchanged or “maintained” mutp53 peaks (n = 18,295; FDR< 0.001) and TNF-α-dependent enriched or “gained” mutp53 peaks (n = 17,772; FDR< 0.001) (Fig. 2.2a). Specifically, 43% of the gained mutp53-binding sites show overlap with p65, and conversely

31% of the p65-occupied regions overlap with the gained mutp53 peaks in response to TNF-α (Fig. 2.8a). In addition, de novo motif analysis identified that NFκB consensus motifs are among the most highly enriched to overlap with the gained mutp53 and NFκB peaks (Fig. 2.2b). We also identified a comparable degree of overlap between p65 and maintained mutp53-binding sites following TNF-α exposure with about half (47%) of the maintained mutp53 regions showing overlap with p65 and 34% of the p65-enriched regions revealing overlap with maintained mutp53-binding sites (Fig. 2.2a; Fig. 2.8a). Motif analysis of the maintained peaks revealed an enrichment of the consensus sequences recognized by transcription factors that include Fra-1/AP-1, TEAD4, and ERG/ETS but not NFκB (Fig. 2.2b). Also as expected, wild-type p53 motifs do not overlap with the gained or maintained mutp53 peaks, which is consistent with the reduced affinity of contact mutp53 for wild-type p53 recognition elements (Freed-Pastor and Prives 2012). Altogether, these findings reveal that chronic TNF-α promotes an overlap in NFκB and mutp53 binding across the genome.

Genome-wide analyses have revealed that the majority of NFκB binding takes place at genomic regions with enhancer-like chromatin features (Barish et al. 2010, John et al. 2011). To explore whether the overlapping mutp53 and NFκB-binding sites occur at enhancers, we compared our mutp53 and NFκB ChIP-seq data to global profiling analysis of H3K27ac and H3K4me1 that demarcate enhancers. As demonstrated at the gained (*MMP9* and *CCL2*) and maintained (*CYP24A1* and *CPA4*) mutp53-bound enhancers, we identified a strong correlation between mutp53 and NFκB enrichment, and H3K4me1 and H3K27ac accumulation that occurs across the genome in response to chronic TNF-α signaling (Fig. 2.2c).

To determine the temporal relationship of mutp53 and NFκB binding at the identified enhancers, we next performed time course ChIP experiments followed by qPCR. Immunoprecipitated DNA was analyzed with primer sets specific to regions with active enhancer

chromatin signatures and centered at NFκB/p65 and mutp53 peaks (Fig. 2.2d, amplicons A and B at *MMP9* and A at *CCL2*, *CYP24A1*, and *CPA4*) and non-specific control regions (Fig. 2.2d, amplicon C at *MMP9* and B at *CCL2*, *CYP24A1*, and *CPA4*). Consistent with our ChIP-seq data, ChIP-qPCR revealed low levels of pre-associated mutp53 and negligible NFκB binding before TNF-α signaling and substantial TNF-α-induced increases in the binding of both factors at the gained enhancers, but not at the control regions of the *MMP9* and *CCL2* genes (Fig. 2.2d). At the maintained enhancers, *CYP24A1* and *CPA4*, we observed comparable levels of mutp53 binding +/−TNF-α, and negligible levels of uninduced NFκB binding that are increased in response to TNF-α (Fig. 2.2d). Consistent with our ChIP-seq findings, H3K4me1 and H3K27ac levels were observed at the mutp53 and NFκB co-bound enhancers with peak levels observed at 8 and 16 h TNF-α (Fig. 2.2d). In addition, the overlap of mutp53, NFκB, and H3K27ac that occurs in response to chronic TNF-α was identified at the *MMP9* and *CPA4* enhancer regions, but not the wild-type p53 *p21* enhancer in MDA-MB-231 cells (Fig. 2.8b). Similarly, wild-type p53 was not found to overlap with NFκB or H3K27ac at the *MMP9* or *CPA4* enhancers in HCT116 cells, despite the enrichment of wild-type p53 at the *p21* enhancer (Fig. 2.8c). These ChIP analyses support differential enhancer targeting of mutant versus wild-type p53 in cancer cells in response to chronic immune signaling.

To investigate simultaneous binding of mutp53 and NFκB at active enhancers, sequential chromatin immunoprecipitation (re-ChIP) for mutp53 followed by NFκB was performed in SW480 cells treated with TNF-α for 16 h. As shown in Fig. 2.2e, qPCR analysis of the re-ChIP DNA revealed NFκB and mutp53 co-occupancy at the *MMP9*, *CCL2*, *CYP24A1*, and *CPA4* enhancers. In comparison, the control (IgG) IP revealed little to no enrichment of DNA in the re-ChIP experiments. The strong parallel between our global and enhancer-specific analyses demonstrate distinct classes of mutp53 and NFκB co-bound enhancers.

2.3.3 **Mutp53 and NFκB form functional interactions**

Given the striking overlap of the mutp53 and NFκB-binding profiles, we next assessed whether these factors form functional interactions. Using purified mutp53 and p65 proteins (Fig. 2.9a), we identified that p65 interacts directly and equivalently with the p53 mutants, R273H, R248W, R248Q, and G245S (Fig. 2.3a). p65 also interacts directly with wild-type p53 (Fig. 2.3a), despite that these factors were not found to overlap at mutp53-bound enhancers (Fig. 2.8c). As shown in Fig. 2.9b, we also identified an association between mutp53 and NFκB in SW480 cells. Specifically, an NFκB/p65 antibody comparably co-immunoprecipitated mutp53 from nuclear extracts prepared before and following TNF-α treatment. These results establish mutp53– NFκB interactions that are consistent with the TNF-α-induced global overlap (Fig. 2.2a, c; Fig. 2.8a) and the simultaneous binding of mutp53 and NFκB at active enhancers (Figs. 2.2d, e).

We next analyzed whether NFκB regulates mutp53 enhancer binding. ChIP-qPCR was performed in SW480 cells transfected with control or NFκB/p65 siRNA, which reduced NFκB mRNA and protein levels without affecting mutp53 levels (Fig. 2.9c). Under TNF-α-induced conditions, p65 knockdown resulted in a comparable loss of p65 binding at the *MMP9* (80%, 90% at amplicons A and B, respectively) and *CCL2* (70%) enhancers (Fig. 2.3b). Notably, decreased p65 binding resulted in a substantial and comparable reduction of mutp53 binding at the *MMP9* (70%, 75% at amplicons A and B, respectively) and *CCL2* (77%) enhancers (Fig. 2.3b). In comparison, little to no effect of p65 knockdown on mutp53 binding was identified at the maintained mutp53 enhancers, *CYP24A1* and *CPA4*, despite the significant decrease (73% and 83%, respectively) in the TNF-α-induced levels of NFκB binding at both enhancers (Fig. 2.3b). This finding is consistent with our motif analysis (Fig. 2.2b), which revealed that NFκB response elements are not enriched, whereas response elements recognized by transcription

factors including ETS2 overlap with the maintained enhancers. Also consistent with the motif analysis (Fig. 2.2b), we identified a comparable enrichment of ETS2 that overlaps with mutp53 binding at the maintained enhancers, *CYP24A1* and *CPA4* before and after TNF-α signaling (Fig. 2.9d), which is consistent with published results showing that ETS2 facilitates mutp53 binding (Do et al. 2012, Zhu et al. 2015). We further investigated the role of NFκB in regulating mutp53 binding at the gained enhancers, *MMP9* and *CCL2* by using the proteasome inhibitor MG132, which prevents degradation of IκB, an endogenous NFκB inhibitor(Lee and Goldberg 1998), while not affecting the protein levels of p65 or mutp53 (Fig. 2.9e). Consistent with the NFκB knockdown experiments (Fig. 2.3b), MG132 significantly reduced p65 binding at the *MMP9* (96%) and *CCL2* (89%) enhancers (Fig. 2.9f), which resulted in substantial losses of TNF-induced mutp53 binding at the *MMP9* (86%, 94% at amplicons A and B, respectively) and *CCL2* (88%) enhancers (Fig. 2.9f). Altogether, these results demonstrate that NFκB is required for mutp53 binding at a subset of enhancers in response to TNF-α signaling.

We next investigated a role for mutp53 in the regulation of NFκB enhancer binding by performing ChIP-qPCR in SW480 cells following mutp53 shRNA and siRNA-mediated knockdown. As shown in Fig. 2.1a, mutp53 knockdown significantly decreased mutp53 mRNA and protein levels, without affecting p65 levels. Under uninduced conditions, mutp53 binding at the maintained, *CYP24A1* (74%) and *CPA4* (66%) enhancers were significantly decreased following mutp53 knockdown, which is consistent with the identification of pre-associated mutp53 binding at this subset of enhancers (Fig. 2.3c). In TNF-α-treated cells, mutp53 knockdown resulted in a comparable and substantial decrease in mutp53 binding at all four enhancers, *MMP9* (80%, 82% at amplicons A and B, respectively), *CCL2* (91%), *CYP24A1* (78%), and *CPA4* (75%) (Fig. 2.3c), which resulted in a significant decrease in p65 binding at the *MMP9* (50%, 67% at amplicons A and B, respectively), *CCL2* (57%), *CYP24A1* (63%), and

CPA4 (68%) enhancers (Fig. 2.3c). The effect of mutp53 in regulating p65 binding at the maintained enhancers that are devoid of NFκB consensus motifs (Fig. 2.2b) is consistent with a mutp53 GOF activity that involves altering NFκB binding to extend the cancer cell transcriptome. The requirement for mutp53 in regulating NFκB recruitment was confirmed using siRNA-mediated knock-down of mutp53 (Fig. 2.9g). The ability of mutp53 and NFκB to impact each other's binding is in agreement with the identification of mutp53– NFκB interactions and the interplay of these factors at specific subsets of enhancers in response to chronic TNF-α signaling.

2.3.4 Potent eRNA synthesis at mutp53 and NFκB co-bound enhancers

Given that active enhancers support eRNA synthesis, we performed global run-on sequencing (GRO-seq) to assay nascent transcription in SW480 cells (+/–TNF-α). As demonstrated at the *MMP9* and *CPA4* enhancers, our GRO-seq data reveals bidirectional transcription at mutp53 and NFκB co-bound enhancers (Fig. 2.4a). Specifically, the gained *MMP9* enhancer revealed low levels of uninduced and markedly induced eRNA levels following TNF-α treatment, which parallels with the induced levels of mutp53 binding (Fig. 2.4a). In comparison, the maintained *CPA4* enhancer supports comparable levels of eRNA synthesis that parallels with mutp53 binding before and following TNF-α (Fig. 2.4a). This correlation between eRNA synthesis and mutp53 binding was further demonstrated at the *CCL2* and *CYP24A1* enhancers, respectively (Fig. 2.10a). To further investigate differential eRNA induction from mutp53 gained and maintained enhancers, we examined the GRO-seq signals from all enhancers parsed by mutp53, NFκB, and H3K27ac enrichment. The vast majority of the mutp53 gained (n = 1506, 58%) and maintained (n = 1864, 68%) enhancers reveal robust TNF-α-inducible eRNA synthesis (Fig. 2.4b). In addition, the higher levels of uninduced eRNA synthesis from the maintained enhancers is consistent with the lower fold eRNA induction that is

identified from the maintained versus gained enhancers (Fig. 2.4b). These results, taken together with the identification of H3K27ac accumulation are consistent with an active state of the mutp53 and NFκB co-bound enhancers in response to chronic TNF signaling. These findings also reveal a strong correlation between mutp53 enhancer localization and enhancer-directed transcription across the genome.

We next wanted to determine whether enhancer transcription at mutp53 and NFκB co-bound enhancers parallels with the transcription of nearby genes on a global scale. Thus, we compared our GRO-seq data at intergenic sites bound by NFκB alone or co-bound by mutp53 and NFκB with the positive strand GRO-seq signals identified at the nearest gene promoters following TNF-α treatment. Notably, the peak GRO-seq signals were significantly higher at the mutp53 and NFκB co-bound enhancers as compared to the NFκB-bound enhancers (Fig. 2.4c, left). Also, there exists a strong parallel between intergenic GRO-seq signals at the two subsets of enhancers and the GRO-seq signals at the nearby promoters (Fig. 2.4c, right). These results indicate that enhancer transcription positively correlates with mutp53 binding and nearby gene activation.

To further investigate the kinetics of enhancer transcription from mutp53 and NFκB co-bound enhancers, eRNA levels were examined in SW480 cells treated with TNF-α for 0, 8, and 16 h. We identified that eRNA induction reached near maximal levels from the maintained (*CYP24A1* and *CPA4*) and gained (*MMP9* and *CCL2*) enhancers by 8 h of TNF-α treatment (Fig. 2.4d; Fig. 2.10b). Consistent with our GRO-seq data (Fig. 2.4a–c), the overall fold induction of eRNA levels are (three- to fourfold) higher at the gained versus maintained mutp53-bound enhancers, which is due to the measurable levels of eRNA synthesis at the maintained but not gained enhancers in uninduced cells (Fig. 2.4d; Fig. 2.10b). The strong correlation between enhancer transcription and nearby-gene activation was further confirmed by qRT-PCR

analyses of the mRNA expression levels of the *MMP9*, *CCL2*, *CYP24A1*, and *CPA4* genes (Fig. 2.4d; Fig. 2.10b). In comparison, negligible levels of eRNA synthesis were identified from the *MMP9*, *CCL2*, *CYP24A1*, and *CPA4* enhancers in wild-type p53-expressing HCT116 cells, which is consistent with the negligible TNF-α-induced mRNA expression levels of all four genes (Fig. 2.4e; Fig. 2.10c). A 250-fold lower level of TNF-α-induced *MMP9* expression was detected in HCT116 as compared to SW480 cells through a mechanism that is independent of mutp53 (Fig. 2.4e; Fig. 2.10c). These enhancer-specific findings and our genome-wide data provide support for a functional interplay between mutp53 enhancer- binding sites, enhancer transcription, and target gene expression.

2.3.5 Mutp53 and NFκB regulate RNAPII binding and eRNA production

We next investigated a direct role for mutp53 in the regulation of eRNA synthesis. First, using ChIP-seq we compared the global-binding profiles of RNAPII and mutp53, which revealed a significant colocalization of RNAPII and mutp53 in response to TNF-α signaling (Fig. 2.5a), and a symmetrical and bidirectional profile for global RNAPII binding (Fig. 2.5a) that is consistent with bidirectional transcription from the mutp53- bound enhancers (Figs 2.4a–c; Fig. 2.10a). Next, we examined a role for mutp53 in the regulation of RNAPII binding at mutp53-bound enhancers by performing RNAPII ChIP following the inducible expression of control or mutp53 shRNA. Under uninduced conditions, negligible levels of mutp53 and RNAPII binding were identified at the gained (*MMP9* and *CCL2*) enhancers (Fig. 2.5b). In comparison, and consistent with pre- associated levels of mutp53 binding at the maintained enhancers, *CYP24A1*, and *CPA4*, we identified that pre-associated RNAPII levels are substantially (52% and 65%, respectively) decreased following mutp53 knockdown (Fig. 2.5b). Under TNF-α-induced conditions, the decrease in mutp53 binding at the enhancer regions of *MMP9* (75%, 84% at amplicons A and B, respectively), *CCL2* (87%), *CYP24A1* (74%), and *CPA4* (71%)

results in a significant loss (64%, 85%, 90%, 71%, and 75%) in RNAPII binding at all four enhancers, respectively (Fig. 2.5b).

Consistent with the identified role of mutp53 in regulating RNAPII binding at the maintained *CYP24A1* and *CPA4* enhancers prior to TNF-α signaling, qRT-PCR analyses revealed a comparable (twofold) reduction in the uninduced eRNA and mRNA expression levels of *CYP24A1* following mutp53 knockdown (Fig. 2.5c). We were unable to detect a change in *CPA4* mRNA levels, which likely relates to its lower uninduced expression levels (Fig. 2.5c). In addition, a significant decrease in the TNF-α-induced eRNA levels from the *MMP9* (fourfold, fivefold at the –3.7 kb and –0.7 kb regions, respectively), *CCL2* (sixfold), *CYP24A1* (fivefold), and *CPA4* (fourfold) enhancers and a comparable decrease in the TNF-α-induced mRNA levels was identified for *MMP9*, *CCL2*, *CYP24A1*, and *CPA4* (eightfold, fivefold, threefold, and fourfold, respectively) following mutp53 knockdown (Fig. 2.5c). siRNA-mediated knockdown of mutp53 revealed an identical requirement for mutp53 in the regulation of RNAPII binding (Fig. 2.11a), eRNA synthesis, and gene activation (Fig. 2.11b). These findings demonstrate a strong correlation between mutp53 and RNAPII enrichment across the genome and a requirement for mutp53 in supporting RNAPII regulation of enhancer and gene activation.

To determine whether NFκB regulates TNF-inducible enhancer transcription, RNAPII ChIP-qPCR was performed in TNF-α-treated SW480 cells transfected with control or NFκB/p65 siRNA. NFκB depletion resulted in an approximately 80% decrease in RNAPII binding at the gained *MMP9* enhancers (Fig. 2.11c), which is consistent with the identification that NFκB depletion reduced the levels of eRNA and mRNA *MMP9* induction by at least twofold and fivefold, respectively (Fig. 2.11d). These findings are consistent with p65 regulation of mutp53 binding (Fig. 2.3b) and mutp53 regulation of RNAPII binding at these enhancers (Fig. 2.5b; Fig. 2.11a). p65 also supports RNAPII binding at the maintained *CYP24A1* enhancer as revealed by

an approximately 50% decrease in RNAPII levels following p65 knockdown (Fig. 2.11c). However, despite the decrease in RNAPII binding, we identified little change in the TNF-α-induced eRNA levels from this enhancer (Fig. 2.11d), which is likely due to the residual levels of RNAPII at this enhancer following p65 knockdown (Fig. 2.11c, amplicon A versus B). In addition, TNF-α-induced *CYP24A1* mRNA levels were significantly (twofold) decreased following p65 knockdown, despite the negligible change in *CYP24A1* eRNA levels (Fig. 2.11d), which suggests that p65 also regulates this target gene through mechanisms that are independent of p65 enhancer functions. Taken together, these findings demonstrate a direct requirement for the functional interplay between mutp53 and NFκB in the activation of enhancer and tumor-promoting genes.

2.3.6 eRNA expression in colon carcinomas expressing mutp53

To explore the clinical significance of mutp53-dependent alterations in the cancer cell transcriptome, qRT-PCR analyses were performed to analyze *MMP9* eRNA and mRNA expression levels in human colorectal carcinomas (CRCs) and matched non-neoplastic tissues isolated from five patients. First, DNA sequencing (Fig. 2.6a) and immunoblot (Fig. 2.12a) analyses confirmed mutp53 versus wild-type p53 expression in CRCs and non-neoplastic tissues, respectively. Notably, we identified a potent activation of *MMP9* eRNA and mRNA expression levels in CRCs that express mutp53, as compared with the negligible levels that are present in the wild-type p53-expressing tissues (Fig. 2.6a). Additional support for these findings is the identification of significant *CCL2* eRNA and mRNA expression levels in the CRCs and not the non-neoplastic tissues (Fig. 2.12b). Thus, these results further underscore the importance of mutant versus wild-type p53 in regulating the observed changes in the cancer cell transcriptome.

2.4 Discussion

Immune cells of the tumor microenvironment influence the course of tumor progression, yet the molecular mechanisms by which immune signaling drives alterations in tumor-specific gene expression remains unclear. Our study highlights an emerging link between chronic proinflammatory signaling pathways and the gene expression landscape controlled by GOF mutations of the tumor suppressor p53. Specifically, our findings reveal that chronic TNF-α signaling prompts a global relationship between mutp53 and NFκB that supports potent enhancer and tumor-promoting gene activation and has significant implications for cancer aggressiveness. Support for a dynamic relationship between mutp53 and NFκB is demonstrated by the identification of a significant gain in the global binding of mutp53 that overlaps with NFκB at active enhancers, kinetic ChIP analyses that show a direct parallel in the temporal-binding profiles of mutp53 and NFκB, and re-ChIP analyses that revealed simultaneous binding of these factors at active enhancers.

Roles for NFκB and mutp53 in the regulation of each other's binding at active enhancers in response to chronic TNF signaling is supported by our demonstration of (1) direct physical inter- actions between purified NFκB and mutp53, (2) the formation of mutp53 and NFκB associations in colon cancer cells, and (3) the decreased binding of NFκB and mutp53 at active enhancers that occurs following the depletion or inactivation of the other factor. Specifically, at the mutp53-gained enhancers, we identified that mutp53 is bound through NFκB interactions as demonstrated by the near complete loss of mutp53 binding that occurs in response to NFκB knockdown and the inhibition of NFκB activation. As the vast majority of p53 mutations localize to the DNA-binding domain and alter the recognition of wild-type p53 sequence- specific DNA elements (Cho et al. 1994), these findings support an additional mechanism for mutp53 DNA-binding that is facilitated by NFκB. We also identified that mutp53 knockdown leads to a

modest, yet significant decrease in NFκB binding at this identical subset of enhancers. These modest effects of mutp53 depletion on NFκB binding are consistent with additional NFκB-enhancer interactions, particularly those that are likely facilitated by NFκB recognition of its consensus motifs that are present at these enhancers. The cooperativity in mutp53 and NFκB-enhancer binding is consistent with the previously described assisted loading mechanism in which factors localized at the same enhancer region facilitate each other's binding (Heinz et al. 2015). An unexpected finding is the identification that mutp53 facilitates NFκB binding at the mutp53-maintained enhancers that are devoid of NFκB recognition sequences and that show significant and comparable levels of mutp53 and ETS2, which was previously shown to recruit mutp53 (Do et al. 2012, Zhu et al. 2015). This finding significantly advances our understanding of the GOF properties of mutp53 by revealing the ability of mutp53 to facilitate NFκB accessing this subset of enhancers, which provides new opportunities for expanding the proinflammatory roles of NFκB in cancer cells. This observation suggests the importance of considering additional roles of mutp53 in regulating NFκB involvement in chronic inflammatory and autoimmune diseases, wherein proinflammatory cytokines drive NFκB activation. Although we are unable to rule out additional cofactors and mechanisms that may contribute to the recruitment and function of mutp53 and NFκB, our results provide strong evidence for the mutual interdependence of mutp53 and NFκB at these classes of enhancers in response to chronic TNF-α signaling.

Growing evidence supports mechanisms underlying mutp53 GOF activities that are connected to the gene regulatory roles of mutp53 (Weisz et al. 2007b). Yet, the full spectrum of mechanisms remains to be elucidated, and little is known about the roles of mutp53 in the regulation of enhancers. Through RNAPII ChIP-seq and GRO-seq (Core, Waterfall and Lis 2008) analyses, we demonstrate that enhancer-specific mutp53 binding events are linked to

RNAPII recruitment and the extensive induction of eRNA synthesis in response to chronic TNF signaling. Also, we provide a global perspective of the relationship that exists between enhancer-directed transcription and tumor-promoting gene activation mediated by the functional interplay between mutp53 and NFκB. Interestingly, the enhancers co-bound by mutp53 and NFκB support significantly higher levels of TNF-induced eRNA synthesis that positively correlates with higher levels of transcription from the nearby gene promoters as compared with the enhancers that are bound only by NFκB. We also demonstrate that mutp53 and NFκB exhibit a direct role in the regulation of RNAPII recruitment and as a result, modulate the TNF-α-inducible activation of enhancers and tumor-promoting genes. Altogether, inducible eRNA synthesis and H3K27ac accumulation are strong indicators that the induced recruitment of mutp53 and NFκB coincides with enhancer activation. This finding is consistent with previously described mechanisms in which signal-dependent transcription factors bind to pre-selected enhancers that consist of H3K4me1 and little to no enrichment of H3K27ac, and transition to an active state that includes enrichment of both H3K4me1 and H3K27ac (Heintzman et al. 2007). Further investigation is needed to determine the additional factors that together with mutp53 and NFκB regulate the step-wise events that lead to enhancer activation.

Our studies also provide support for mutant versus wild-type p53 in the regulation of these enhancer-directed alterations in the cancer cell transcriptome. Although we identified comparable NFκB interactions with p53 mutants and wild-type p53, wild-type p53 was not found to overlap with NFκB at the mutp53 maintained or gained enhancers before or after TNF signaling. In addition, wild-type p53 was not found to have a role in the induction of eRNA or mRNA synthesis in response to TNF signaling. Consistent with these cell-based experiments, additional transcriptional analyses revealed increased expression of eRNA and mRNA levels of the gained target gene loci, *MMP9* and *CCL2* in solid colon tumors that express mutp53 relative

to the matched normal tissues that express wild-type p53. However, we were unable to detect an increase in the eRNA and mRNA levels of the maintained genes, *CYP24A1* and *CPA4*, which we believe may relate to the lower overall eRNA and mRNA expression levels of the maintained relative to the gained gene loci. Thus, our data supporting a mutp53-specific role in enhancer regulation that is mediated by NFκB interactions is consistent with previous studies (Beckerman and Prives 2010) that have shown that wild-type p53 will be recruited to its typical sites within the genome consisting of wild-type p53 DNA- binding motifs (as was shown in this study by revealing wild-type p53 recruitment to its target gene, *p21*), whereas the vast majority of p53 mutants will be mislocalized to other regions in the genome based on interactions with other transcriptional regulators (i.e., NFκB in this study). Overall, the effects on enhancer and gene activation by mutp53 and NFκB enhancer landscapes in response to chronic TNF-α signaling support our proposed model (Fig. 2.6b), which is consistent with an emerging regulatory network of mutp53 in orchestrating chronic inflammation-induced colon cancer.

2.5 Methods

Cell culture and treatments

Human SW480 and HCT116 cells were purchased from American Type Culture Collection (ATCC) and grown in Dulbecco's modified Eagle medium (DMEM, Gibco) supplemented with 10% fetal bovine serum (FBS, Gibco). MDA-MB-231 cells were also purchased from ATCC and were grown in RPMI 1640 (Gibco) medium supplemented with 10% FBS. SW480 cells that stably and inducibly express short hairpins against LacZ or p53 were kindly provided by Xinbin Chen (UC Davis) and were grown in standard DMEM medium containing 1× penicillin and streptomycin (Gemini Bio-Products), 1.5 μg ml^{-1} puromycin (Sigma), and were induced with 1 μg ml^{-1} doxycycline (Sigma). MG132 treatment experiments were performed by treating SW480 cells with 5 μM MG132 (Sigma) or vehicle (DMSO, Fisher

Scientific) and with 12.5 ng ml^{-1} TNF-α (R&D Systems) for 0 or 16 h before harvesting for gene expression or ChIP analyses. All cell lines mentioned have tested negative for mycoplasma contamination by PCR.

RNA interference experiments

SW480 and MDA-MB-231 cells were transfected with 100 nM non-targeting siRNA control, human RelA siRNA SMART pool, or p53 siRNA duplexes (listed in Supplementary Table 2.1) (all siRNAs are from Thermo Scientific). Forty-eight hours after transfection, cells were treated with 12.5 ng ml^{-1} TNF-α for 0 or 16 h before harvesting for gene expression or ChIP analyses.

Immunoblotting

Protein samples were incubated at 95 °C for 5 min, separated by SDS-PAGE, and transferred to PVDF membranes (EMD Millipore) that were probed with the indicated antibodies. Reactive bands were detected by ECL (Thermo Scientific Pierce) and exposed to Blue Devil Lite ECL films (Genesee Scientific). Full scans of all western blots are provided in Fig. 2.13.

Antibodies

Antibodies used for ChIP assays were obtained commercially as followed: anti-H3 (ab1791, 1 µg), anti-H3K4me1 (ab8895, 1 µg), and anti- H3K427ac (ab4729, 1 µg) from Abcam; anti-RNA Pol II (N20, sc899, 2 µg), anti-p53 (FL393, sc6243, 2 µg), anti-ETS2 (sc351, 2 µg), anti-p65 (sc372x, 2 µg), and anti-IgG (sc2027, 2 µg) from Santa Cruz Biotechnology. Antibodies used for immunoblotting were obtained as followed: anti-p53 (DO1, sc126, 1:2000 dilution) and anti-β-Actin (sc47778, 1:2000 dilution) from Santa Cruz Biotechnology, and anti-p65 (ab7970, 1:1000 dilution) from Abcam.

RNA purification and quantitative real-time PCR

Total RNA was extracted with TRIzol LS reagent (Invitrogen) from SW480, MDA-MB-231, HCT116, and SW480 stably expressing LacZ or p53 shRNA and treated with 12.5 ng ml^{-1} TNF-α for the indicated time points. Reactions were performed using SYBR Green PCR Master Mix (Applied Biosystems) in duplicate using samples from at least three independent cell harvests and the specificity of amplification was examined by melting curve analysis. Primers used for qRT-PCR analysis are listed in Supplementary Table 2.3. The relative levels of eRNA and mRNA expression were calculated according to the ($\Delta\Delta$Ct) method(Livak and Schmittgen 2001) and individual expression data was normalized to GAPDH. The gene expression levels determined after TNF-α treatment are relative to the levels before TNF-α treatment.

Invasion assay

Invasion assays were performed using SW480 cells that inducibly express shRNA against LacZ or mutp53 and were pre-treated with or without 12.5 ng ml^{-1} recombinant TNF-α in low-serum media (0.1% serum) for 24 h prior to plating 1–2× 10^5 cells from each condition on 24-well-PET inserts with 8 μm pore size (Falcon), coated with BD Matrigel (BD Bioscience). The lower chamber was filled with high-serum media (20% serum) without TNF-α. Cells that passed through the Matrigel after 24 h were fixed, stained, imaged, and counted after. Representative scale bars were added using ImageJ.

Colorectal carcinoma tumor analysis

Five colorectal carcinoma tumors and their corresponding paired normal colon tissue were obtained from Biorepository Tissue Technology Shared Resource at Moores Cancer Center (UC San Diego), following informed consent from patients. Samples were dissected by pathologists, and frozen in liquid nitrogen for molecular analyses. Briefly, RNA extraction from the tissue samples was done using TRIzol LS reagent (Invitrogen). Extracted RNA was subsequently treated with DNase I (Worthington Biochem) before being reverse-transcribed with

the SuperScript III First-Strand Synthesis System (Invitrogen), and amplified with SYBR Green PCR master mix. qRT-PCR primer sequences can be found in Supplementary Table 2.3. The DNA-binding domain of p53 was amplified from cDNA by PCR and submitted for sequencing. Primers used for PCR amplification are listed in Supplementary Table 2.4. For extraction of protein from the tumor samples, genomic DNA was first precipitated with ethanol and isolated by centrifuging the organic phase after TRIzol purification of the RNA. Isopropanol was added to the phenol–ethanol supernatant obtained after isolation of the genomic DNA to precipitate the protein. The protein precipitate was washed with 0.3 M guanidine hydrochloride in 95% ethanol and then dissolved in 1% SDS at 50 °C. Extracted proteins were quantified using Protein Assay Reagent Dye Concentrate (Bio-Rad) and 20 μg of total protein was analyzed by immunoblot.

Purification of recombinant proteins

GOF p53 mutants were generated by site-directed mutagenesis (Agilent Technologies). Wild-type and GOF p53 mutants were expressed in bacteria and purified on M2 agarose (Sigma). The p65 protein, which was kindly provided by Gourisankar Ghosh (UC San Diego) was purified on Ni-NTA beads (Qiagen) and Superdex 200 (GE Healthcare) columns following expression from pFAST-BAC1 vector in Sf9 cells.

***In vitro* protein-binding assay**

For binding assays, excess His-tagged p65 protein was incubated with FLAG-tagged p53 proteins in binding buffer (150 mM NaCl, 20 mM Hepes at pH 7.9, 0.1% NP40) for 2 h at 4 °C. The protein complexes were then incubated with M2 agarose for 30 min at 4 °C. Beads were washed five times with wash buffer (20 mM Tris-HCl at pH 7.9, 20% glycerol, 0.1 mM EDTA, 150 mM KCl, 0.1% NP40). Bound proteins were eluted in sample buffer and analyzed by immunoblot.

Co-immunoprecipitation

For co-immunoprecipitation assays, SW480 cells were treated with 12.5 ng ml^{-1} TNF-α for 0 or 16 h, crosslinked in 1% formaldehyde (Sigma), harvested, and washed with PBS. The cell pellet was resuspended in RIPA lysis buffer (50 mM Tris-HCl at pH 7.9, 150 mM NaCl, 1% NP40, 0.1% SDS, 0.5% Na-deoxycholate), supplemented with protease inhibitor cocktail (Sigma) and incubated on ice for 30 min before isolating the nuclear pellet by centrifugation at 4 °C. The pellet was then further lysed by resuspension in hypotonic buffer (20 mM Hepes at pH 7.9, 1.5 mM MgCl2, 20 mM KCl, 25% glycerol) and high-salt buffer (20 mM Hepes at pH 7.9, 1.5 mM MgCl2, 800 mM KCl, 25% glycerol, 1% NP40) followed by rotation at 4 °C. Lysates were cleared by centrifugation and incubated with indicated antibodies for 2 h at 4 °C. After an additional 2 h incubation with Protein A Sepharose (Rockland Inc.), beads were washed with wash buffer (20 mM Tris-HCl at pH 7.9, 20% glycerol, 0.1 mM EDTA, 150 mM KCl, 0.1% NP40) five times and analyzed by immunoblotting.

RNA-seq analysis

Total RNA was extracted with TRIzol LS reagent from SW480- expressing short hairpin RNA against either LacZ or p53, treated with 12.5 ng ml^{-1} TNF-α for 0 or 16 h. Strand-specific libraries from two biological replicates were generated from 1 μg total RNA, following the dUTP second strand cDNA method(Borodina, Adjaye and Sultan 2011). Briefly, RNA Isolation was subjected to two consecutive rounds of oligo (dT) enrichment using magnetic beads (New England Biolabs) followed by fragmentation. Isolated RNA species were then used for First-Strand cDNA Synthesis using SuperScript III in the presence of Actinomycin D (Invitrogen). Strand specificity was maintained by second-Strand synthesis with dUTP. The ends on the double stranded DNA were then repaired, followed by the addition of the A-tail. Adaptor ligation was performed using NEXTflex barcodes (Bioo Scientific) and Uracil-DNA-Glycosylase (UDG) treatment was performed to selectively degrade the strand marked with dUTP. The remaining

strand was PCR amplified for nine cycles to generate a sequencing library. Final PCR products were then size selected to have an average size of 250 bp and purified using DNA Clean & Concentrator Kit (Zymo Research). DNA concentrations were determined using Qubit 2.0 fluorometer (Invitrogen) and pooled for sequencing. cDNA libraries were single-end sequenced (50 bp) on Illumina HiSeq 4000. Sequencing reads were mapped to hg38 human genome using STAR (Dobin et al. 2013). Gene expression levels were counted per gene model (not counting differentiated splices) and differential expression across samples were determined using edgeR (Robinson, McCarthy and Smyth 2010). Gene ontology enrichment (GO) analysis was performed using Metascape (Tripathi et al. 2015).

Chromatin immunoprecipitation

p53, RNAPII, and histone chromatin immunoprecipitation (ChIP) assays were performed using SW480, MDA-MB-231, or HCT116 cells that were (i) untreated or treated with 12.5 ng ml^{-1} TNF-α for the indicated time points or (ii) transfected with indicated siRNAs and treated with 12.5 ng ml^{-1} TNF-α for 0 or 16 h. Cells were reversibly cross-linked using a final concentration of 1% formaldehyde for 10 min at room temperature and quenched by adding glycine (Fisher Scientific) to a final concentration of 125 mM. In place of tip-sonication, isolated chromatin was fragmented to an average size of 200–600 bp with a biorupter Pico (Diagenode). Precleared chromatin was immunoprecipitated overnight at 4 °C and immunocomplexes were collected with Protein A agarose coupled with salmon sperm DNA (EMD Millipore) for 2 h at 4 °C. The immunocomplexes were washed and eluted, crosslinks were reversed at 65 °C for 4 h or overnight, and DNA was purified using DNA Clean & Concentrator Kit according to the manufacturer's instructions. qPCR was performed using ABI Real-Time PCR machine to measure the relative amounts of ChIP DNA and results were quantified relative to inputs as

detailed(Lauberth et al. 2007). The levels of H3K4me1 and H3K27ac were determined relative to the total H3 levels. Primer sets are listed in Supplementary Table 2.2.

p65 ChIP and ChIP-seq

For p65 ChIP-qPCR and all ChIP-seq assays (p53, p65, RNAPII, H3K4me1, and H3K27ac), 20–24 million cells were first crosslinked in 6 mM disuccinimidyl glutarate (ProteoChem) in PBS for 30 min, then subsequently in 1% formaldehyde in PBS for 10 min at room temperature. Crosslinking was then quenched by addition of glycine to a final concentration of 125 mM. Cells were then resuspended in lysis buffer (20 mM Tris-HCl pH 7.5, 300 mM NaCl, 2 mM EDTA, 0.5% NP40, 1% Triton X-100) and incubated on ice for 30 min. The resuspended cells were then transferred to an ice-cold homogenizer and dounced for 10 strokes. Nuclei were collected and resuspended in shearing buffer (0.1% SDS, 0.5% N-lauroylsarcosine, 1% Triton X-100, 10mM Tris-HCl pH 8.1, 100mM NaCl, 1 mM EDTA) and the isolated chromatin was fragmented to an average size of 200–600 bp with biorupter Pico sonicator. Immunocomplexes were collected from 65 µg of sheared chromatin with Protein A Dynabeads (Invitrogen) overnight at 4 °C. Following the overnight incubation, immunocomplexes bound to Dynabeads were resuspended in wash buffer (50 mM Hepes at pH 7.6, 500 mM LiCl, 1 mM EDTA, 1% NP40, 0.7% Na-deoxycholate). The beads were washed eight times followed by two additional TE (1× TE at pH 8, 50mM NaCl) washes. The immunocomplexes were eluted in elution buffer (50 mM Tris-HCl at pH 8, 10 mM EDTA, 1% SDS) and the crosslinks were reversed overnight at 65 °C. Samples were subsequently treated with RNase A at 37 °C for 1 h and 0.2 μg ml^{-1} proteinase K for 2 h. The ChIP DNA was isolated using the DNA Clean & Concentrator Kit according to manufacturer's instructions. qPCR was performed to measure the relative amounts of ChIP DNA and results were quantified relative to inputs as detailed (Lauberth et al. 2007).

Sequential ChIP experiments were performed exactly as described above with

minor modifications. Specifically, 150 µg of sheared chromatin was used to perform the IP. Following the washes after the first IP, immunocomplexes were eluted in re-IP elution buffer (50 mM Tris-HCl at pH 8, 1% SDS, 1 mM EDTA, 1 mM DTT), diluted 10-fold in dilution buffer (16.7 mM Tris-HCl at pH 8, 167 mM NaCl, 0.01% SDS, 1% Triton X-100, 1.2 mM EDTA), and incubated with the second IP antibodies overnight at 4 °C, followed by additional washes and the final elution as described above.

For ChIP-seq experiments, the IP's were performed as described above and the eluted ChIP DNA was quantified using a Qubit 2.0 fluorometer, and 2–5ng of ChIP DNA was used to prepare the sequencing libraries from two biological replicates using the TruSeq ChIP Sample Prep Kit according to the manufacturer's instructions (Illumina). Briefly, ChIP DNA was end-repaired and Illumina TruSeq adaptors were ligated to the ends of the ChIP fragments. Adaptor-ligated ChIP DNA fragments with average size of 350 bp were used to construct libraries according to Illumina's specifications. Prepared libraries were single-end sequenced (50 bp) on Illumina HiSeq 4000. Sequencing reads were mapped to the hg38 human genome using Bowtie2 software (Langmead and Salzberg 2012) and default parameters. The mapped reads were then processed to make TagDirectory module using HOMER(Heinz et al. 2010) for filtering. Briefly, PCR duplications were removed and only uniquely mapped reads were kept for further analysis. The genome browser files for the resulting reads were generated by using makeUCSCfile module from HOMER. Enriched regions for p65 or histone-modification deposition were called using findPeaks module from HOMER by using preset options, factor or histone styles, respectively, and compared with the corresponding inputs. For p53 R273H peak calling, p53-enriched regions were first generated by HOMER in comparison to corresponding inputs. The resulting regions were split into subpeaks using PeakSplitter (http://www.ebi.ac.uk/research/bertone/software). For the identification of mutp53 and p65 peak colocalization, p65 peaks were first divided into two groups with and without uninduced mutp53

binding by using the co-bound option of the mergePeak module from HOMER. Induced mutp53 peaks that were co-bound with p65 with and without 0 h p53 peaks identified in the previous step were defined as maintained and gained p53 peaks. Deeptools were used to generate heat maps(Ramírez et al. 2016). De novo motif analysis was performed from the top peaks, which were rank-ordered by the intensity of mutp53 and NFκB/p65 peaks and grouped as described above for defining maintained and gained mutp53 peaks using "findMotifsGenome.pl" of Homer with ±100 bp window relative to the peak center. Putative motif loci of motifs from each category (gained versus maintained) were extracted from merged mutp53 and NFκB peaks with de novo motifs using "annotatePeaks.pl". The length of the motifs was adjusted and merged to one bed file using "intersectBed", and motif consensus sequence logos were generated by the "seqLogo" package of R.

Global run on-seq

Global run-on reactions were performed using SW480 cells treated with 12.5 ng ml^{-1} TNF-α for 0 or 16 h. 5 million nuclei in 100 μl freezing buffer (40% glycerol, 5 mM MgCl2, 0.1 mM EDTA, 50 mM Tris-HCl pH 7.8) were run on by addition of 50 μl NRO-reaction buffer (15 mM Tris-HCl pH 8, 500 mM KCl, 7.5 mM MgCl2, 1.5% Sarkosyl, 1.5 mM DTT, 0.2 U ml^{-1} SUPERase-in (ThermoFisher Scientific), 375 μM ATP, 375 μM GTP, 0.6 μM CTP, 375 μM BrUTP (Sigma) for 5 min at 30 °C. Reactions were stopped by addition of 750 μl TRIzol LS and purified following manufacturer's instructions. RNA was fragmented in 10 mM Tris-HCl pH 7.5, 10mM $ZnCl_2$, 0.05% Tween 20 at 70 °C for 15 min and stopped by addition of 2× EDTA. For nascent RNA enrichment, fragmented RNA samples were incubated with 50 μl equilibrated Anti-BrdU agarose beads (Santa Cruz Biotechnology) in 500 μl GRO-binding buffer (0.25× SSPE, 0.05% Tween, 37.5 mM NaCl, 1 mM EDTA) at 4 °C for 1 h under gentle rotation. Anti-BrdU beads were equilibrated by washing once with GRO- binding buffer, followed by one wash with

binding buffer with 500 mM NaCl and two consecutives washes with GRO-binding buffer. Following the IP, beads were transferred to Ultrafree MC column (EMD Millipore) and spun at 1000 rcf for 30 s. Flow through was discarded and beads were washed three times with GRO-binding buffer for 5 min. The columns were then moved to fresh tubes and RNA samples were eluted twice with 200 μl TRIzol LS under gentle shaking for 3–5 min. RNA repair and libraries were prepared from two biological replicates. Libraries were amplified for 12 cycles, size selected for 165–215 bp, and sequenced on Illumina HiSeq 4000. Reads were then mapped to hg38 genome using bowtie2. Only uniquely mapped reads were kept and at most three reads at each unique genomic position. GRO-seq reads were counted 1000 bp around specified transcription factors peaks and normalized to 10 million total reads using default setting of annotatePeaks module of HOMER. Five reads (RPKM > 0.5) were used as the threshold for defining significant eRNA synthesis.

2.6 Data availability

All sequencing data that support the findings of this study have been deposited in the National Center for Biotechnology Information Gene Expression Omnibus (GEO) and are accessible through GEO Series Accession Number GSE102796. All other relevant data are available from the corresponding author upon reasonable request.

2.7 Author contributions

Conceptualization: H.R., H.L., and S.M.L.; methodology: H.R., H.L., and S.M.L.; investigation: H.R., H.L., and S.H.D; formal analysis: H.R., H.L., S.M.L., and C.B.; writing—original draft: S.M.L. and H.R.; writing—review and editing: S.M.L., H.R., and C.K.G.; funding acquisition: S.M.L.; supervision: S.M.L.

2.8 Figures

Figure 2.1. Mutp53 regulates chronic TNF-α induction of protumorgenic genes. (a) qRT-PCR (top) and immunoblot (bottom) analyses of SW480 cells induced to express LacZ (control) or p53 (p53) shRNA and treated with TNF-α for 0 or 16 hr. The expression levels following TNF-α treatment are relative to the levels before TNF-α exposure. The bar graph represents the average of three independent experiments with the error bars denoting the standard error. **(b)** Venn diagram depicting the number of genes affected by mutp53 depletion in SW480 cells treated as described in (a). Genes were sorted prior to (green, 0 hr) or after (pink, 16 hr) TNF-α treatment (FDR <0.05). **(c)** Gene Ontology analysis using Metascape of the 772 mutp53 regulated genes upon 16 hr TNF-α treatment, corresponding to the pink only portion of the Venn diagram in (b). **(d)** Heat map of the differentially expressed RefSeq genes induced by 2-fold or higher (FDR <0.05) after TNF-α induction in the control relative to the mutp53 knockdown cells. **(e)** qRT-PCR analyses of mutp53 target genes (left) and known wild-type p53 target genes (right) in control and p53 shRNA SW480 cells that were treated with TNF-α for 0 or 16 hr. The expression levels shown after TNF-α are relative to the levels before treatment. The bar graph represents the average of three independent experiments with the error bars denoting the standard error. **(f)** Representative images (left) and quantitation (right) of invasion assays performed with SW480 cells treated as described in (a) that were fixed and detected by Giemsa staining (scale bar: 0.2 mm). The bar graph represents the average number of cells invaded through the Matrigel-coated membrane from three independent experiments with the error bars denoting the standard error.

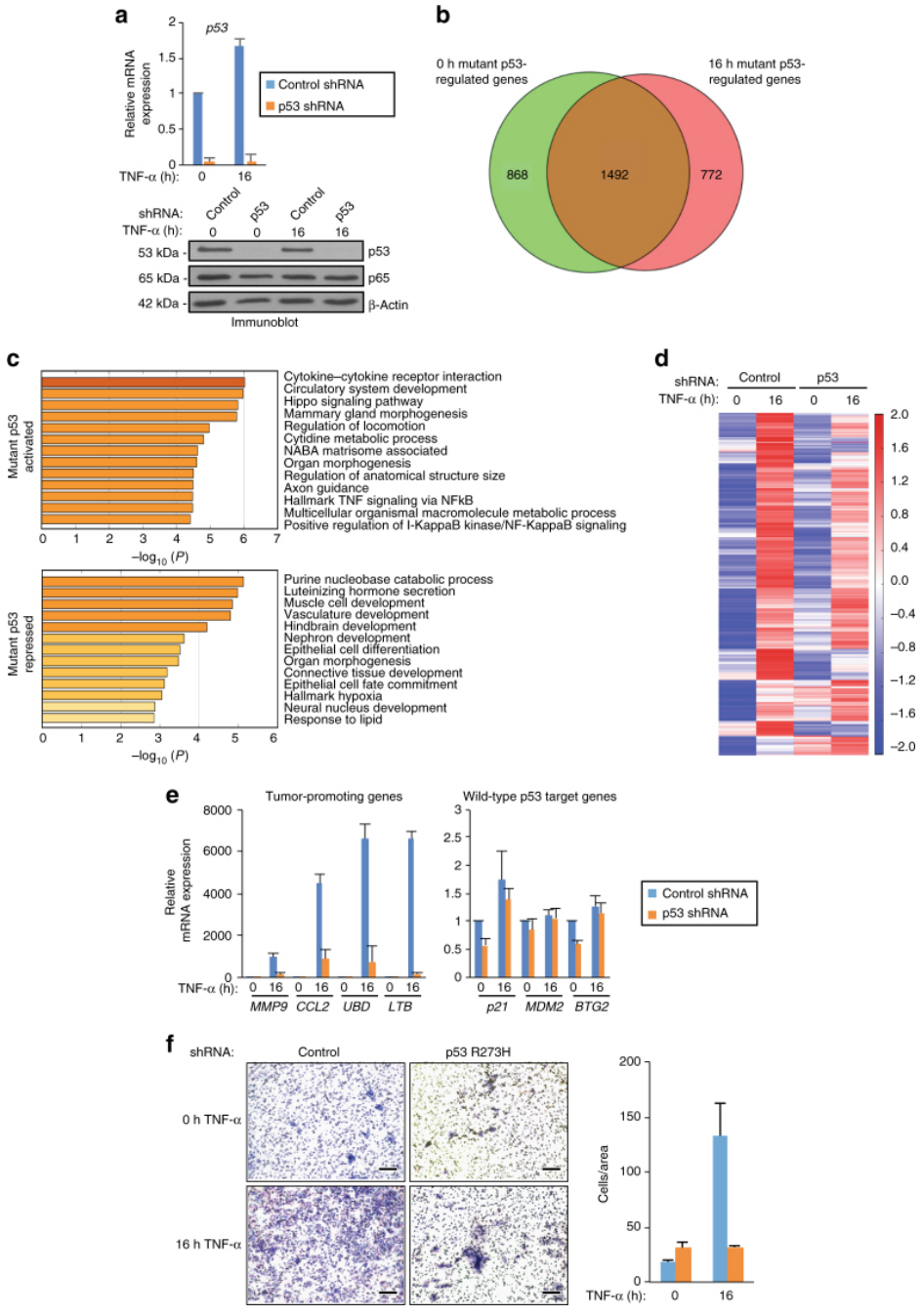
a
p53
Relative mRNA expression
Control shRNA
p53 shRNA
TNF-α (h): 0 16
shRNA: Control p53 Control p53
TNF-α (h): 0 0 16 16
53 kDa
65 kDa
42 kDa
p53
p65
β-Actin
Immunoblot
b
0 h mutant p53-regulated genes
16 h mutant p53-regulated genes
868
1492
772
c
Mutant p53 activated
Cytokine–cytokine receptor interaction
Circulatory system development
Hippo signaling pathway
Mammary gland morphogenesis
Regulation of locomotion
Cytidine metabolic process
NABA matrisome associated
Organ morphogenesis
Regulation of anatomical structure size
Axon guidance
Hallmark TNF signaling via NFkB
Multicellular organismal macromolecule metabolic process
Positive regulation of I-KappaB kinase/NF-KappaB signaling
–log10 (P)
Mutant p53 repressed
Purine nucleobase catabolic process
Luteinizing hormone secretion
Muscle cell development
Vasculature development
Hindbrain development
Nephron development
Epithelial cell differentiation
Organ morphogenesis
Connective tissue development
Epithelial cell fate commitment
Hallmark hypoxia
Neural nucleus development
Response to lipid
–log10 (P)
d
shRNA: Control p53
TNF-α (h): 0 16 0 16
e
Tumor-promoting genes
Wild-type p53 target genes
Relative mRNA expression
Control shRNA
p53 shRNA
TNF-α (h): 0 16 0 16 0 16 0 16
MMP9 CCL2 UBD LTB
p21 MDM2 BTG2
f
shRNA: Control p53 R273H
0 h TNF-α
16 h TNF-α
Cells/area
TNF-α (h): 0 16

Figure 2.2. chronic TNF-α signaling alters mutp53 and NFκB binding in colon cancer cells. (a) Heat maps of p53 R273H and NFκB/p65 ChIP-seq reads in SW480 cells treated with TNF-α for 0 or 16 hr. Each row shows ±2 kb centered on p65 peaks, rank-ordered by the intensity of mutp53 and NFκB/p65 peaks and grouped by gained versus maintained mutp53 peaks. **(b)** *De novo* motif analyses of the TNF-gained and maintained mutp53 overlapping NFκB/p65 binding sites as noted in (a). **(c)** UCSC genome browser tracks of ChIP-seq signals for p53 R273H, NFκB/p65, H3K27ac, and H3K4me1 at the *MMP9, CCL2, CYP24A1,* and *CPA4* gene loci in untreated (purple) or TNF-α 16 hr (pink) treated SW480 cells. The y-axis depicts the ChIP-seq signal and the x-axis locates the genomic position with the enhancer regions highlighted in yellow. **(d)** Schematics of ChIP-qPCR amplicons and ChIP analyses with the indicated antibodies at the enhancers and nonspecific regions of *MMP9, CCL2, CYP24A1,* and *CPA4* gene loci. ChIP-qPCR amplicons were designed to amplify the enhancer (A and B at *MMP9* and A at *CCL2*, *CYP24A1*, and *CPA4*) or nonspecific (C at *MMP9* and B at *CCL2*, *CYP24A1*, and *CPA4*) regions of the target gene loci. ChIP experiments were performed using SW480 cells treated with TNF-α for 0, 8, 16, and 32 hr. ChIPs for histone marks were normalized to H3. An average of two independent ChIP experiments that are representative of at least three is shown with error bars denoting the standard error. **(e)** Sequential ChIP (re-ChIP) with p53 antibody followed by IgG (control) and NFκB/p65 antibody performed in SW480 cells treated with TNF-α for 16 hr. The ChIP-qPCR amplicons are identical to those used in (d). An average of two independent re-ChIP experiments that are representative of at least three is shown with error bars denoting the standard error.

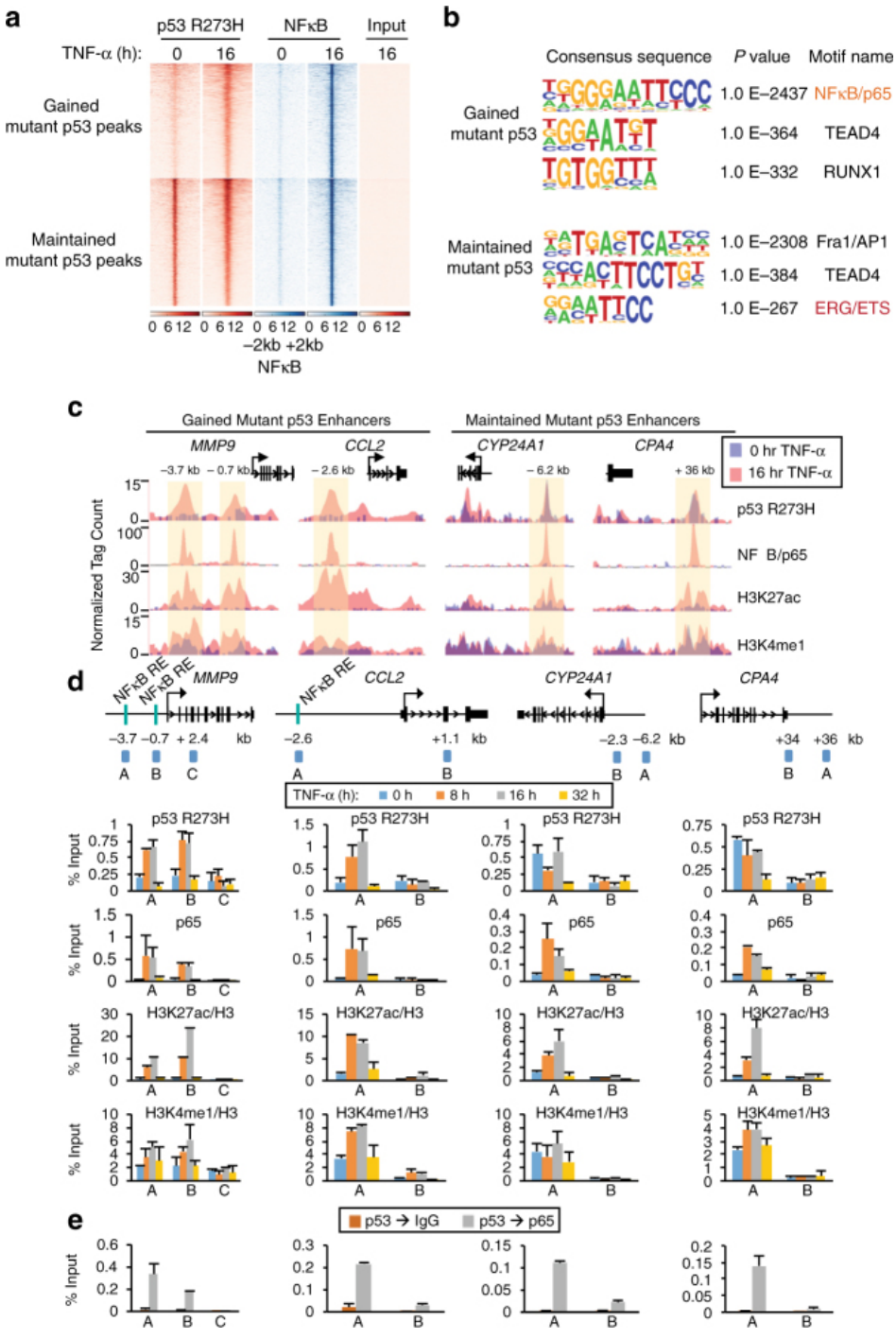
a
p53 R273H
NFκB
Input
TNF-α (h):
0
16
0
16
16
Gained mutant p53 peaks
Maintained mutant p53 peaks
0 6 12 0 6 12 0 6 12 0 6 12 0 6 12
−2kb +2kb
NFκB
b
Consensus sequence
P value
Motif name
Gained mutant p53
1.0 E−2437 NFκB/p65
1.0 E−364 TEAD4
1.0 E−332 RUNX1
Maintained mutant p53
1.0 E−2308 Fra1/AP1
1.0 E−384 TEAD4
1.0 E−267 ERG/ETS
c
Gained Mutant p53 Enhancers
Maintained Mutant p53 Enhancers
MMP9
CCL2
CYP24A1
CPA4
−3.7 kb
−0.7 kb
−2.6 kb
−6.2 kb
+36 kb
0 hr TNF-α
16 hr TNF-α
Normalized Tag Count
p53 R273H
NF B/p65
H3K27ac
H3K4me1
d
NFκB RE
NFκB RE
MMP9
NFκB RE
CCL2
CYP24A1
CPA4
−3.7 −0.7 + 2.4 kb
−2.6
+1.1 kb
−2.3 −6.2 kb
+34 +36 kb
A B C
A B
B A
B A
TNF-α (h): 0 h 8 h 16 h 32 h
p53 R273H
p65
H3K27ac/H3
H3K4me1/H3
% Input
e
p53 → IgG
p53 → p65
% Input

Figure 2.3. Mutp53 and NFκB interact and impact each other's binding at enhancers. **(a)** Purified Wild-type and mutp53 proteins bind directly to purified NFκB/p65 as revealed by immunoblot analysis with an antibody that recognizes p65. Input samples for the p53 proteins were also analyzed by immunoblot analysis with an antibody that recognizes both wild-type and mutp53. Three independent interaction assays were performed. **(b)** ChIP-qPCR analyses of NFκB/p65 and p53 R273H at the enhancer (A and B at *MMP9* and A at *CCL2*, *CYP24A1*, and *CPA4*) or nonspecific (C at *MMP9* and B at *CCL2*, *CYP24A1*, and *CPA4*) regions of the target gene loci in SW480 cells transfected with non-targeting control or p65 siRNA and following TNF-α treatment for 0 or 16 hr. **(c)** ChIP-qPCR analyses of p53 R273H and NFκB/p65 binding at identical genomic regions examined in (b). The SW480 cells were induced to express LacZ (control) or p53 (p53) shRNA and treated with TNF-α for 0 or 16 hr. For both ChIP experiments, an average of two independent experiments that are representative of at least three is shown with error bars denoting the standard error.

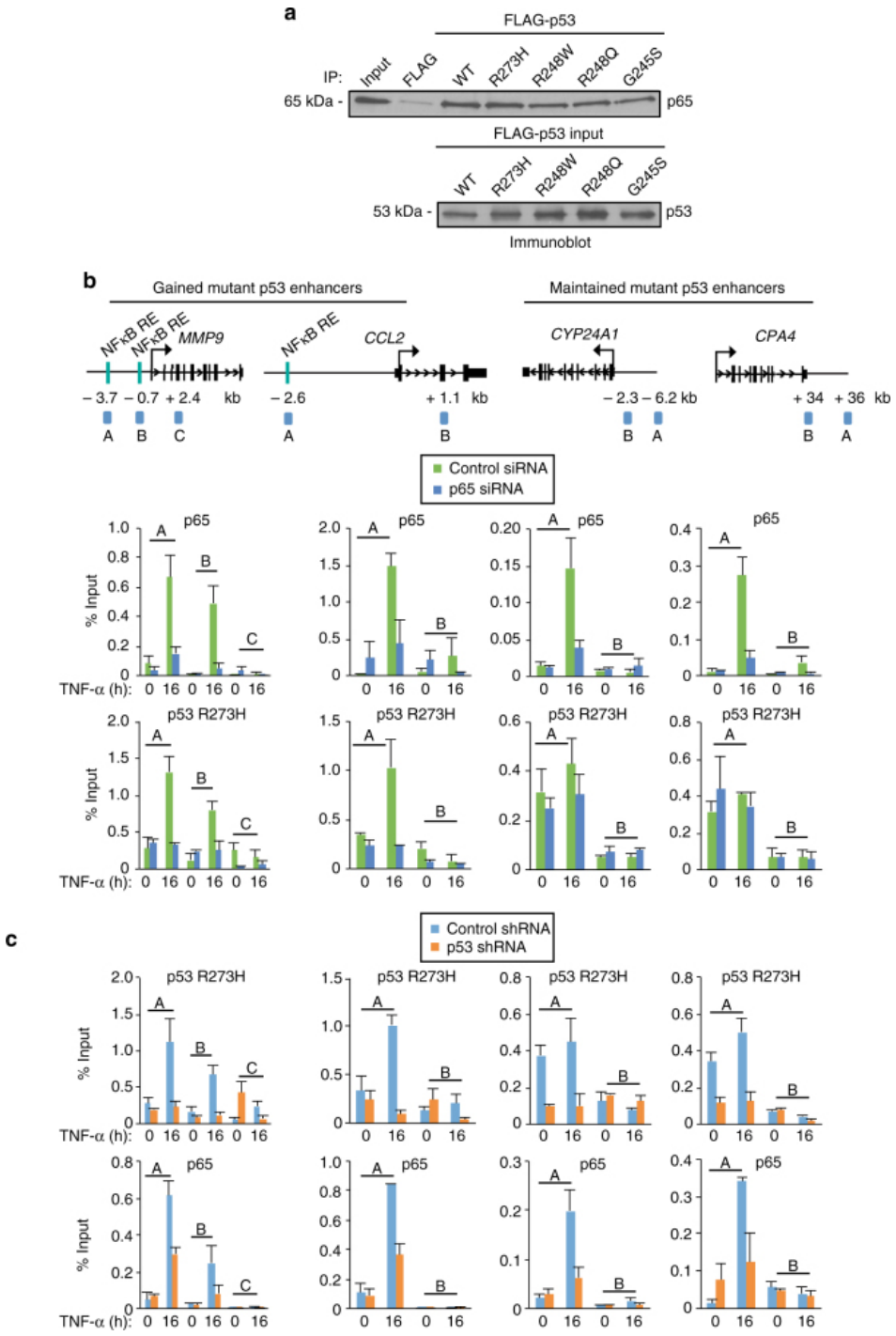
a
FLAG-p53
IP:
Input
FLAG
WT
R273H
R248W
R248Q
G245S
65 kDa -
p65
FLAG-p53 input
WT
R273H
R248W
R248Q
G245S
53 kDa -
p53
Immunoblot
b
Gained mutant p53 enhancers
Maintained mutant p53 enhancers
NFκB RE
NFκB RE
MMP9
NFκB RE
CCL2
CYP24A1
CPA4
– 3.7 – 0.7 + 2.4 kb
– 2.6
+ 1.1 kb
– 2.3 – 6.2 kb
+ 34 + 36 kb
A B C
A
B
B A
B A
Control siRNA
p65 siRNA
p65
p53 R273H
% Input
TNF-α (h): 0 16 0 16 0 16
c
Control shRNA
p53 shRNA
p53 R273H
p65
% Input
TNF-α (h): 0 16 0 16 0 16

Figure 2.4. Mutp53 enhancer binding is positively correlated with enhancer transcription. **(a)** UCSC genome browser images for *MMP9* and *CPA4* gene loci showing the ChIP-seq signal for mutp53 binding and GRO-seq peaks with the enhancer regions highlighted in yellow. **(b)** Boxplots showing $\log_2$ fold change in response to TNF-α in GRO-seq signal of nascent transcripts centered upon intergenic gained or maintained mutp53 peaks that overlap with NFκB and H3K27ac peaks. **(c)** Analyses of **(left)** GRO-seq reads per bp per intergenic ChIP-seq peaks of mutp53 and NFκB/p65, as indicated, and **(right)** GRO-seq reads per bp per TSS at promoters closest to intergenic ChIP-seq peaks defined in the left panel. **(d)** qRT-PCR analyses of the indicated eRNAs and mRNAs in SW480 cells and **(e)** HCT116 cells treated with TNF-α for 0, 8 or 16 hr. The expression levels shown after TNF-α treatment are relative to the levels before treatment. The bar graphs represent the average of three independent experiments with the error bars denoting the standard error.

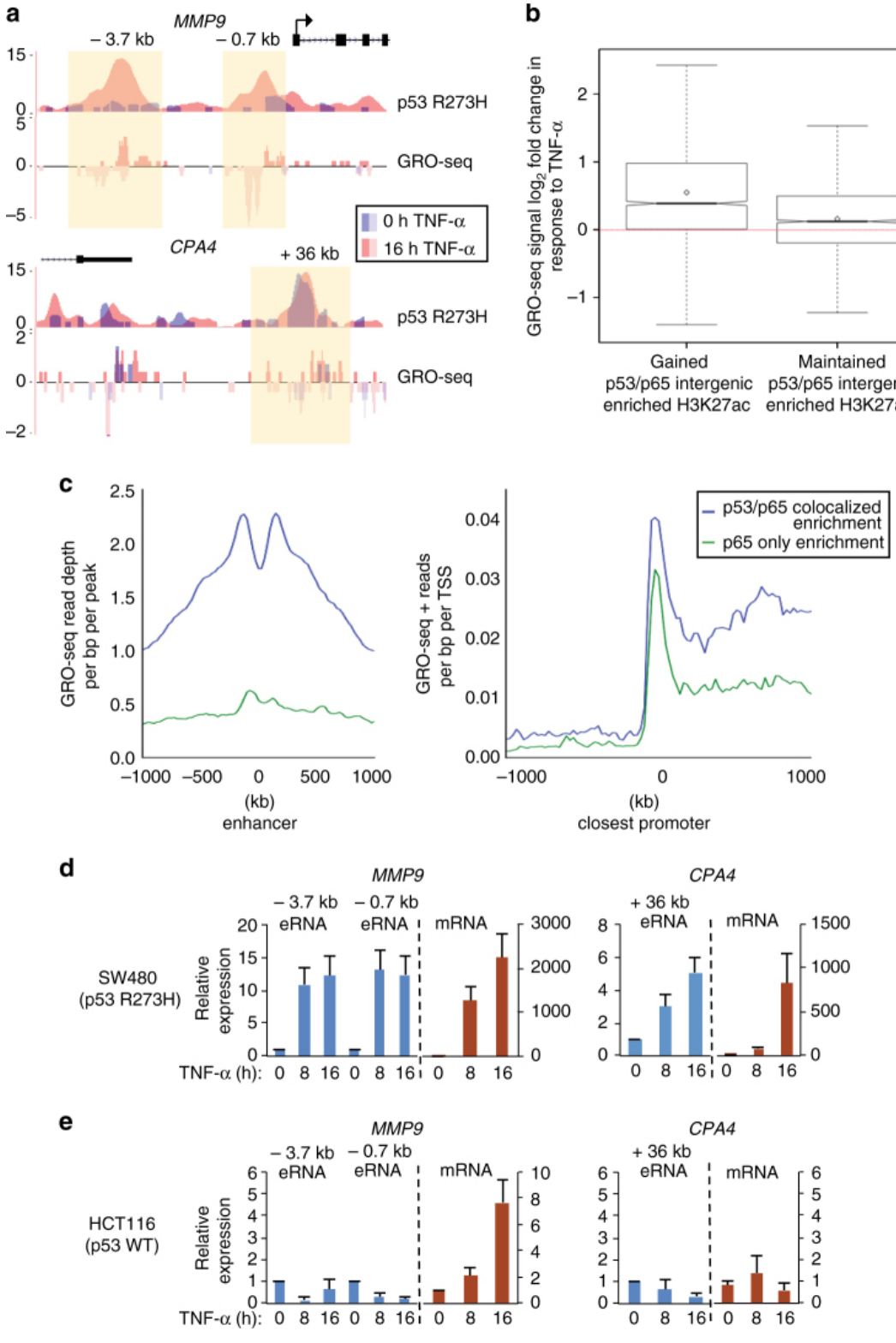
a
MMP9
– 3.7 kb
– 0.7 kb
p53 R273H
GRO-seq
0 h TNF-α
16 h TNF-α
CPA4
+ 36 kb
b
GRO-seq signal log2 fold change in response to TNF-α
Gained p53/p65 intergenic enriched H3K27ac
Maintained p53/p65 intergenic enriched H3K27ac
c
GRO-seq read depth per bp per peak
(kb) enhancer
GRO-seq + reads per bp per TSS
p53/p65 colocalized enrichment
p65 only enrichment
(kb) closest promoter
d
MMP9
CPA4
eRNA
mRNA
SW480 (p53 R273H)
Relative expression
TNF-α (h):
e
HCT116 (p53 WT)

Figure 2.5. Mutp53 regulates RNAPII recruitment and enhancer transcription. (a) RNAPII ChIP-seq peaks overlapping with mutp53 peaks following 16 hr TNF-α treatment. **(b)** ChIP-qPCR analyses of p53 R273H and RNAPII enrichment at *MMP9, CCL2, CYP24A1,* and *CPA4* enhancers in SW480 cells expressing control (LacZ) or p53 shRNA and treated with TNF-α for 0 or 16 hr. An average of two independent ChIP experiments that are representative of at least three is shown with error bars denoting the standard error. The amplicons used for ChIP-qPCR are shown in the schematics and were designed to recognize the enhancer (A and B at *MMP9* and A at *CCL2*, *CYP24A1*, and *CPA4*) or nonspecific (C at *MMP9* and B at *CCL2*, *CYP24A1*, and *CPA4*) regions of the target gene loci. **(c)** qRT-PCR analyses of the indicated eRNAs and mRNAs in SW480 cells treated as described in (b). The expression levels shown after TNF-α treatment are relative to the levels before treatment. The bar graphs represent the average of three independent experiments with the error bars denoting the standard error.

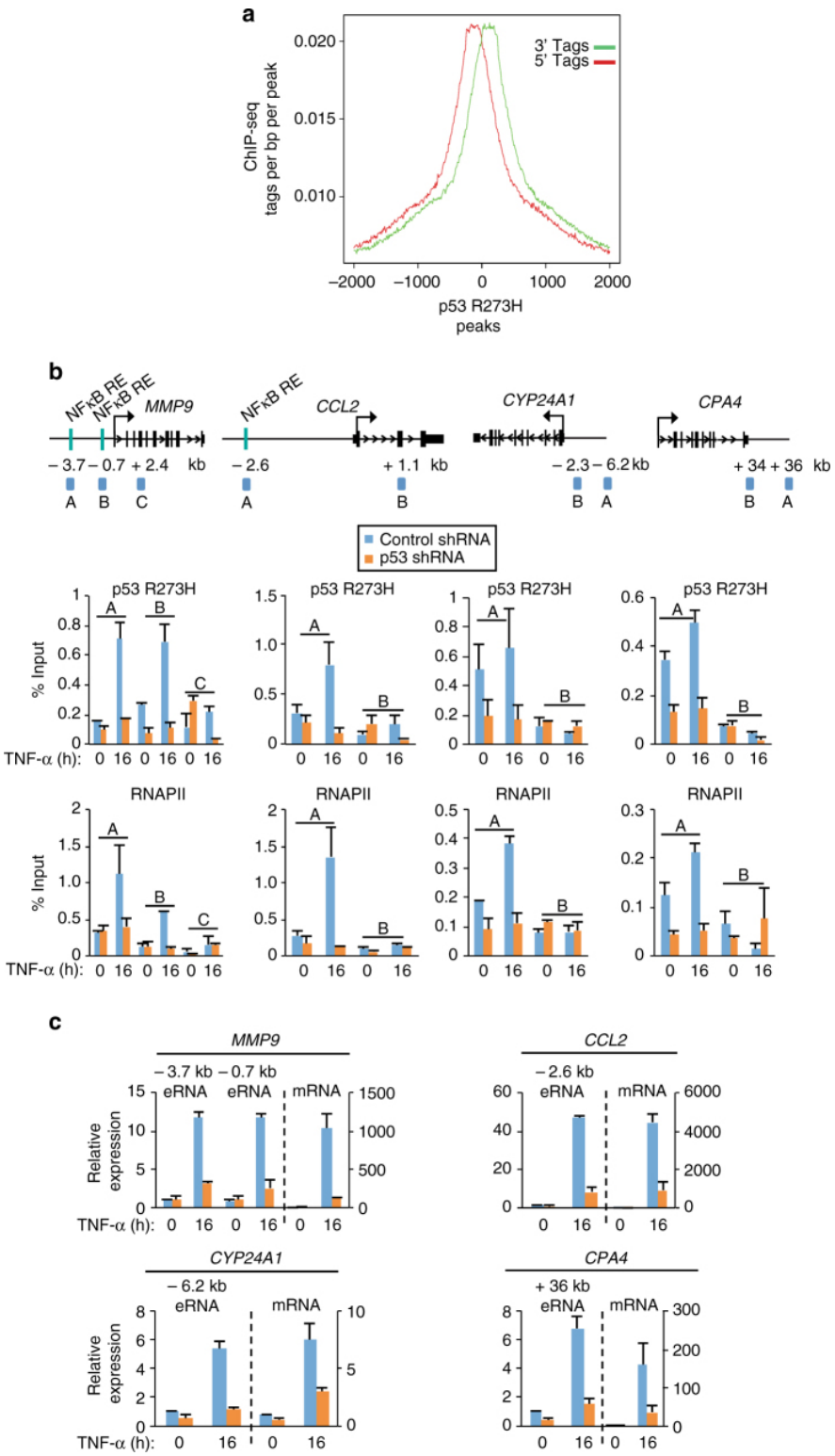
a
ChIP-seq tags per bp per peak
0.020
0.015
0.010
3' Tags
5' Tags
−2000 −1000 0 1000 2000
p53 R273H peaks
b
NFκB RE
NFκB RE
MMP9
NFκB RE
CCL2
CYP24A1
CPA4
− 3.7 − 0.7 + 2.4 kb
− 2.6
+ 1.1 kb
− 2.3 − 6.2 kb
+ 34 + 36 kb
A B C
A
B
B A
B A
Control shRNA
p53 shRNA
p53 R273H
% Input
TNF-α (h): 0 16 0 16 0 16
RNAPII
c
MMP9
− 3.7 kb − 0.7 kb
eRNA eRNA mRNA
CCL2
− 2.6 kb
CYP24A1
− 6.2 kb
CPA4
+ 36 kb
Relative expression

Figure 2.6. Mutp53 enhancer and gene activation in human colon tissues. (a) qRT-PCR analysis of *MMP9* eRNA from the -3.7 kb enhancer and mRNA expression levels from five independent cases of paired non-neoplastic (NT) and colorectal carcinomas (CRC) expressing wild-type and mutant forms of p53, respectively. mRNA expression levels of NT and CRC samples were normalized to β-Actin levels. The expression levels shown for each CRC sample is relative to the expression levels of its corresponding NT sample. **(b)** Proposed model in which mutp53 through interactions with NFκB directs enhanced RNAPII recruitment that is required for the potent induction of enhancer transcription and pro-tumorigenic gene expression in response to chronic TNF signaling. The contributions of wild-type p53 were also examined in this study and are included in our model to show that the TNF-α-induced changes in gene expression are mutp53-dependent since wild-type p53 is neither recruited to the mutp53 bound enhancer regions, nor regulates enhancer activation and gene induction.

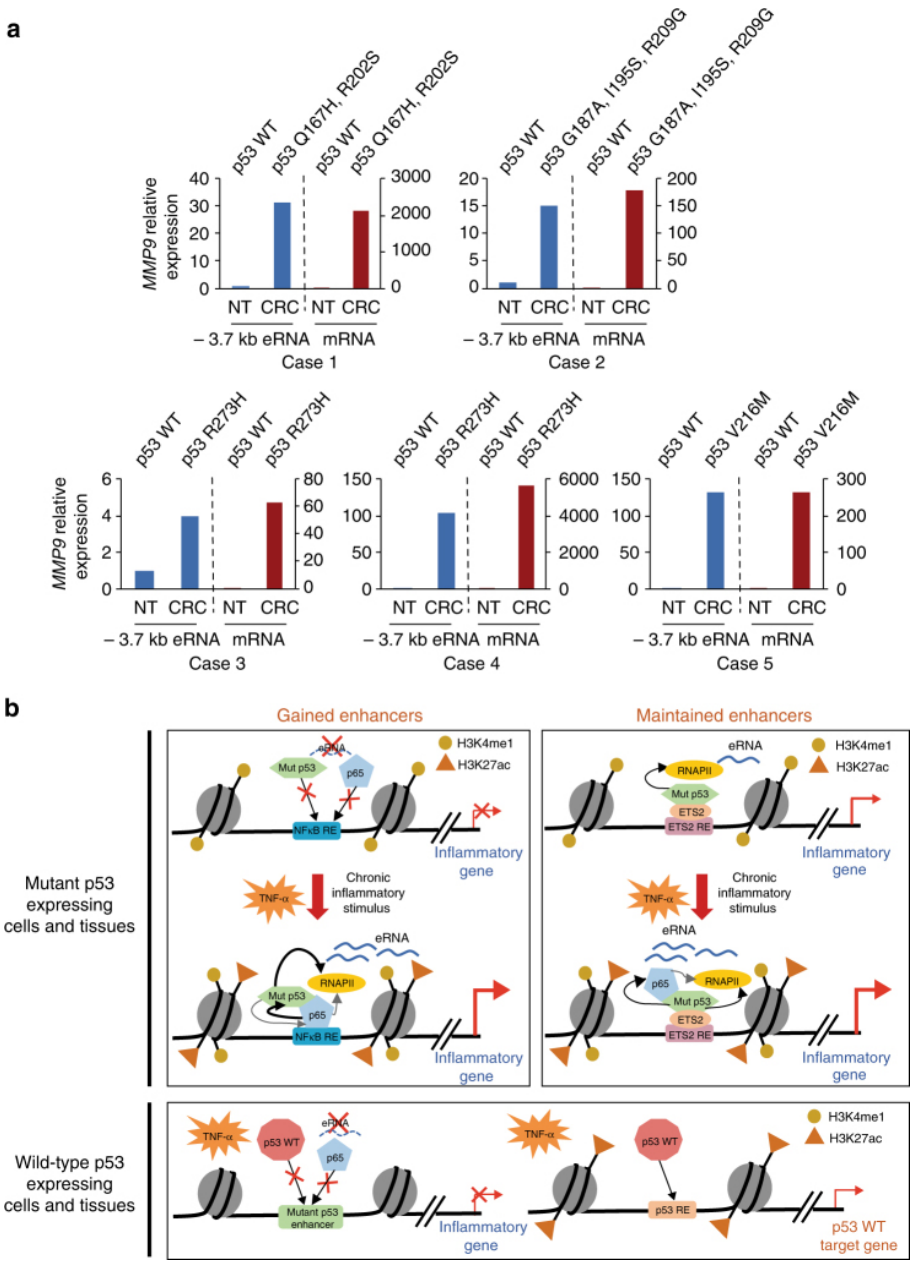
a
MMP9 relative expression
p53 WT
p53 Q167H, R202S
p53 G187A, I195S, R209G
p53 R273H
p53 V216M
NT CRC NT CRC
– 3.7 kb eRNA mRNA
Case 1
Case 2
Case 3
Case 4
Case 5
b
Gained enhancers
Maintained enhancers
Mutant p53 expressing cells and tissues
Wild-type p53 expressing cells and tissues
H3K4me1
H3K27ac
eRNA
Mut p53
p65
NFκB RE
RNAPII
ETS2
ETS2 RE
TNF-α
Chronic inflammatory stimulus
Inflammatory gene
p53 WT
Mutant p53 enhancer
p53 RE
p53 WT target gene

2.9 Supplemental information

2.9.1 Supplemental figures

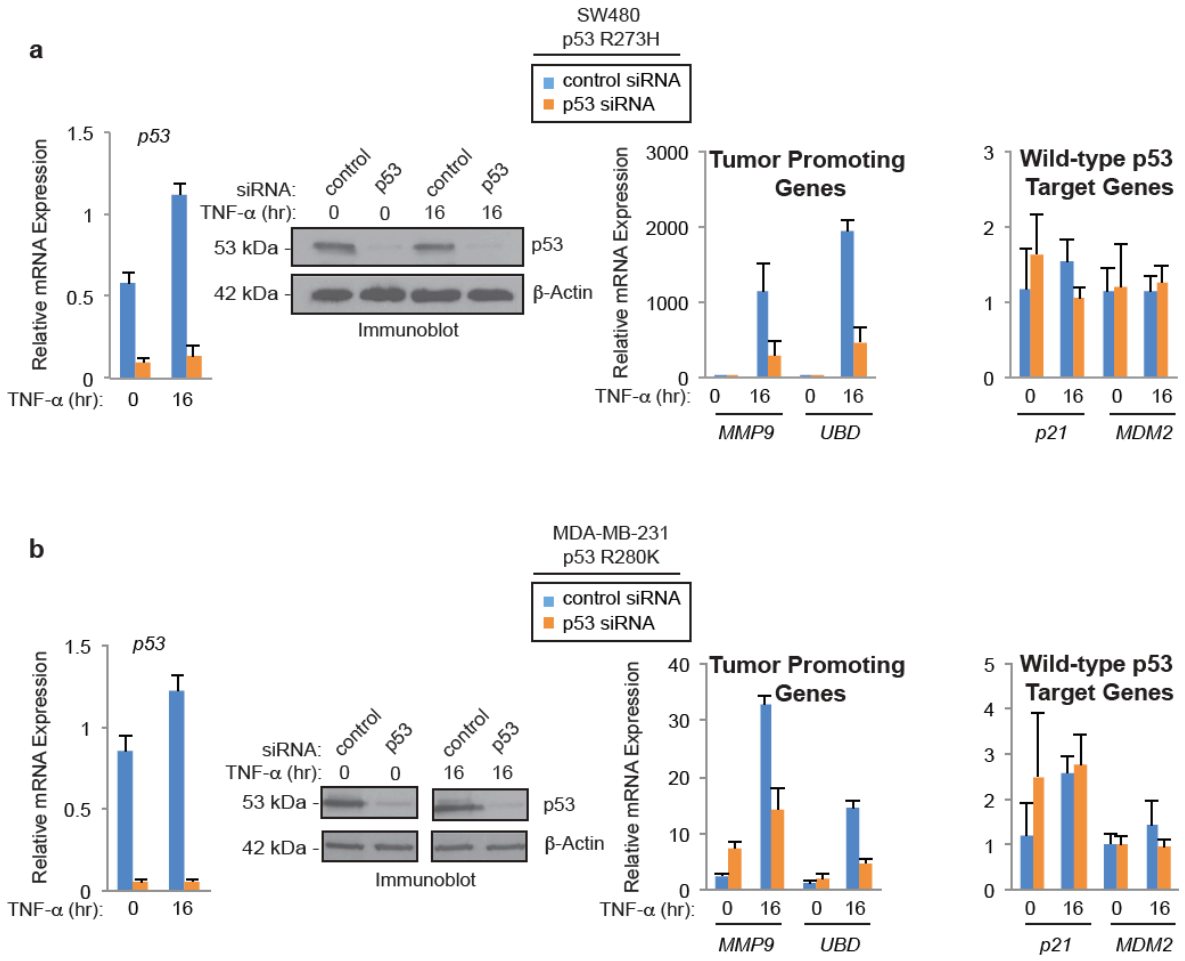

Figure 2.7. Mutp53 knockdown disrupts TNF-α-induced gene expression in colon and breast cancer cells. (Left) qRT-PCR and immunoblot analysis of **(a)** SW480 cells or **(b)** MDA-MB-231 cells transfected with nonspecific control or p53 siRNAs and treated with TNF-α for 0 or 16 hr. **(Right)** qRT-PCR analyses to examine the relative mRNA expression levels of mutp53 and wild-type p53 target genes in SW480 and MDA-MB-231 cells treated as described above. The expression levels upon TNF-α treatment are relative to the levels before treatment. The bar graphs represent the average of three independent experiments with the error bars denoting the standard error.

Figure 2.8. p53 and NFκB binding upon chronic TNF-α signaling in mutp53 expressing breast and wild-type p53 expressing colon cancer cells. (a) Venn diagram showing the overlap of NFκB/p65 with the gained or maintained mutp53 binding sites after 16 hr TNF-α. **(b)** ChIP analyses with the indicated antibodies were performed using MDA-MB-231 (p53 R280K) or **(c)** HCT116 (p53 WT) cells that were treated with TNF-α for 0 or 16 hr. The amplicons used for ChIP-qPCR are represented in the schematics of the target gene loci. Also, the amplicon for the wild-type p53 target gene, p21 was designed to amplify the region of p21 that overlaps with a wild-type p53 response element. ChIPs for H3K27ac were normalized to H3. An average of two independent ChIP experiments that are representative of at least three is shown with error bars denoting the standard error.

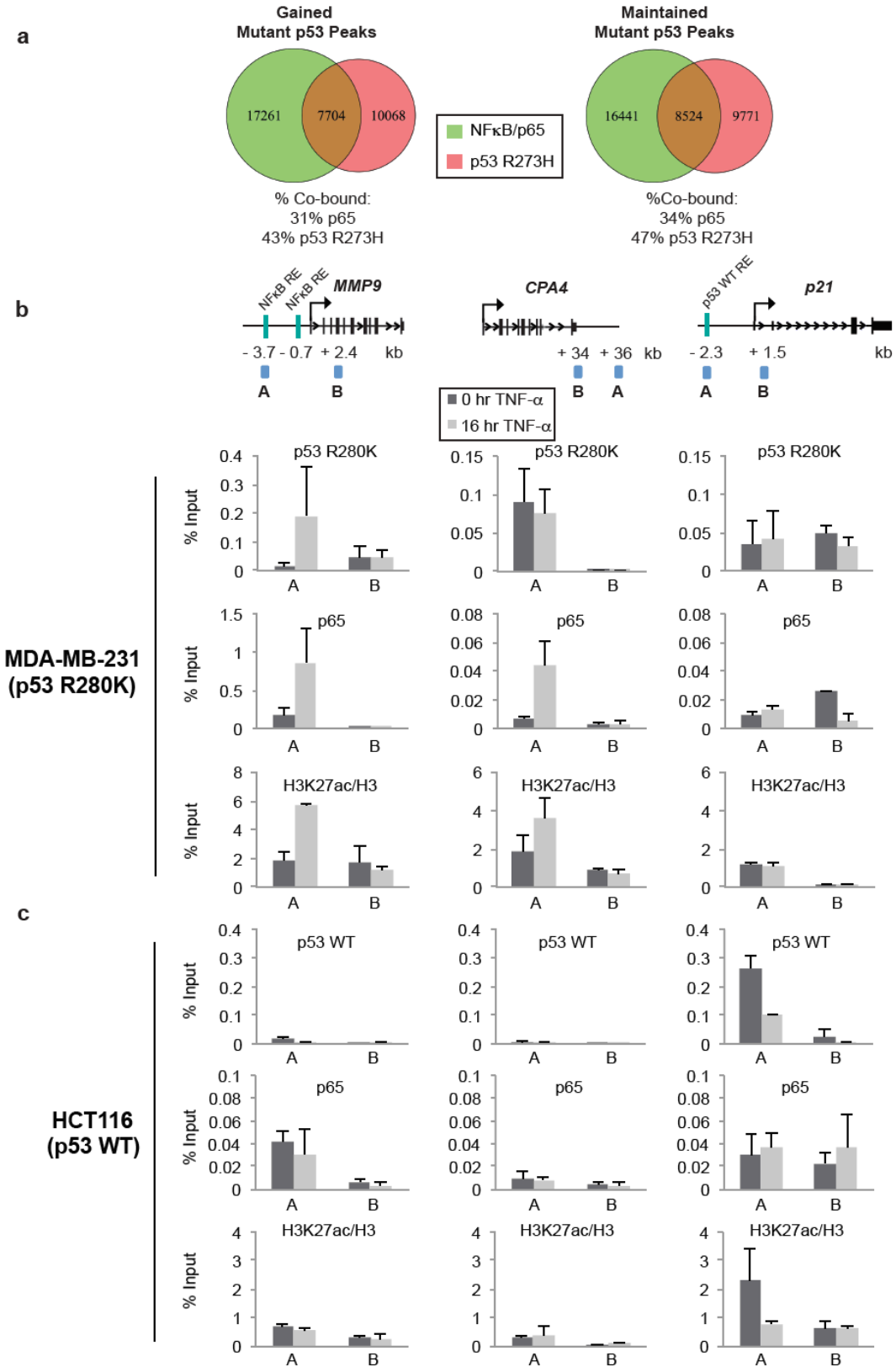
a
Gained
Mutant p53 Peaks
17261
7704
10068
% Co-bound:
31% p65
43% p53 R273H
NFκB/p65
p53 R273H
Maintained
Mutant p53 Peaks
16441
8524
9771
%Co-bound:
34% p65
47% p53 R273H
b
NFκB RE
NFκB RE
MMP9
- 3.7 - 0.7 + 2.4 kb
A
B
CPA4
+ 34 + 36 kb
B
A
p53 WT RE
p21
- 2.3 + 1.5 kb
A
B
0 hr TNF-α
16 hr TNF-α
MDA-MB-231
(p53 R280K)
p53 R280K
p65
H3K27ac/H3
% Input
c
HCT116
(p53 WT)
p53 WT
p65
H3K27ac/H3
% Input

Figure 2.9. Analysis of NFκB and mutp53 at proinflammatory target gene enhancers. (a) Analysis of purified p53 and p65 proteins by SDS-PAGE with Coomassie Brilliant Blue (CBB) staining. **(b)** Immunoblot analyses following p65 Co-IP performed with nuclear extract from SW480 cells treated with TNF-α for 0 or 16 hr with indicated antibodies that recognize mutp53 and p65. Three independent Co-IP assays were performed. **(c)** qRT-PCR and Immunoblot analysis of SW480 cells that were transfected with non-targeting control or NFκB/p65 siRNA, following TNF-α treatment for 0 or 16 hr with indicated antibodies. The expression levels upon TNF-α treatment are relative to the levels before treatment. The bar graphs represent the average of three independent experiments with the error bars denoting the standard error. **(d)** ETS2 ChIP-qPCR analysis in SW480 cells following TNF-α treatment for 0 or 16 hr at *CYP24A1* and *CPA4* enhancer and nonspecific regions. The amplicons used for ChIP-qPCR are shown in the schematics of the target gene loci. **(e)** Immunoblot analysis of SW480 cells treated with vehicle or MG132 and TNF-α for 0 or 16 hr with indicated antibodies. **(f)** ChIP analyses to examine NFκB/p65 and mutp53 binding at the enhancers and nonspecific regions of *MMP9* and *CCL2* in SW480 cells treated with vehicle or MG132 and TNF-α for the indicated time points. The amplicons used for ChIP-qPCR are shown in the schematics of the target gene loci. **(g)** ChIP analyses of p53 R273H and NFκB/p65 binding at the enhancers and nonspecific regions of *MMP9* and *CYP24A1* in SW480 cells transfected with control or p53 siRNA and treated with TNF-α for the indicated time points. The amplicons used for ChIP-qPCR are shown in the schematics of the target gene loci. For all ChIP assays, an average of two independent ChIP experiments that are representative of at least three is shown with error bars denoting the standard error.

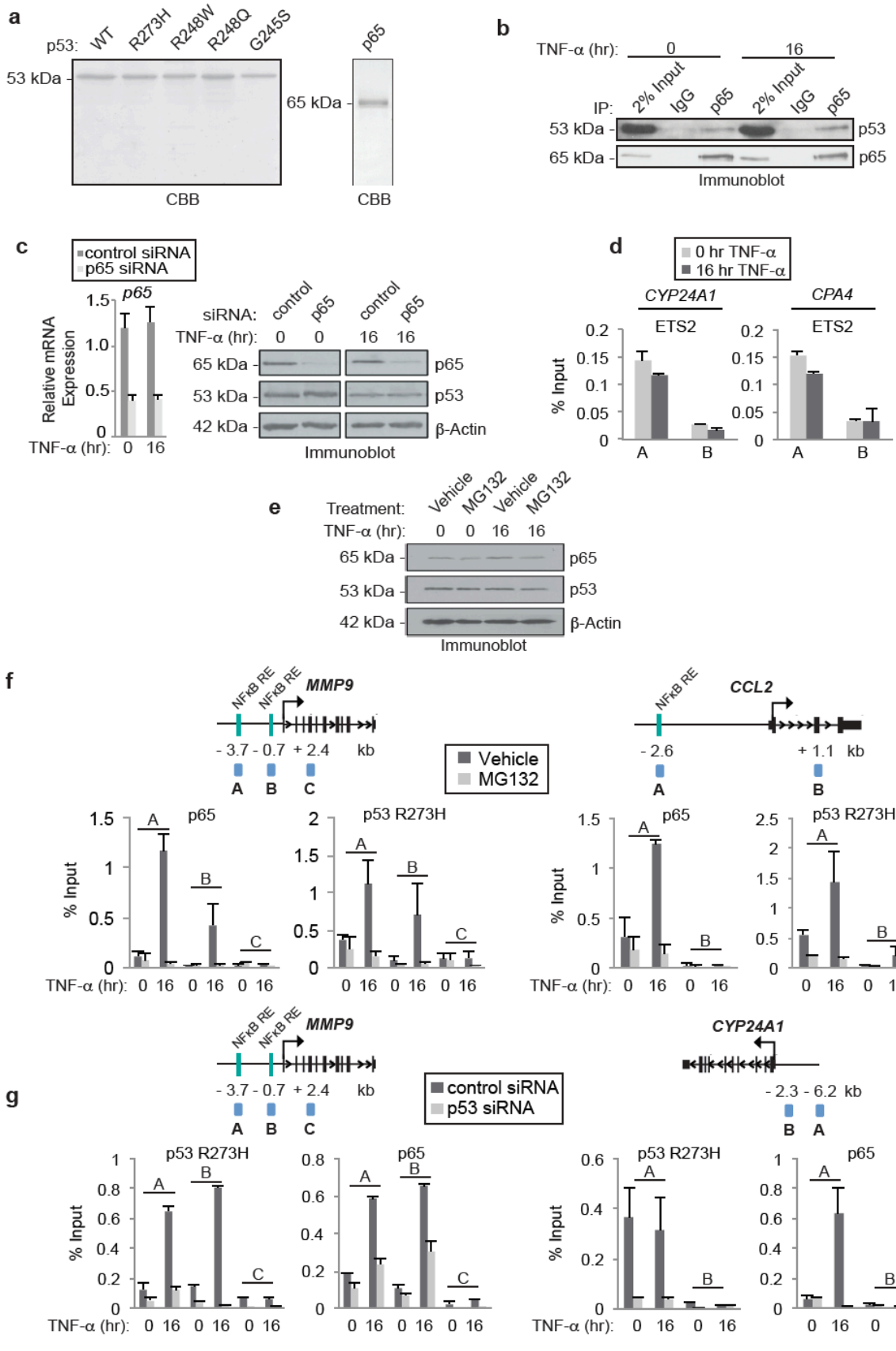
a
p53: WT R273H R248W R248Q G245S
53 kDa
CBB
p65
65 kDa
CBB
b
TNF-α (hr): 0 16
IP: 2% Input IgG p65 2% Input IgG p65
53 kDa
p53
65 kDa
p65
Immunoblot
c
control siRNA
p65 siRNA
p65
Relative mRNA Expression
TNF-α (hr): 0 16
siRNA: control p65 control p65
TNF-α (hr): 0 0 16 16
65 kDa
p65
53 kDa
p53
42 kDa
β-Actin
Immunoblot
d
0 hr TNF-α
16 hr TNF-α
CYP24A1
CPA4
ETS2
% Input
A B
e
Treatment: Vehicle MG132 Vehicle MG132
TNF-α (hr): 0 0 16 16
65 kDa
p65
53 kDa
p53
42 kDa
β-Actin
Immunoblot
f
NFκB RE
MMP9
- 3.7 - 0.7 + 2.4 kb
A B C
CCL2
- 2.6 + 1.1 kb
Vehicle
MG132
p65
p53 R273H
% Input
TNF-α (hr): 0 16 0 16 0 16
g
control siRNA
p53 siRNA
CYP24A1
- 2.3 - 6.2 kb
B A

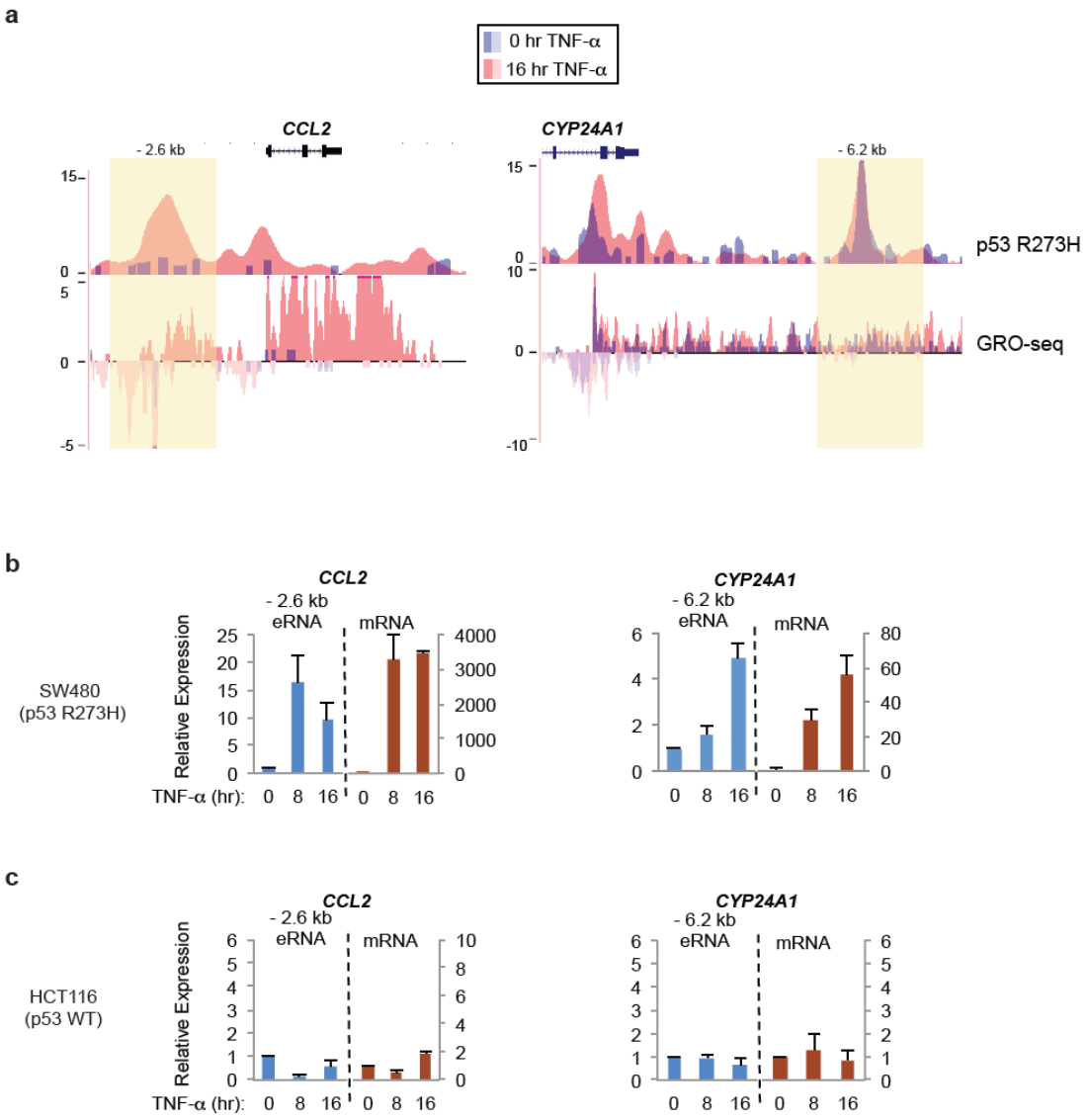

Figure 2.10. Mutp53 enhancer binding is positively correlated with enhancer transcription and gene activation. (a) UCSC genome browser images of genomic loci for *CCL2* and *CYP24A1* showing the ChIP-seq signal for mutp53 ChIP-seq and GRO-seq peaks with the enhancer regions highlighted in yellow. **(b)** qRT-PCR analysis of the indicated eRNAs and mRNAs in SW480 cells (p53 R273H), and **(c)** HCT116 cells (p53 WT) treated with TNF-α for 0, 8 or 16 hr. The expression levels shown after TNF-α treatment are relative to the levels before treatment. The bar graphs represent the average of three independent experiments with the error bars denoting the standard error.

Figure 2.11. Regulation of RNAPII recruitment, eRNA synthesis and mRNA expression by mutp53 and NFκB. (a) ChIP-qPCR analyses of RNAPII binding at the enhancers and nonspecific regions of *MMP9* and *CYP24A1* in SW480 cells transfected with control or p53 siRNA and treated with TNF-α for 0 or 16 hr. The amplicons used for ChIP-qPCR are shown in the schematics of the target gene loci. An average of two independent ChIP experiments is shown with error bars denoting the standard error. See Supplementary Fig. 2.7 and 2.8 for the relative mRNA, protein levels of mutp53, and mutp53 recruitment following p53 siRNA-mediated knockdown in SW480 cells. **(b)** qRT-PCR analysis of the *MMP9* and *CYP24A1* eRNAs and mRNAs in SW480 cells treated as described in (a). The expression levels shown after TNF-α treatment are relative to the levels before treatment. The bar graphs represent the average of three independent experiments with the error bars denoting the standard error. **(c)** ChIP-qPCR analyses of RNAPII binding at the enhancers and nonspecific regions of *MMP9* and *CYP24A1* in SW480 cells transfected with control or NFκB/p65 siRNA and treated with TNF-α for 16hr. The amplicons used for ChIP-qPCR are shown in the schematics of the target gene loci. An average of two independent ChIP experiments that are representative of at least three is shown with error bars denoting the standard error. See Fig. 2.9 and Fig. 2.3 for NFκB/p65 mRNA, protein levels, and recruitment following NFκB/p65 siRNA-mediated knockdown in SW480 cells. **(d)** qRT-PCR analysis of the *MMP9* and *CYP24A1* eRNAs and mRNAs in SW480 cells treated as described in (c). The expression levels shown after TNF-α treatment are relative to the levels before treatment. The bar graphs represent the average of three independent experiments with the error bars denoting the standard error.

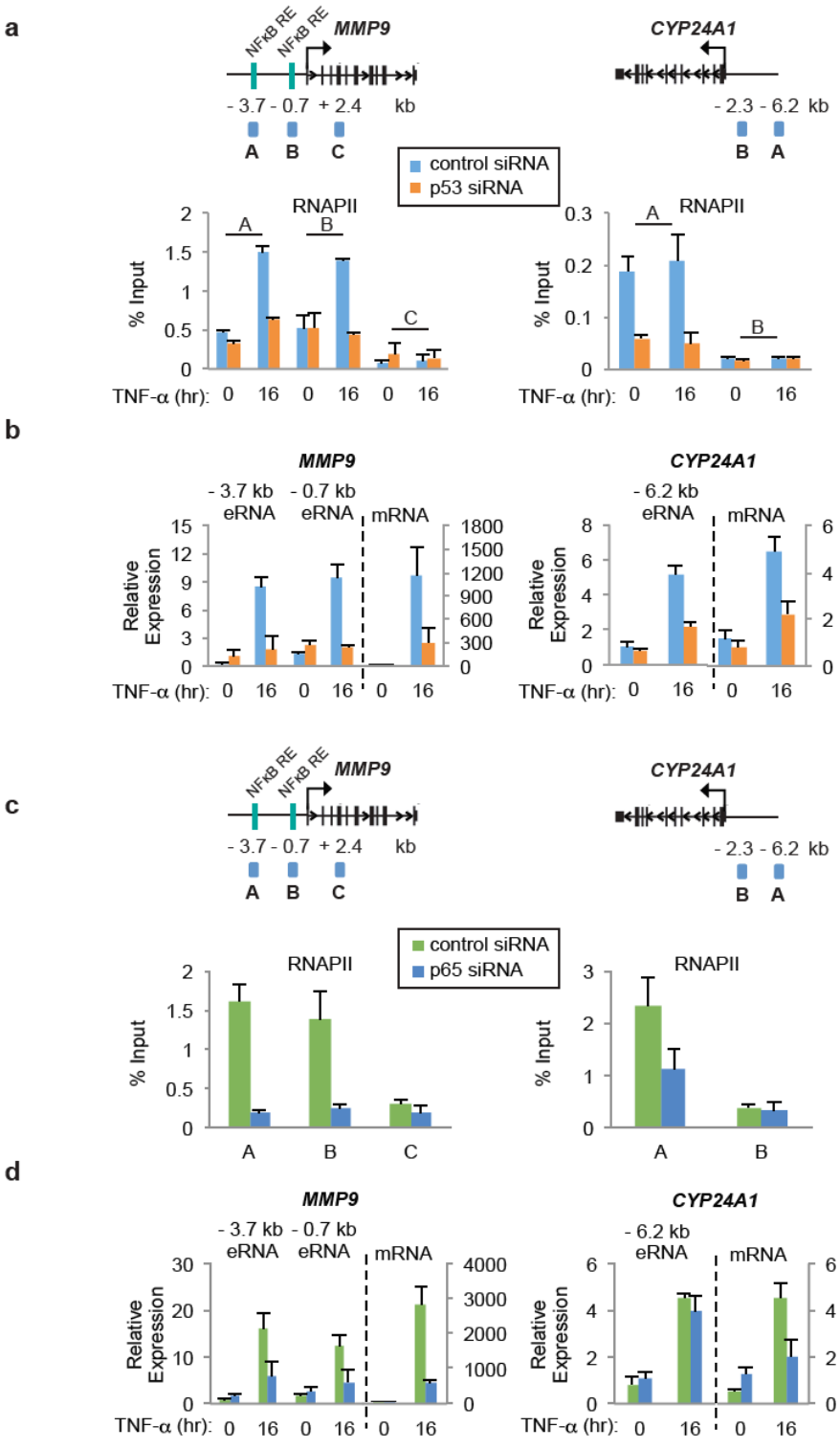
a
NFκB RE
NFκB RE
MMP9
- 3.7 - 0.7 + 2.4 kb
A B C
CYP24A1
- 2.3 - 6.2 kb
B A
control siRNA
p53 siRNA
RNAPII
% Input
TNF-α (hr): 0 16 0 16 0 16
b
MMP9
- 3.7 kb eRNA
- 0.7 kb eRNA
mRNA
Relative Expression
CYP24A1
- 6.2 kb eRNA
c
control siRNA
p65 siRNA
d

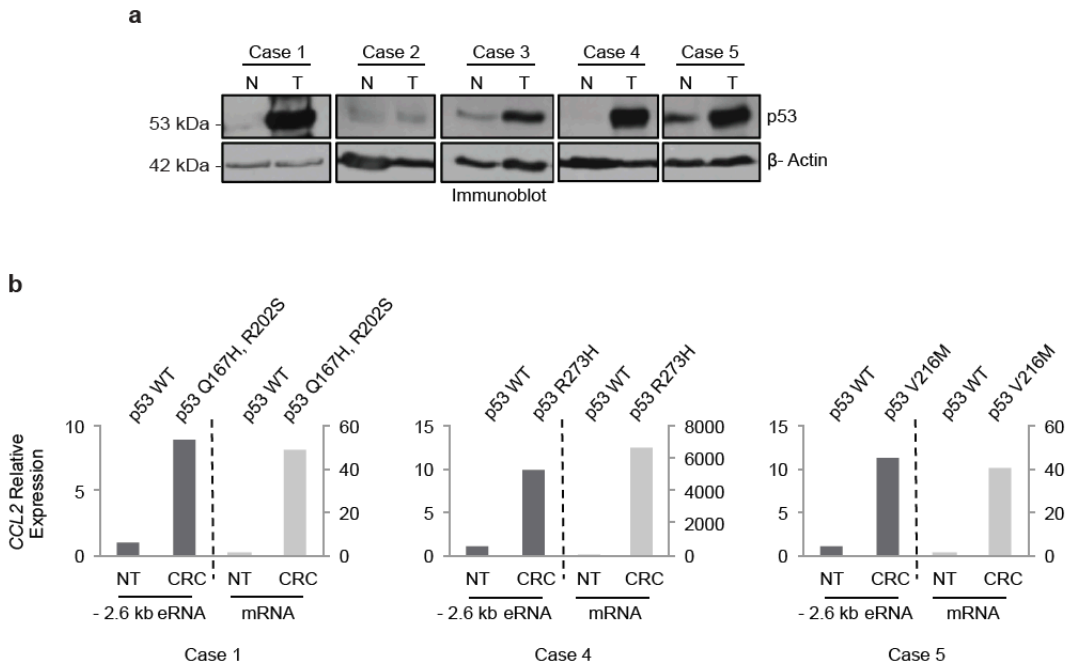

Figure 2.12. eRNA and mRNA expression analysis in human colon cancer tissues. (a) Immunoblot analysis of whole lysates derived from the five cases of paired non-neoplastic (NT) and colorectal carcinomas (CRC) samples with indicated antibodies. **(b)** qRT-PCR analysis of *CCL2* - 2.6 kb eRNA and mRNA from three of the five independent cases of paired NT and CRC samples prepared and analyzed as described in Figure 2.6a.

a

shRNA-mediated p53 knockdown in SW480 cells, corresponding to Figure 1a:

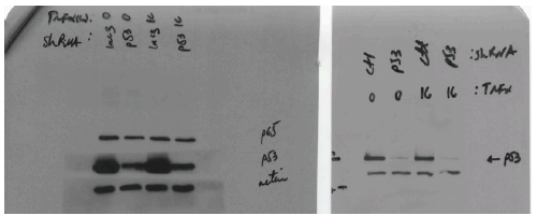

b

siRNA-mediated p53 knockdown in SW480 cells, corresponding to Supplementary Figure 1a:

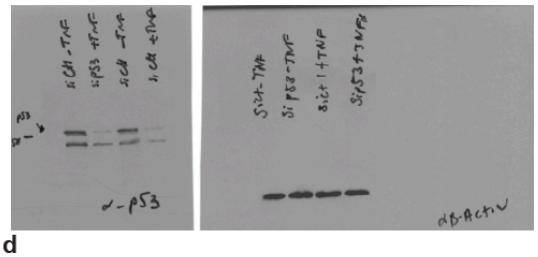

c

siRNA-mediated p53 knockdown in MDA-MB-231 cells, corresponding to Supplementary Figure 1b:

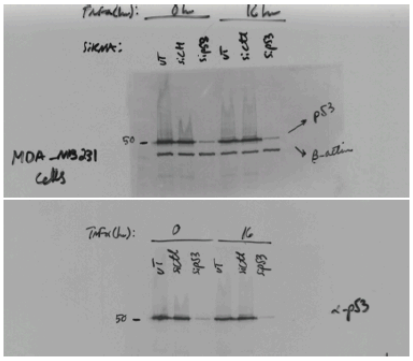

d

Direct p53-p65 interaction assay, corresponding to Figure 3a

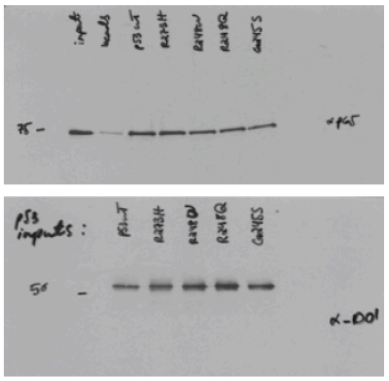

e

siRNA-mediated p65 knockdown in SW480 cells, corresponding to Supplementary Figure 3c:

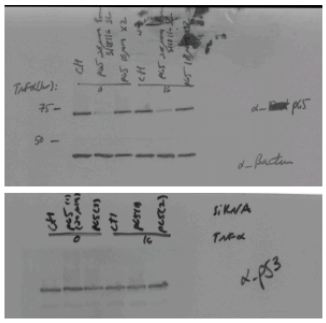

f

MG132 treatment of SW480 cells, corresponding to Supplementary Figure 3d:

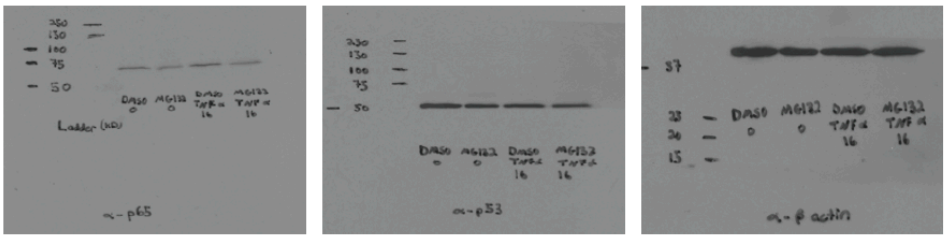

Figure 2.13. Uncropped images of western blot figures shown in the main paper

2.9.2 Supplemental tables

Supplementary Table 2.1. p53 and Rel-A siRNA sequences, Related to Experimental Procedures

siRNA	Sequence
Individual siGENOME TP53	GCUUCGAGAUGUUCCGAGA
SMART pool siGENOME RELA	GGAUUGAGGAGAAACGUAA CUCAAGAUCUGCCGAGUGA GGCUAUAACUCGCCUAGUG GAUUGAGGAGAAACGUAAA

Supplementary Table 2.2. Oligonucleotide sequences for ChIP analysis of the *MMP9*, *CCL2*, *CYP24A1, CPA4,* and *CDKN1A* genes, related to experimental procedures

Region	Forward Primer	Reverse Primer
MMP9 A	AGGGTCTTGGCTAAACTCTATT	TGGACAGAGCTTGGCTTTC
MMP9 B	CCCTTTACTGCCCTGAAGATT	TTCTTTGACTCAGCTTCCTCTC
MMP9 C	GATGGTCCTGGGTTCTAATTCC	GCAGTTCATCCCATCTCTCATC
CCL2 A	TTTGTGCCAGAGCCTAACC	AGTTCCCAGATCCCGTAGAA
CCL2 B	CAAAGAAGCTGTGATGTGAGTTC	GCACTCTCTGACTCTAGGTTTATG
CYP24A1 A	TACGCAGTCTTTGTGCAGTAG	GGAGGTTACATCGCTGTTCTC
CYP24A1 B	AATGCCTACCATGTCAGTATGT	CTACACTCAGCCAGAGCTATTC
CPA4 A	TTCTTTCTCTGGGAGCTTTCC	GTTTGGAAGCTGGACCTATGA
CPA4 B	GGGCAATCATAGCTCACTGTAG	TGCCTGTAATCCCAGCATTT
CDKN1A A	AGCAGGCTGTGGCTCTGATT	CAAAATAGCCACCAGCCTCTTCT
CDKN1A B	TTTGGGCGTGGAGATAAGGTGGA	GGGCGTGTGTGTGTGTGTGT

Supplementary Table 2.3. Oligonucleotide sequences for RT-PCR analysis of gene expression, related to experimental procedures

Gene	Forward Primer	Reverse Primer
GAPDH	ATTTGGTCGTATTGGGCGCCTG	AGCCTTGACGGTGCCATGGAATTT
β-Actin	ACCATGTACCCTGGCATTG	TACTTGCGCTCAGGAGGA
p53	GTTTCCGTCTGGGCTTCTT	GCAGGTCTTGGCCAGTT
p65	AGCACAGATACCACCAAGAC	CGGCAGTCCTTTCCTACAA
MMP9	GACCTGGGCAGATTCCAAA	GGCAAGTCTTCCGAGTAGTTT
CCL2	CAGCCAGATGCAATCAATGCC	TGGAATCCTGAACCCACTTCT
CYP24A1	TGGAGATCAAACCGTGGAAGG	GAAGACTGGCAGCGGGT
CPA4	GTCAGAAATGGAGACGAGATCAG	CTTCAATCGGCCTGTGGAT
LTB	TTTCAGAAGCTGCCAGAGG	AAACGCCTGTTCCTTCGT
UBD	CAATGCTTCCTGCCTCTGT	TCACGCTGTCATATGGGTTG
MMP9 3.7kb eRNA	TGATGGAGCTACCTCAGTG	CCACAATAGAGTTTAGCCAAGA
MMP9 0.7kb eRNA	CCCTTTACTGCCCTGAAGATT	TTCTTTGACTCAGCTTCCTCTC
CCL2 eRNA	TTGTGGAGCAAGGGACAAG	CCCTTGGGTGCCTCAGTTT
CYP24A1 eRNA	TACGCAGTCTTTGTGCAGTAG	GGAGGTTACATCGCTGTTCTC
CPA4 eRNA	TTCTTTCTCTGGGAGCTTTCC	GTTTGGAAGCTGGACCTATGA
p21	TGGAGACTCTCAGGGTCGAAAACGGC	AGGGCTTCCTCTTGGAGAAGATCA
MDM2	AGGGCTTCCTCTTGGAGAAGATCA	GTGCACCAACAGACTTTAATAACT TCA
PTG2	GAGTGTGGGATTTGACCAGTAT	TGTGTTTGGAGTGGGTTTCA

Supplementary Table 2.4. Oligonucleotide sequences for amplification of p53 from colorectal carcinoma tumor samples prior to sequencing, related to experimental procedures

	Forward Primer	Reverse Primer
p53 DBD	CAGCTGTGGGTTGATTCC	AGGGATCCTCAGTCTGAGTCAGGCCCTT

2.10 Acknowledgements

We are grateful to Trenton Massey and Zhengxi Sun for technical assistance; Graham McVicker (Salk Institute) for insightful discussions of the project; Xinbin Chen (UC Davis) for providing the SW480 shLacZ and shp53 cell lines, and Gourisankar Ghosh (UC San Diego) for providing purified p65 protein. This work was supported by the Research Scholar Award from the Sidney Kimmel Foundation for Cancer Research #857A6A to S.M.L. and CRI-Irvington Fellowship to S.H.D.

Chapter 2, in full, is a reprint of the material as it occurs in *Nature Communications*, Rahnamoun, H.; Lu, H.; Duttke, S. H.; Benner, C.; Glass, C. K.; Lauberth, S. M.; Nature Research, 2017. Rahnamoun, H. was the primary author.

Chapter 3

TOP1 interactions with RNAs regulate its protein interactome

3.1 Abstract

Human Topoisomerase 1 (TOP1) is a dynamic enzyme that primarily functions to overcome topological constraints on the DNA that are caused by strand separation. In this chapter, we demonstrate that TOP1 functions as a noncanonical RNA-binding protein in colon cancer cells following acute TNF signaling. Through biochemical analyses, we found that TOP1-RNA associations are essential for maintaining its protein interactome, particularly those ribonucleoprotein complexes that are critical for processing of pre-ribosomal RNAs.

3.2 Introduction

DNA topoisomerase I (TOP1) is a key enzyme that modulates essential cellular processes such as DNA replication, transcription, and chromatin remodeling by regulating the topology of the DNA double helix (Liu and Wang 1987, Durand-Dubief et al. 2010, Durand-Dubief et al. 2011, Pommier et al. 2016). Rapid unwinding of the DNA strands in such processes results in extensive torsional stress that, if left unresolved, leads to the formation of RNA-DNA hybrids known as R-loops and double-stranded DNA breaks (DSBs) (Ma, Bai and Wang 2013, Roca 2011, Aguilera and García-Muse 2012, Liu and Wang 1987, Kouzine et al. 2013). TOP1 acts to relieve DNA supercoiling by cutting the DNA backbone through its catalytic

intermediate known as the TOP1 cleavable complex (TOP1cc) and allowing the cut ends to swivel past each other to a more relaxed conformation before ligating the phosphodiester bonds to reform an intact double helix (Champoux 2001). Treatment with TOP1 poisons such as camptothecin (CPT) stabilizes the TOP1cc intermediate, causing R-loop accumulation and DSB formation that result in downregulation of gene expression (reviewed in (Pommier 2013)).

TOP1 is primarily found in the nucleolus where the transcription of ribosomal RNAs (rRNAs) which account for ~75% of total RNAs in growing cells is a highly dynamic and topologically taxing process (Brill et al. 1987, Schultz et al. 1992). Evidence in yeast cells has demonstrated that loss of TOP1 leads to transcriptional blocks at ribosomal DNA (rDNA) repeats and truncation of rRNA transcripts (El Hage et al. 2010). Consistent, systematic characterization of over 600 nucleolar proteins in HeLa cells identified TOP1 as a *trans*-acting processing factor that regulates pre-rRNA levels in the nucleolus (Tafforeau et al. 2013). Moreover, TOP1 depletion has been shown to morphologically change the nucleoli to be smaller in size and exhibit a more rounded shape (Shen et al. 2017). Given that the nucleolus size directly correlates with rRNA transcription, cell growth, and metabolic rates, coordinated nucleolar positioning of TOP1 is also critical for other nucleolar functions that relate to its size and structure (Boulon et al. 2010).

Notably, TOP1 is also a crucial cofactor for proper transcription of nucleoplasmic genes (Stewart and Schütz 1987, Kretzschmar, Meisterernst and Roeder 1993, Merino et al. 1993, Shykind et al. 1997, Durand-Dubief et al. 2010, Pedersen et al. 2012). More specifically, TOP1 was identified as a cofactor for activator-dependent transcription by RNA Polymerase II (RNAPII) (Kretzschmar et al. 1993) and shown to enhance the assembly of TFIID-TFIIA complex during transcription activation (Shykind et al. 1997). In yeast models, TOP1 nicking activity was also directly linked to efficient nucleosome disassembly at promoter regions (Durand-Dubief et al. 2010). More recently, it was demonstrated that TOP1 activity is stimulated

through its interactions with the BRD4-phosphorylated C-terminal domain of RNAPII to support efficient transcription (Baranello et al. 2016). Additionally, TOP1 was shown to be essential for activation of androgen receptor (AR)-bound enhancers in prostate cancer cell and Aire-regulated super-enhancers in medullary thymic epithelial cells (Puc et al. 2015, Bansal et al. 2017).

Given the critical roles of TOP1 at highly transcribed genomic loci, this enzyme is tightly controlled through different mechanisms. Namely, TOP1 relaxation activity is stimulated through its interactions with various transcription regulators such as p53, ARF and NKX3.1 (Karayan et al. 2001, Bowen et al. 2007, Mao et al. 2000). TOP1 activity was also reported to be attenuated through interactions with the tumor suppressor PAR-4 which sequesters TOP1 from the DNA to prevent TOP1-induced genomic instability (Goswami et al. 2008). Moreover, post-translational modifications of TOP1 also play a crucial role in its regulation. Namely, SUMOylation of TOP1 at highly transcribed regions assists in the recruitment of splicing factors to prevent R-loop accumulation and DSBs (Li et al. 2015a).

While several mechanisms underlying the regulation of TOP1 at highly transcribed regions have been explored, the reciprocal roles of RNAs in regulating TOP1 remain unknown. Interestingly, many DNA-binding proteins have been shown to exhibit RNA binding capabilities (Cassiday and Maher 2002). Consistent with this, a few recent studies have identified TOP1 to be among many noncanonical RNA binding factors through unbiased approaches (Castello et al. 2012, Baltz et al. 2012, He et al. 2016). In addition, the long non-coding RNA (lncRNA) *NORAD* was found to control the ability of RBMX to assemble a TOP1-containing ribonucleoprotein complex that is essential for maintaining genomic stability (Munschauer et al. 2018). Recently, TOP1 was also identified to be among the many factors that exhibit RNA-dependency (Caudron-Herger et al. 2019). While these studies have underscored the potential roles of TOP1 as an RNA-binding protein (RBP), analysis of various classes of transcripts that

are in association with TOP1 and the functional consequences of these complexes remain unexplored.

In this chapter, we characterize TOP1 as an RBP by demonstrating its association with various classes of transcripts under physiological conditions and direct interaction with RNAs, *in vitro*. We also establish that RNAs regulate TOP1's protein interactome by maintaining the integrity of the TOP1-containing ribonucleoprotein complex that is crucial for pre-rRNA processing.

3.3 Results

3.3.1 TOP1 associates and forms direct interactions with RNAs

While the largest requirement for TOP1 activity is in the nucleolus where transcription of the rRNA genes is most topologically taxing, TOP1 also functions within the nucleoplasm and in rapid response to various stimuli such as UV irradiation and ligand-induced transcription activity (Puc et al. 2015, Lanza et al. 1996). To gain a broad sense of various nucleoplasmic and nucleolar RNAs that associate with TOP1, we performed ultraviolet-cross-linked RNA immunoprecipitation (UV-RIP) in human SW480 colon cancer cells treated with tumor necrosis factor alpha (TNF-α) for 1 h. As shown in Fig. 3.1a, an antibody specific to TOP1 coimmunoprecipitated nucleoplasmic RNA species that include the *NORAD* lncRNA, an enhancer RNA (eRNA) produced from the +19 kb *CSF2* locus, and the corresponding *CSF2* mRNA. We also observed enrichment of nucleolar RNAs such as the C/D box 118 small nucleolar RNA (snoRNA) as well as the 18s and 45s rRNAs with TOP1 immunoprecipitation (Fig. 3.1a).

To further investigate the direct binding of TOP1 to RNAs, we next carried out electrophoretic mobility shift assays (EMSAs). Incubation of purified TOP1 FL (Fig. 3.3a) with a 286-base pair-long, ^{32}P-labeled RNA probe revealed the formation of a distinct TOP1–RNA

complex (Fig. 3.1b). Notably, we also confirmed the well-characterized TOP1 interactions with DNA by performing EMSAs with equimolar amounts of the corresponding double-stranded DNA (dsDNA) probe (Fig. 3.3b). We next performed RNA pulldowns using TOP1 FL protein and various *in vitro*–transcribed RNA probes corresponding to the 45s rRNA as well as *CCL2* and *MMP9* eRNAs (Fig. 3.1c). Consistent with the UV-RIP results, this analysis revealed that TOP1 can pull down different RNA species, independent of their sequence (Fig. 3.1c). Taken together, these findings demonstrate that TOP1 associates with different classes of RNAs under physiological conditions and can form direct interactions with RNA species, *in vitro*.

3.3.2 TOP1 forms RNA-dependent protein complexes

To gain insights into functional consequences of RNA associating with TOP1, we next investigated the role of RNAs in regulating the protein interactome of TOP1. Recently, a proteome-wide density gradient ultracentrifugation screen identified TOP1 to be among a group of RNA-dependent proteins as revealed by their differential migration patterns through sucrose gradients without and with RNA degradation (Caudron-Herger et al. 2019). Thus, to identify the TOP1 interactome that is RNA-dependent, we employed a similar methodology where control (-RNase) and RNase-treated (+RNase) whole cell lysates obtained from SW480 cells following 1 h TNF were subjected to sucrose-gradient ultracentrifugation. Notably, RNA analysis of cell lysates ± RNase treatment revealed significant degradation of cellular RNA species following treatment with the RNase cocktail (Fig. 3.3c). As shown in Fig. 3.2a, immunoblot analysis of the collected sucrose fractions revealed an RNA-dependent shift in fractions where TOP1 was detected. More specifically, TOP1 mainly migrated within higher sucrose density fractions (15 to 23) in the -RNase conditions while in the +RNase conditions, it migrated among lower sucrose density fractions (5 to 10) (Fig. 3.2a). Consistent with previous reporting (Caudron-Herger et al.

2019), our results are indicative of TOP1 being an RNA-dependent factor that loses its native protein associations following RNA degradation.

To identify the specific proteins that interact with TOP1 in an RNA-dependent manner, we coupled our sucrose density gradient ultracentrifugation with TOP1 immunoprecipitation. Specifically, the -RNase fractions (19-23) and +RNase fractions (6-10) in which TOP1 was detected following the sucrose density gradient ultracentrifugation in 1 h TNF-induced conditions were pooled together (Fig. 3.2b). The pooled fractions were subsequently used for immunoprecipitation with nonspecific IgG or TOP1 antibodies followed by silver stain or mass spectrometry (MS) analyses of the resulting eluates (Fig. 3.2b). The silver stain analysis of TOP1-associating factors in ± RNase conditions demonstrated specific enrichment of TOP1-associating peptides as compared to the IgG control (Fig. 3.2c). This analysis also revealed lost or decreased enrichment of several factors with TOP1 in +RNase conditions (Fig. 3.2c, denoted with asterisks). Liquid chromatography and tandem mass spectrometry (LC-MS/MS) analysis of the bound proteins in ± RNase conditions identified 14 factors that were in association with TOP1 in -RNase conditions and 10 that immunoprecipitated with TOP1 in +RNase conditions ($-\log_{10}(P) \geq 30$, % coverage ≥ twofold over IgG) (Fig. 3.2d). Among these proteins, 2 were found to be common between ± RNase conditions and they were TOP1 and mitochondrial TOP1, leaving 12 proteins that were uniquely enriched in the -RNase conditions and 8 that were exclusively identified in +RNase samples (Fig. 3.2d; Figs 3.3d, e). As listed in Fig. 3.3d, among the factors that lose their association with TOP1 following RNase treatment were nucleophosmin 1 (NPM1) and Heat shock protein 70 family member, HSP72 which were previously reported to associate with TOP1(Li et al. 2015b, Liccardi, Hartley and Hochhauser 2014, Ciavarra et al. 1994, Giffard et al. 2008). Moreover, 4 out of these 12 factors were directly related to ribosomes (RPL29, RPS6, RPL17, and RRBP1) of which RPL17, RPL29, and RPS6 along with NPM1, MYBBP1, and TOP1 were previously identified to be present in pre-rRNA

processing complexes(Hayano et al. 2003) (Fig. 3.3d). Notably, we validated the effect of RNA degradation on these TOP1-associating factors by performing TOP1 co-immunoprecipitation in ± RNase conditions and immunoblotting for NPM1. As shown in Fig. 3.3f, this analysis was consistent with our IP-MS results and verified that TOP1-NPM1 associations are diminished in the absence of RNAs.

On the other hand, factors that associated with TOP1 exclusively in +RNase conditions included TCOF which is a nucleolar factor linked to transcription and methylation of rRNAs (Hayano et al. 2003, Valdez et al. 2004, Gonzales et al. 2005) and IWS1 that is a critical transcription elongation factor for the RNAPII machinery(Krogan et al. 2002). Two ribosomal proteins (RLA0 and RLA0L) as well as two catalytic subunits of protein kinase A (PRKACB and PRKACA) and a regulator of the protein kinase A activity (RPGF3) were also identified among proteins that associated with TOP1 in +RNase conditions (Fig. 3.3e).

Next, we visualized the functional relationships among the 12 identified factors that lose their associations with TOP1 following RNA degradation by the STRING database (Szklarczyk et al. 2015) (Fig. 3.2e). Notably, this analysis further underscored the identification of previously unrecognized TOP1 associations with various regulatory factors such as leucine-rich repeat kinase (LRRK2), telomere-associated protein (RIF1), and zinc finger protein 638 (ZNF638) (Fig. 3.2e).

Gene ontology (GO) enrichment analysis by the Metascape tool(Zhou et al. 2019) further revealed different overrepresented biological pathways in the RNA-dependent TOP1 interactome (Fig. 3.2f). More specifically, Metascape analysis of the 12 proteins found in association with TOP1 in -RNase conditions showed enrichment of the previously identified Nop56p-associated pre-rRNA complex (Hayano et al. 2003) based on the presence of NPM1, RPL17, RPL29, RPS6, and MYBBP1A proteins (Fig. 3.2f). Other enriched pathways in the GO analysis included ribosome biogenesis and regulation of cell cycle and stress response

processes. This proteomic analysis, together with our biochemical characterization of TOP1 as an RBP, establishes the significance of RNA associations with TOP1 in regulating its ribonucleoprotein complexes and adds an additional layer of complexity to our current understanding of the mechanisms that regulate TOP1.

3.4 Discussion

TOP1 resolves topological constraints resulting from separation of DNA strands during replication and transcription. Given the ability of this enzyme to introduce transient yet detrimental DNA nicks, understanding the previously unrecognized mechanisms that regulate TOP1 function is of great significance. This study advances our current understanding of the conventional roles of TOP1 in gene expression by characterizing this factor as a noncanonical RBP. Notably, we have identified the ability of TOP1 to form stringent associations with different classes of RNAs that include protein-coding mRNAs as well as a wide array of noncoding transcripts. Moreover, our data underscores the importance of RNA interactions for maintaining TOP1's protein interactome, particularly those that are critical for pre-rRNA complex assembly within the nucleolus.

Establishment of TOP1 as a noncanonical RBP is supported by our UV-RIP analyses under physiological conditions as well as our *in vitro* RNA EMSA and pulldown assays. Having demonstrated that RNA interactions add an additional layer of complexity to TOP1 regulation, further identification of RNA binding regions (RBRs) within this protein is essential to explore the clinical implications of TOP1 targeting in cancer treatment. Notably, recent unbiased and high resolution mapping of RBRs in nuclear proteins using mouse embryonic stem cells not only classified TOP1 as an RBP, but further identified a 13-amino acid peptide that lies within its DNA-binding domain (DBD) as the RBR (He et al. 2016). While further validation and *in vitro* characterization of this 13-residue RBR is needed, given its complete sequence conservation

from mice to humans, it is highly plausible that the same region in human TOP1 would similarly support RNA binding. Notably, RNAs interacting with TOP1 through its DBD could be significant with regards to its therapeutic targeting given that the current chemotherapeutic agents against TOP1 stabilize its covalent engagement on DNA. Thus, understanding the potential consequences of TOP1 interacting with RNAs through its DBD and assessing whether RNA associations with TOP1 are able to sequester it away from the DNA at highly transcribed loci may uncover additional mechanisms that are critical for efficient TOP1 targeting.

Our proteomic analysis has established the global role of RNAs in maintaining TOP1-protein associations. More specifically, stringent TOP1 IP-MS in TNF-exposed cell lysates that were untreated or treated with a cocktail of RNases prior to being subjected to sucrose density gradient ultracentrifugation identified 12 factors that lost their associations with TOP1 following degradation of RNAs. GO analysis of these factors revealed enrichment of the Nop56p-associated pre-ribosomal ribonucleoprotein (pre-rRNP) complexes due the presence of MYBBP1A, RPL17, RPL29, RPS6, and NPM1 proteins within this list that were previously identified to be present in this complex along with TOP1 (Hayano et al. 2003). Notably, during ribosome biogenesis, various *trans*-acting proteins and snoRNAs that are not present in mature ribosomes form pre-rRNP complexes which play critical functions in processing pre-rRNAs as well as assembling rRNAs with ribosomal proteins (Lafontaine and Tollervey 1995, Tollervey 1996, Newman et al. 2000). Importantly, extensive biochemical and genetic analyses have identified a number of transcriptional regulators such as TOP1 and MYBBP1A that also function as *trans*-acting factors within these pre-rRNP complexes (Tafforeau et al. 2013, Hayano et al. 2003). Notably, while the precise roles for this subset of *trans*-acting factors within the pre-rRNP complexes remain to be fully examined, we have identified the dependency of TOP1 on its interaction with RNAs to remain within such complexes.

Moreover, Identification of cytoplasmic ribosomal proteins RPL17, RPL29, and RPS6 as factors that associate with TOP1 in an RNA-dependent manner is consistent with previous reporting that many ribosome components are also found in the nucleus and at transcriptionally active regions (Brogna, Sato and Rosbash 2002) where TOP1 is commonly found as well. This primes such factors to be potentially involved in the transcription of pre-ribosomal components.

In our analysis, the multifunctional and abundant nucleolar factor, NPM1 also exhibited RNA dependency in its association with TOP1. Notably, NPM1 which also demonstrates nucleic acid binding capabilities, has been shown to stimulate rRNA synthesis by binding to rDNA promoters and by exerting its histone chaperone activity (Murano et al. 2008, Wang et al. 1994). NPM1 also undergoes liquid-liquid phase separation by forming associations with rRNAs and other nucleolar proteins (Mitrea et al. 2018). Thus, it is plausible that RNA-mediated maintenance of TOP1 and NPM1 within the same RNP complex contributes to the phase-separated compartmentalization of the nucleolus, given that depletion of both factors independently alters the nucleolar morphology (Feric et al. 2016, Frottin et al. 2019, Shen et al. 2017, Mitrea et al. 2018).

Importantly, the nucleolus has been characterized as the main hub for response to cellular stress by sensing various stimuli and mediating cell cycle arrest or apoptosis (Lam, Trinkle-Mulcahy and Lamond 2005, Pfister 2019). Consistent with this, our proteomic analysis also identified RNA-dependent TOP1 associations for factors that are involved in cell cycle processing and stress response. Thus, it is likely that disrupting TOP1-containing complexes through RNA degradation delocalizes TOP1 and perturbs the structure integrity of the nucleolus which ultimately affects ribosome biogenesis and triggers the stress response (Boulon et al. 2010).

Lastly, while our proteomic analysis primarily identified nucleolar and pre-rRNA associating factors as RNA-dependent TOP1 interactors, there were other proteins such as LRRK2 and ZNF638 that were also determined to complex with TOP1 in a similar fashion. Moreover, factors such as NPM1 and TOP1 itself also associate with chromatin and exhibit critical roles within the nucleoplasm (Lindström 2011). Thus, further examination of how TOP1-RNA associations may be affecting regulatory events within the nucleoplasm are needed to better grasp the broad implications of TOP1 as a noncanonical RNA binding factor. In relation to this, follow up IP-MS analyses with milder binding and wash conditions are needed to examine the roles of RNAs in modulating TOP1's weaker and more transient associations with other proteins that may play critical roles in signal-dependent regulatory events.

3.5 Ongoing efforts and future directions

To explore the transcriptional roles of TOP1 in response to acute immune signaling, we have begun to assess TOP1's catalytic engagement before and after 1 h TNF-α treatment in colon cancer cells using the established TOP1-seq methodology (Baranello et al. 2016). Notably, we are performing these analyses prior to and following rapid TNF stimulation to induce some level of TOP1 translocation that would allow us to extend our examination of TOP1 engagement also on nucleoplasmic regulatory elements. This assay is performed by briefly treating the cells with the TOP1-selective inhibitor, CPT which will trap the enzyme in its TOP1cc intermediate form without altering TOP1 protein levels or the chromatin state (Baranello et al. 2016) and following immunoprecipitation of TOP1, DNA libraries are prepared for sequencing. Analysis of TOP1-enriched regions from the resulting datasets will reveal where the majority of TOP1 engagement occurs, both in the nucleolus and within the nucleoplasm,

To determine if TOP1 catalytic activity correlates with transcription levels in response to acute TNF-α signaling, I have also assayed nascent transcription in SW480 cells that were

treated with TNF-α for 1 h by performing precision nuclear run-on sequencing (PRO-seq) (Mahat et al. 2016). Importantly, both replicates of this assay have been successful, and we hope to use this dataset in parallel with the TOP1-engagement analyses described above to examine the correlation between transcription levels and catalytic potentials of TOP1.

Moreover, to extend our targeted UV-RIP analysis and globally identify endogenous RNAs that are in association with TOP1, I have prepared sequencing libraries from two biological replicates of Single-end Enhanced Crosslinking and Immunoprecipitation (seCLIP) (Van Nostrand et al. 2017) and size-matched input controls in SW480 cells following 1 h TNF-α induction. We expect that examination of this dataset identifies the different classes of RNAs (coding and noncoding) that TOP1 associates with. Further assessment of this data can also shed light on whether TOP1 has preferential binding to RNAs that contain specific sequence motifs. Lastly, comparison of TOP1-associating RNAs with the PRO-seq and TOP1-seq profiles will reveal whether there exists a correlation between TOP1-RNA complexes forming at sites where there are high levels of transcription and TOP1 catalytic engagement.

3.6 Methods

Antibodies

The antibodies used for IP analyses were obtained as follows: anti-TOP1 (ab219735, 2 μg) from Abcam and anti-IgG (2729, 2 μg) from Cell Signaling Technology. The antibodies used for immunoblotting analyses were obtained as follows: anti-TOP1 (sc-32736 1:1000 dilution) and anti-β-actin (sc-47778 1:2000 dilution) from Santa Cruz Biotechnology.

Immunoblotting

Protein samples denatured at 95 °C for 5 min were separated by SDS-PAGE and transferred to PVDF membranes (EMD Millipore). The membranes were blocked in 3% milk and probed with the indicated antibodies. Reactive bands were detected by ECL reagent and visualized using Odyssey Fc Imaging System (LI-COR).

Ultraviolet-RNA Immunoprecipitation (UV-RIP)

20 million SW480 cells that were untreated or treated with 12.5 ng ml^{-1} TNF-α for 1 h were crosslinked by UV irradiation (150 mJ per cm^2 at 254 nm) using a Stratalinker. The cells were lysed in RIP lysis buffer [25 mM HEPES-KOH pH 7.5, 150 mM KCl, 0.5% NP40, 1.5 mM $MgCl_2$, 10% glycerol, 1 mM EDTA, 0.4 U RNaseOUT (Thermo Fisher Scientific), protease inhibitor cocktails (PICs)] on ice for 30 min and cleared cell lysates were used for IP with TOP1 and IgG-antibody bound Protein A Dynabeads (Invitrogen) for 12-16 h. Beads were subsequently washed three times with RIP lysis buffer and RNA samples were eluted using TRIzol LS reagent (Invitrogen). cDNA samples were prepared as described below and analyzed by qRT-PCR primers listed in Supplementary Table 5.1.

RNA Purification and RT-qPCR

RNAs were extracted using TRIzol reagent (Invitrogen) following manufacturer's instructions and was used for cDNA synthesis with the ProtoScript II First Strand cDNA Synthesis Kit (NEB). PCR reactions were set up using SYBR Green PCR Master Mix (Applied Biosystems) on an Applied Biosystems Step One Plus real-time PCR systems. The specificity of amplification was confirmed by melting curve analysis. For UV-RIP analyses, RNA enrichment in IgG and TOP1 IP samples was normalized to *GAPDH* from input samples. Primers for qRT-PCR are listed in Supplementary Table 5.1.

***In vitro* RNA synthesis and refolding**

Primers were designed to amplify desired genomic regions that correspond to the *45s rRNA, CCL2* and *MMP9* eRNAs. The T7 promoter sequence was added to the forward primer for amplification from cDNA synthesized from SW480 colon cancer cells. The primers used for PCR amplification can be found in Supplementary Table 5.2. The amplified DNA was subsequently used for RNA synthesis using the T7 RiboMAX Express Large-Scale RNA Production System (Promega) followed by purification with MicroSpin G-25 Columns (GE Healthcare Life Sciences). RNAs were quantitated by Nanodrop (Invitrogen) and their integrity was verified on a 5% TBE urea gel followed by staining with SYBR Gold (Life Technologies) for 20 min prior to imaging using LI-COR Odyssey Fc Imaging System.

RNA probes were refolded by incubation at 85°C for 2 min followed by a 10-fold dilution with cold RNA refolding buffer (10 mM Tris-HCl pH 7, 10 mM $MgCl_2$, 100 mM KCl) and snap-cooling on an ice-cold metal rack for 5 min. RNAs were allowed to refold by bringing the sample to room temperature for 30 min.

Electrophoretic Mobility Shift Assays

EMSAs were performed based on established protocols with a few modifications(Rahnamoun et al. 2018). The 286 bp DNA probes were generated by PCR using

primers amplifying the *CCL2* enhancer region corresponding to the maximal RNA peak according to our published GRO-seq data(Rahnamoun et al. 2017). The 286 bp DNA product was used as the template for T7-synthesis of the RNA probe. Labeling reactions were carried out with 10 pmol of DNA or 10 μg of RNA, T4 polynucleotide kinase (NEB) and γ-^{32}P-ATP (Perkin Elmer). Unincorporated γ-^{32}P-ATP was removed from DNA by purification with MicroSpin G-25 Columns (GE Healthcare Life Sciences) and from RNA by extraction from 5% TBE urea gel using the ZR small-RNA PAGE Recovery Kit (Zymo Research). Labeled samples were quantified by running known amounts of unlabeled nucleic acid on an agarose gel for DNA or 5% TBE urea gel for RNA. Standard curves were generated following the quantification of the intensity of the nucleic acid bands using ImageJ.

Binding reactions were performed using 1 nM of labeled nucleic acids in 1X EMSA buffer [20 mM Tris-HCl pH 7.4, 100 mM KCl, 1mM EDTA, 1% glycerol, 0.05% NP40, 0.5 mM ZnCl2, 0.1 mg ml^{-1} BSA (Fisher), 0.1 mg ml^{-1} yeast tRNA (Sigma), 2 mM DTT) supplemented with 0.4U RNaseOUT (Thermo Fisher Scientific)] for RNA EMSAs. The RNA probe was refolded prior to addition to the reaction. The binding reactions were initiated by the addition of various doses (200-800 nM) of FLAG-TOP1 protein and incubation at 4°C for 30 min. Reactions were loaded on a 4% native polyacrylamide gel that was pre-chilled overnight and pre-run for 1 h at 150V. The gel was run for 4 h at 150V and exposed to autoradiography screen for 12-16 h prior to imaging with Typhoon phophorimager (GE Healthcare Life Sciences).

***In vitro* pull-down RNA binding assays**

Binding reactions were set up using 10 nM of FLAG-tagged proteins and 50nM of refolded RNA in RNA binding buffer (20 mM Tris-HCl at pH 7.4, 100 mM KCl, 0.2 mM EDTA, 0.05% NP40, 0.4 U RNase inhibitor, PICs) and incubated at 4°C for 1 h. Protein-RNA complexes were recovered using FLAG M2 agarose beads for 1 h at 4°C. Beads were washed

three times with RNA wash buffer (20 mM Tris-HCl at pH 7.4, 200 mM KCl, 0.2 mM EDTA, 0.05% NP40, PICs) and RNA samples were eluted using TRIzol LS reagent. Purified RNA samples were resolved on a denaturing 5% TBE urea gel and stained with SYBR gold for 20 min before imaging using LI-COR Odyssey Fc Imaging System.

SW480 cell lysate preparation for sucrose density gradient ultracentrifugation

This assay was performed following previously established protocols(Caudron-Herger et al. 2019). 20 – 24 million SW480 cells that were untreated or treated with 12.5 ng ml^{-1} TNF-α for 1 h were harvested and collected by centrifugation. Cell pellets were resuspended in 150 μL of lysis buffer (20 mM Tris-HCl pH 7.5, 300 mM NaCl, 2 mM EDTA, 0.5% NP40, 1% Triton X-100, 1 mM PMSF, PICs), incubated on ice for 30 min, and gently vortexed every 5 min. Cell resuspensions were next snap frozen in liquid nitrogen and quickly thawed twice to fully lyse the cells. Lysates were cleared by centrifugation at 13,000 rpm for 10 min at 4 ºC and protein concentrations were determined against bovine serum albumin (BSA) standard solutions.

RNase treatment of SW480 cell lysates

2 to 2.5 mg of protein lysate that was prepared as described above was pre-incubated with 50 μg RNase A (Fisher Scientific), 50 U RNase I (Life technologies), 5000 U RNase T1 (Sigma), and 50 U RNase H (NEB) at 4°C for 1 h. 50 μL of lysis buffer was added to control samples and incubated at 4°C for 1 h.

Sucrose density gradient ultracentrifugation

To prepare the sucrose density gradient, ten 1 ml sucrose solutions from 50% to 5% in 10 mM Tris-HCl pH 7.5, 100 mM NaCl, and 1 mM EDTA were layered on top of each other in ultra-clear tubes (Beckman Coulter) with the 50% sucrose solution on the bottom. Each layer was frozen at -80 ºC for 10 min before the addition of the next layer. Prepared sucrose gradients were stored at -20 ºC and slowly thawed at 4 ºC an hour prior to starting the spin. 2-

2.5 mg of untreated and RNase-treated cell lysates were gently layered on top of the sucrose gradient without perturbing the layers. Centrifugation was performed using a Beckman ultracentrifuge with a SW41 swinging bucket rotor at 30,000 rpm for 18 h at 4 ºC. Following ultracentrifugation, gradient tubes were removed from the rotor without disturbing the layers and starting from the top, 25 fractions of 400 μL each were collected into fresh 1.5 ml tubes. 5% of each fraction was taken for western blot analysis and the reminder of fractions were kept on ice until processed for immunoprecipitation.

TOP1 immunoprecipitation followed by mass spectrometry

Following immunoblot analysis of TOP1 in control and RNase-treated sucrose gradient fractions, those fractions that showed highest levels of TOP1 protein in each condition were pooled together. Pooled control (no RNase treatment) fractions were diluted twofold with 10 mM Tris-HCl pH 7.5, 100 mM NaCl, and 1 mM EDTA to adjust the sucrose concentration to the same level of the RNase-treated fractions. Protein A Dynabeads that were pre-coupled to TOP1 and IgG antibodies in 1 mg ml^{-1} BSA and crosslinked with dimethyl pimelimidate (DMP; Life technologies) were subsequently used for immunoprecipitation from the pooled sucrose fractions overnight at 4 ºC. Immunocomplexes were washed five times in ice-cold wash buffer (50 mM Tris-HCl pH 7.4, 500 mM NaCl, 0.5% sodium deoxycholate, 1% SDS, 1% NP-40) and three times in 1X PBS. After the removal of last PBS wash, protein-bound beads were either denatured at 70 ºC for 10 min for SDS-PAGE and silver stain analysis or frozen at -80 ºC for storage prior to mass-spectrometry analysis.

Sample preparation for mass spectrometry

Following previously established methods(Guttman et al. 2009, McCormack et al. 1997), protein samples from two biological replicates were diluted in TNE buffer (50 mM Tris-HCl pH 8.0, 100 mM NaCl, 1 mM EDTA). RapiGest SF reagent (Waters Corp.) was added to the mix to 0.1% final concentration and samples were boiled for 5 min. TCEP (Tris (2-carboxyethyl)

phosphine) was added to final concentration of 1 mM and the samples were incubated at 37°C for 30 min. This was followed by carboxymethylation of samples with 0.5 mg ml^{-1} of iodoacetamide for 30 min at 37°C and subsequent neutralization with 2 mM TCEP (final concentration). Samples were next digested with trypsin at the trypsin to protein ratio of 1 to 50 overnight at 37°C. RapiGest reagent was degraded and removed from the samples by treating them with 250 mM HCl at 37°C for 1 h, followed by centrifugation at 14000 rpm for 30 min at 4°C. Soluble fractions were subsequently transferred to fresh tubes and peptides were extracted using C18 desalting columns (Thermo Scientific, PI-87782). Following quantification of peptides using BCA assay, 1 μg of total peptides from each samples were injected for LC-MS analysis.

Liquid chromatography coupled with tandem mass spectroscopy (LC-MS/MS)

This analysis was performed following previously established protocols(Guttman et al. 2009, McCormack et al. 1997). Trypsin-digested peptides were analyzed by ultra high-pressure liquid chromatography (UPLC) coupled with tandem mass spectroscopy (LC-MS/MS) using nano-spray ionization. The nanospray ionization experiments were performed using a Orbitrap fusion Lumos hybrid mass spectrometer (Thermo) interfaced with nano-scale reversed-phase UPLC (Thermo Dionex UltiMate™ 3000 RSLC nano System) using a 25 cm, 75-micron ID glass capillary packed with 1.7-μm C18 (130) BEH™ beads (Waters corporation). Peptides were eluted from the C18 column into the mass spectrometer using a linear gradient (5–80%) of ACN (Acetonitrile) at a flow rate of 375 μl min^{-1} for 1 h. The buffers used to create the ACN gradient were: Buffer A (98% H_2O, 2% ACN, 0.1% formic acid) and Buffer B (100% ACN, 0.1% formic acid). Mass spectrometer parameters were set as follows; an MS1 survey scan using the orbitrap detector (mass range (m/z): 400-1500 (using quadrupole isolation), 120000 resolution setting, spray voltage of 2200 V, Ion transfer tube temperature of 275 C, AGC target of 400000, and maximum injection time of 50 ms was followed by data dependent scans (top speed for

most intense ions) with charge state set to only include +2-5 ions, and 5 second exclusion time, while selecting ions with minimal intensities of 50000 at in which the collision event was carried out in the high energy collision cell (HCD Collision Energy of 30%). The fragment masses where analyzed in the ion trap mass analyzer (With ion trap scan rate of turbo, first mass m/z was 100, AGC Target 5000 and maximum injection time of 35ms). Protein identification and label free quantification was carried out using Peaks Studio 8.5 (Bioinformatics solutions Inc.). Proteins with $-\log_{10}$ p-value of 30 and higher were retained as statistically significant and further filtered to remove all those that were also identified in the IgG IPs without being enriched in the TOP1 IPs by at least twofold based on their % coverage values. Keratins and trypsin which are introduced during the IP-MS procedure were deleted from the results. STRING network and Metascape GO analyses were performed on the list of factors identified following these criteria in both biological replicates of control and RNase conditions.

3.7 Figures

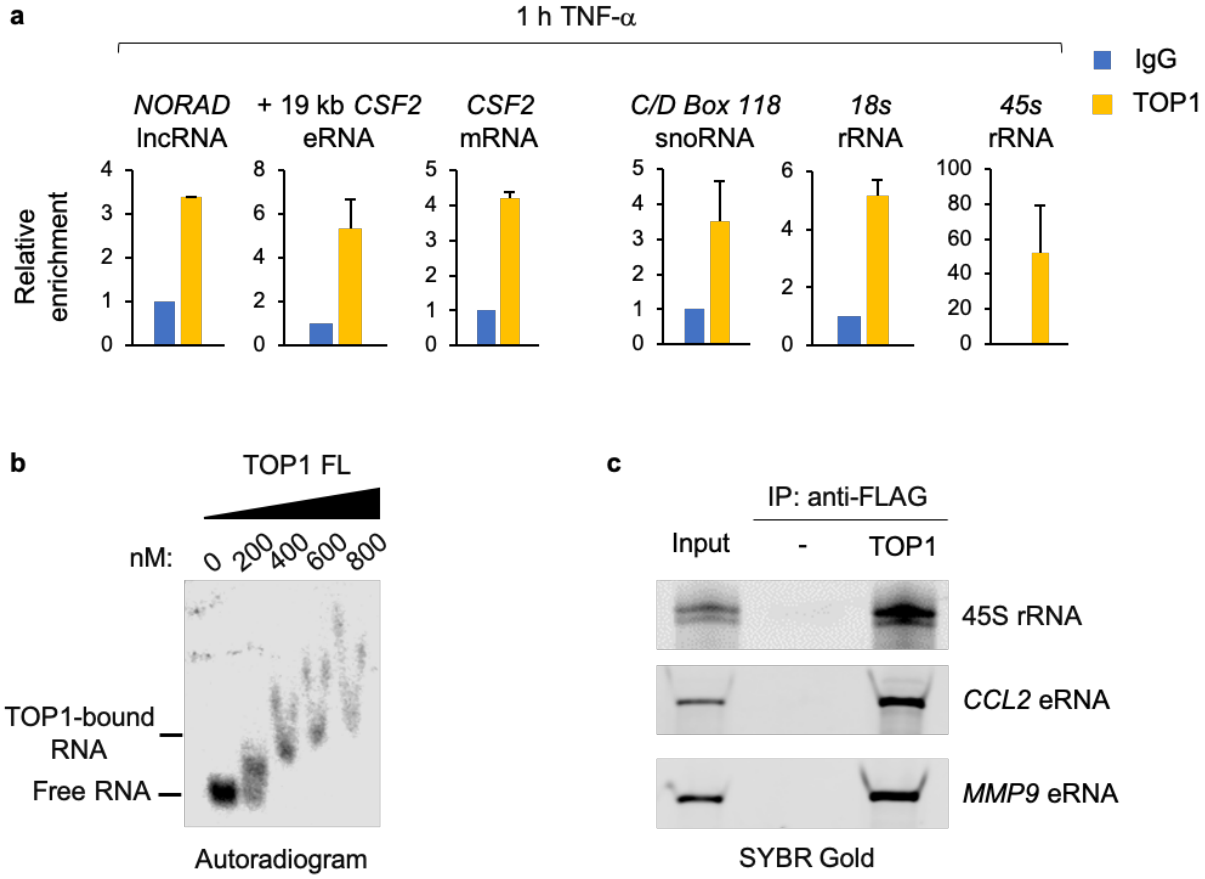

Figure 3.1. TOP1 associates with and directly interacts with different classes of RNAs. **(a)** qRT–PCR analysis of indicated RNAs following UV-RIP with IgG or TOP1 antibodies in SW480 cells treated with TNF-α for 1 h. Enrichment levels for TOP1 immunoprecipitation are relative IgG, and data represent the mean and s.e.m. of n = 2 independent experiments that are representative of at least three replicates. **(b)** RNA EMSA performed with 1 nM *in vitro* transcribed ^{32}P-labeled 286-bp RNA probe and increasing titrations of TOP1 FL. **(c)** SYBR Gold staining analysis of *in vitro* pulldown of indicated RNAs with FLAG-tagged TOP1 FL protein. n = 3 independent experiments for all RNA EMSAs and *in vitro* binding assays, with representative images for each assay shown in the corresponding panels.

Figure 3.2. TOP1 forms RNA-dependent protein complexes. (a) Immunoblot analysis of TOP1 in 25 fractions of the sucrose density gradient following ultracentrifugation using lysates from SW480 cells induced with TNF-α for 1 h, ± RNase treatment. n = 3 independent experiments. **(b)** schematic of IgG and TOP1 IP from TOP1-containing sucrose density gradient fractions following ultracentrifugation in cells treated as described in (a). **(c)** Silver stain analysis of IgG and TOP1 IPs as described in (b). Asterisks denote proteins that lose association with TOP1 in +RNase conditions. n = 3 independent experiments. **(d)** Venn diagram indicating the number of TOP1-associating proteins uniquely identified in -RNase and +RNase conditions following TOP1 IP as described in (b) following LC-MS/MS analysis. **(e)** Protein-protein interaction networks of -RNase only TOP1 interactors, extracted from the STRING 10.5 database. Proteins are represented as nodes and edges represent previously reported associations found from experimental analysis or curated databases. **(f)** Gene Ontology analysis using Metascape for the 12 factors identified to associate with TOP1 only in -RNase conditions, as identified in (d). For d-f, n = 2 independent experiments.

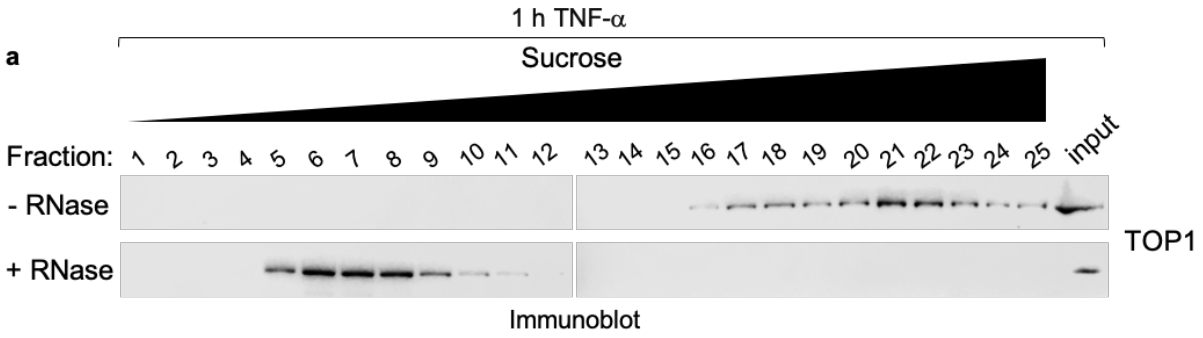
a
1 h TNF-α
Sucrose
Fraction: 1 2 3 4 5 6 7 8 9 10 11 12 13 14 15 16 17 18 19 20 21 22 23 24 25 input
- RNase
+ RNase
TOP1
Immunoblot

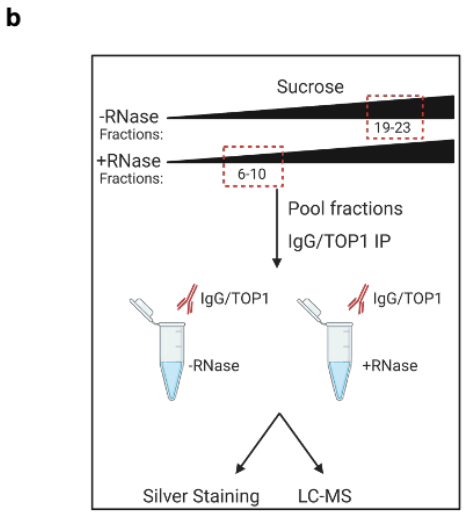
b
Sucrose
-RNase Fractions:
19-23
+RNase Fractions:
6-10
Pool fractions
IgG/TOP1 IP
IgG/TOP1
IgG/TOP1
-RNase
+RNase
Silver Staining
LC-MS

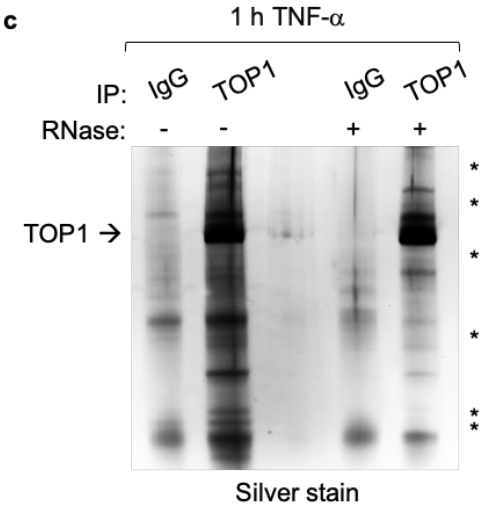
c
1 h TNF-α
IP: IgG TOP1 IgG TOP1
RNase: - - + +
TOP1 →
Silver stain


d
- RNase
+ RNase
12
2
8

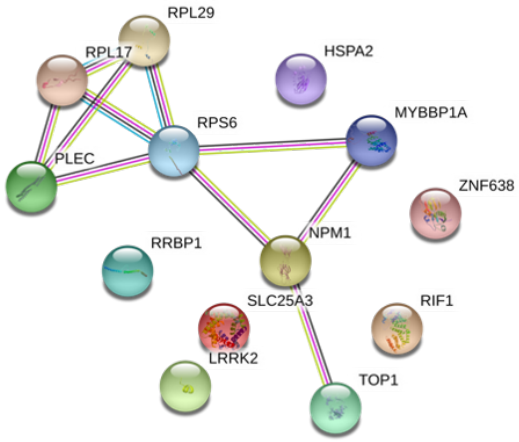
e
RPL29
RPL17
HSPA2
MYBBP1A
RPS6
PLEC
ZNF638
RRBP1
NPM1
SLC25A3
RIF1
LRRK2
TOP1

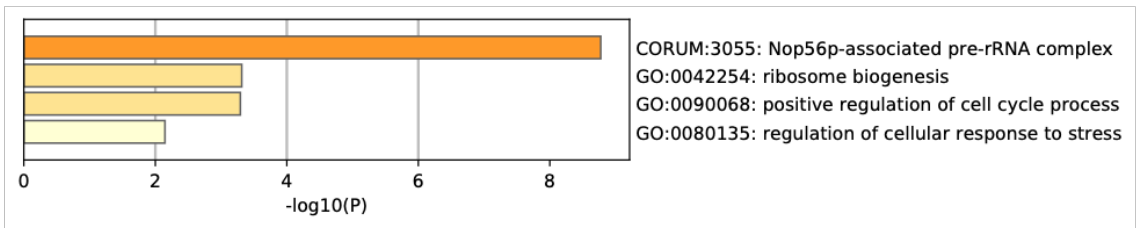
f
0
2
4
6
8
-log10(P)
CORUM:3055: Nop56p-associated pre-rRNA complex
GO:0042254: ribosome biogenesis
GO:0090068: positive regulation of cell cycle process
GO:0080135: regulation of cellular response to stress

3.8 Supplemental information

3.8.1 Supplemental figure

Figure 3.3. Supplemental information related to TOP1-RNA associations. (a) Coomassie staining analysis of the affinity purified TOP1 FL protein. **(b)** DNA EMSA performed with 1 nM ^{32}P-labeled, 286-bp dsDNA probe and increasing titrations of TOP1 FL. (**c**) SYBR Gold staining analysis of total RNA in lysates from SW480 cells induced with TNF-α for 1 h, ± RNase treatment. **(d), (e)** list of proteins identified from TOP1 IP-MS using lysates from SW480 cells induced with TNF-α for 1 h and **(d)** left untreated or **(e)** treated with RNases; corresponding to Fig. 3.2d. **(f)** Immunoblot analyses of TOP1 and co-immunoprecipitation with lysates prepared as described in (c). For b, c, f, n = 3 independent experiments.

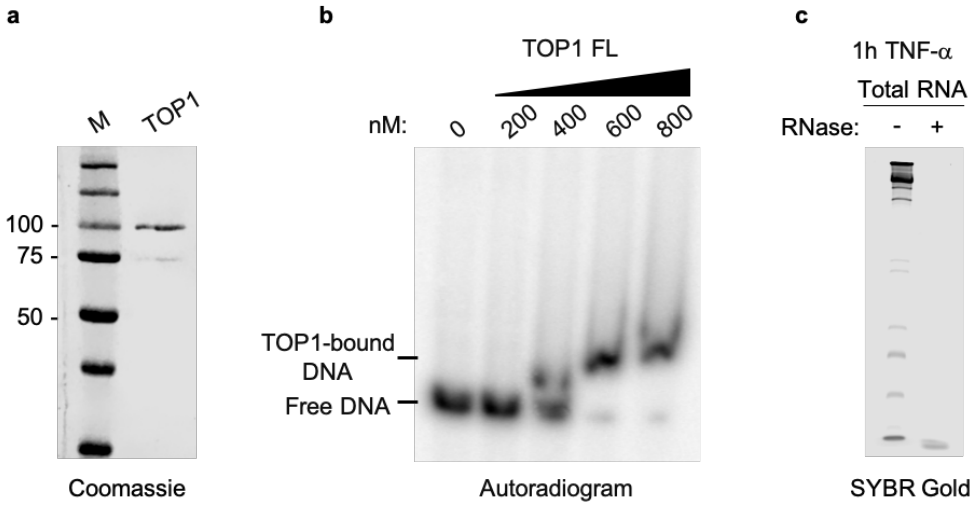

d

TOP1-associating proteins (-RNase)

Protein ID	MW (kDa)	- $\log_{10}$ P
Q9P2E9|RRBP1_HUMAN	152.472	115.8
Q14966|ZN638_HUMAN	220.623	98.13
Q00325|MPCP_HUMAN	40.095	48.60
P54652|HSP72_HUMAN	70.021	63.36
P47914|RPL29_HUMAN	17.752	51.61
P06748|NPM_HUMAN	32.575	73.18
Q9BQG0|MYBB1A_HUMAN	148.854	41.18
Q5UIP0|RIF1_HUMAN	274.464	42.19
P62753|RPS6_HUMAN	28.681	36.92
Q15149|PLEC_HUMAN	531.796	32.99
P18621|RPL17_HUMAN	21.397	38.99
Q5S007|LRRK2_HUMAN	286.100	87.44

e

TOP1-associating proteins (+RNase)

Protein ID	MW (kDa)	- $\log_{10}$ P
Q13428|TCOF_HUMAN	152.105	174.7
Q96ST2|IWS1_HUMAN	91.955	118.8
O95398|RPGF3_HUMAN	103.751	108.9
P22694|KAPCB_HUMAN	40.623	79.39
P17612|KAPCA_HUMAN	40.590	81.91
P46013|KI67_HUMAN	358.695	81.40
P05388|RLA0_HUMAN	34.274	99.94
Q8NHW5|RLA0L_HUMAN	34.364	98.48

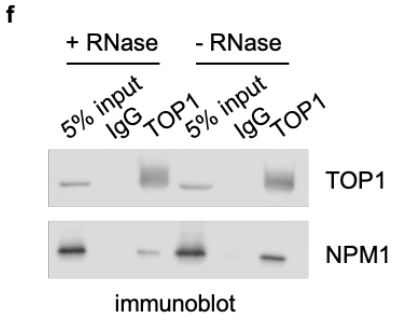

3.8.2 Supplemental tables

Supplementary Table 3.1. Oligonucleotide sequences for RT-PCR analysis of UV-RIP assays, related to the experimental procedures

Name	Sequence
GAPDH F	ATTTGGTCGTATTGGGCGCCTG
GAPDH R	AGCCTTGACGGTGCCATGGAATTT
NORAD F	CTCTGCTGTGGCTGCCC
NORAD R	GGGTGGGAAAGAGAGGTTCG
18S rRNA F	GCTTAATTTGACTCAACACGGGA
18S rRNA R	AGCTATCAATCTGTCAATCCTGTC
snoRNA 118 F	GGTGGGATAATCCTTACCTGTTC
snoRNA 118 R	CCTGATTACGCAGAGACGTTAAT
CSF2 eRNA F	CTGAAGCTGTGAGCAGAGAAA
CSF2 eRNA R	CCAAGTAGCAGGAAGAGTGATG
CSF2 mRNA F	GTCTCCTGAACCTGAGTAGAGA
CSF2 mRNA R	GGTCAAACATTTCTGAGATGACTTC
45S rRNA F	CACGGACAGGATTGACAGATT
45S rRNA R	GCCAGAGTCTCGTTCGTTATC

Supplementary Table 3.2. Oligonucleotide sequences for amplification of genomic regions corresponding to various RNA species used for *in vitro* RNA synthesis, related to experimental procedures

Name	Primer Sequence	RNA length
NORAD F	CCGGATCCTAATACGACTCACTATAGAGTTCCGGTCCGGCAGAGAT	800 bp
NORAD R	TTGCGGCCGCTTGGGGTGGAGTTGAGAGC	
45S rRNA F	CCGGTACCTAATACGACTCACTATAGGAAGCCAGAGGAAACTCT	250 bp
45S rRNA R	TTCTCGAGTACCCATTTAAAGTTTGAGAATAG	
MMP9 eRNA F	CCGGTACCTAATACGACTCACTATAGGCTGGCATATATGATGACT	260 bp
MMP9 eRNA R	TTCTCGAGGCTGGCATATCAGACAG	
CCL2 eRNA F	CCGGTACCTAATACGACTCACTATAGCTTTATCTATGAGTTGATAG	286 bp
CCL2 eRNA R	TTCTCGAGAGCTTTGGAAGTTCCCAG	

3.9 Acknowledgements

Chapter 3, in part, is unpublished material coauthored with Orozco, P. and Vukovic, L. Rahnamoun, H. was the primary author of this chapter.

Chapter 4

Concluding remarks

4.1 Mutant p53-dependent activation of proinflammatory enhancers

The tumor microenvironment greatly influences tumor initiation and progression, yet the mechanisms by which immune signaling drives alterations in tumor-specific gene expression programs remain unclear. Towards understanding the roles of mutant p53 in driving inflammation-induced tumorigenesis, we have identified that chronic TNF-α signaling shapes an active enhancer landscape in human colon cancer cells (Rahnamoun et al. 2017). Our analysis underscores an emerging crosstalk between chronic inflammation and the gene expression programs that are controlled by GOF *p53* mutations. Specifically, we reveal that chronic TNF-α signaling elicits a global relationship between mutant p53 and the master proinflammatory regulator, NFκB that subsequently triggers aberrant activation of pro-oncogenic enhancers and tumor-promoting genes.

4.2 Convergence of mutant p53 and NFκB in response to chronic TNF signaling

Our analyses identified that mutant p53 and NFκB directly interact with one another and regulate each other's recruitment to distinct classes of enhancers (Rahnamoun et al. 2017). Specifically, we established that in response to chronic immune signaling, mutant p53 is recruited through its associations with NFκB to a subset of enhancers that contain NFκB binding motifs. Given that the majority of p53 mutations occur within the DNA binding domain of the protein and diminish its ability to recognize WT p53 response elements (Cho et al. 1994), such

redistribution of mutant p53 to proinflammatory enhancers underscores a new GOF mechanism for this oncoprotein.

Remarkably, we also identified the expansion NFκB binding events following chronic TNF signaling at sites that are devoid of NFκB recognition motifs. This second class of enhancers display high levels of mutant p53 and ETS2, which was previously demonstrated to interact with and recruit mutant p53 (Do et al. 2012, Zhu et al. 2015). This observation revealed mutant p53's ability to expand NFκB's access to a subset of enhancers that it does not typically occupy, which extends the proinflammatory roles of NFκB in colon cancer. Notably, while we have extensively examined the mutual coordination between mutant p53 and NFκB at active enhancers in response to chronic TNF-α signaling, our genome-wide analysis point to more regulatory mechanisms at play with other TFs that include RUNX1, TEAD4, and AP1 and remain to be explored.

Importantly, the cooperative binding of mutant p53 and NFκB at enhancers promoted markedly higher levels of eRNA transcription when compared to those enhancers that were only bound by NFκB (Rahnamoun et al. 2017). Moreover, WT p53 was not identified to induce activation of pro-tumorigenic eRNAs or mRNAs in response to TNF signaling as it did not overlap with NFκB at the same category of proinflammatory enhancers that are co-occupied by mutant p53. Notably, this was consistent with our transcriptional analysis of *MMP9* and *CCL2* eRNA and mRNA levels in colorectal carcinoma tumors that harbored different mutations of *p53* relative to their paired normal tissues with WT *p53* which revealed increased expression of these nascent transcripts in mutant p53-expressing tumor samples.

Altogether, the effects of mutant p53 and NFκB on gene activation by facilitating the formation of active enhancer landscapes in response to chronic TNF-α induction is consistent with the emerging roles of this oncoprotein in coordinating inflammation-induced tumorigenesis.

A fundamental question that remains to be answered is how various p53 mutants may differentially regulate eRNA-associated gene expression programs. This question is of special significance given that various missense p53 mutants exhibit differential GOF activities which ultimately leads to distinct oncogenic lesions and phenotypes (Hanel et al. 2013, Xu et al. 2014).

4.3 Consequences of enhancer-derived transcripts on gene regulation

Given that the human genome contains hundreds of thousands of enhancers (Shlyueva, Stampfel and Stark 2014), understanding the regulation and function of these elements is a crucial goal. Intriguingly, recent advancements in the field of genomics have facilitated the identification that many enhancers also serve as transcription units that result in the generation of eRNAs (Djebali et al. 2012, Li et al. 2016, Andersson et al. 2014, Arner et al. 2015). These eRNA-producing enhancers are distinct from non-transcribing enhancers by exhibiting higher co-activator binding and enrichment of active histone marks such as H3K27ac (Melgar, Collins and Sethupathy 2011, Zhu et al. 2013), greater chromatin accessibility, and enhanced loop formation with their corresponding promoters (Sanyal et al. 2012). Notably, several studies (Bonn et al. 2012, Wang et al. 2011a, Kaikkonen et al. 2013, Bose et al. 2017, Schaukowitch et al. 2014, Mousavi et al. 2013) and recent efforts from our lab have shown that transcription of specific eRNAs promotes higher expression levels of their cognate mRNAs.

Many ncRNA-mediated regulatory events occur through the coupling of these transcripts with various factors to serve as allosteric modulators, molecular guides, or provide scaffolds for the assembly of multi-subunit complexes (Ferrè, Colantoni and Helmer-Citterich 2016, Wang and Chang 2011, Wang et al. 2008). Likewise, eRNAs have been shown to exert their functions through similar mechanisms (Hsieh et al. 2014, Li et al. 2013, Schaukowitch et al. 2014). More recently, eRNAs were shown to stimulate the HAT activity of CBP by interacting with its autoinhibitory loop region (Bose et al. 2017) which was the first indication that eRNAs play

causal roles in modulating the deposition of PTMs that give rise to an altered chromatin landscape. Since then, we have identified that eRNAs augment the engagement BRD4 with acetylated chromatin by directly interacting with the tandem bromodomains (BDs) of this epigenetic regulator (Rahnamoun et al. 2018).

4.4 Dual functionality of chromatin reader domains as RNA binding modules

Histone modifications serve as docking sites for chromatin effector proteins that specifically recognize and bind to different PTMs through unique recognition domains. Intriguingly, recent efforts to identify noncanonical RNA-associating proteins have revealed that many chromatin-associating complexes, including histone reader proteins have RNA binding capabilities (He et al. 2016, Caudron-Herger et al. 2019). Consistent with this, out of the 23 known histone reader domains to date, 6 have been shown to interact with nucleic acids (Weaver, Morrison and Musselman 2018). Most notably, chromodomains which recognize methylated histone residues have also been shown to serve as RNA binding modules (Akhtar, Zink and Becker 2000, He et al. 2016, Yap et al. 2010). Moreover, *in vitro* examination of BDs of BET family members and BRG1/human BRM demonstrated that this acetyl-binding domain also interacts with DNA (Miller et al. 2016, Morrison et al. 2017). Consistent with these, our group has further demonstrated the ability of BDs to also interact with RNAs. Yet, systematic analysis of other chromatin-associating modules is needed to uncover atypical functions of other effector domains.

Our analysis of eRNA-BD interactions included other BET family proteins as well as non-BET factors, BRG1, and BRD7 (Rahnamoun et al. 2018). Notably however, we observed differences in how much RNA was pulled down amongst various BDs which is likely due to differences in the amino acids that reside within the BD loops of these factors as well as their distinct structural and conformational features. The variability in BD interactions with eRNAs

raises the intriguing question of whether these nascent transcripts underlie differential targeting and regulation of various chromatin reader proteins by preferentially binding to a specific factor as opposed to another. This question is of great significance given that the 42 different BD containing proteins identified to date contribute to gene regulation through various mechanisms. As an example, BD-containing protein, TRIM28 associates with heterochromatin-related factors HP1 and the NuRD complex to promote chromatin compaction and transcriptional repression while other BD containing factors such as TRIM24, TRIM33, and ZMYND8 function as transcriptional co-activators (Fujisawa and Filippakopoulos 2017, Cammas et al. 2002, Tsai et al. 2010b, Malovannaya et al. 2011). Therefore, one exciting possibility is that the recruitment and/or activity of these BD-containing proteins can be modulated through their potentially variable interactions with RNAs at different loci to subsequently alter the activity state of that particular region.

Another thought-provoking question that is raised in relation to RNA contacts with chromatin associating factors is the specificity and significance of the interaction domains. The majority of chromatin-modifying and reader proteins are large, multi-subunit complexes that contain a number of catalytic and recognition domains. While recent findings regarding eRNA-BRD4 and eRNA-CBP interactions established that these associations primarily affect the function of the domain that supports eRNA binding, it can be postulated that other functions of these factors that are not directly linked to the RNA interacting domain may also be affected. For example, BRD4 phosphorylates RNAPII CTD and has been shown to exhibit HAT activity that results in deposition of the histone H3 lysine 22 acetylation (H3K122ac) mark (Devaiah et al. 2012, Devaiah et al. 2016). Thus, it would be interesting to assess whether eRNA interactions with the BDs of BRD4 would also affect its kinase or HAT activities.

Furthermore, several BD-containing factors that include CBP, BPTF, TIP5, TRIM24, TRIM33, and BAZ2B also have a histone methyl binding, plant homeodomain (PHD) finger

adjacent to their BDs (Tallant et al. 2015, Fujisawa and Filippakopoulos 2017). Investigating potential effects of BD-eRNA interactions on recognition and binding of the nearby PHD finger to methylated histone marks may reveal another layer of complexity in the bivalent recognition of histone modifications. Moreover, similar to the phenomena shown for the hMSL-3 chromobarrel which exhibits robust binding to the H4K20me1 histone peptide only in the presence DNA (Kim et al. 2010a), for factors that contain adjacent nucleic acid and histone binding domains, RNA interactions may play a critical in providing specificity in reader domain-histone tail interactions.

Lastly, given that RNAs are able to associate with intrinsically disordered regions (IDRs) of some protein complexes (Lin et al. 2015, Molliex et al. 2015, Sabari et al. 2018), investigating eRNA-mediated regulation of histone modifying and effector proteins that contain both chromatin associating and low complexity IDRs will further underscore the significance of ncRNAs in modulating gene expression programs. This will be of great significance given the recently established roles of IDRs and eRNA binding complexes in condensate formation and gene regulation (Sabari et al. 2018, Nair et al. 2019).

4.5 Future directions for characterization of eRNA functions

Given the significance of eRNA associations with a few chromatin regulatory factors, systematic identification of the interactome of these nascent RNAs through unbiased proteomic analyses will provide further mechanistic insights into their function. This analysis has the potential to not only reveal complexes that are affected by eRNAs, but also mechanisms that directly contribute to the regulation and biogenesis of these transcripts themselves.

Moreover, while we have begun to assign functional significance to eRNA molecules as independent modulators under different cellular conditions, the consequential effects of the act of enhancer transcription itself cannot be overlooked (Ling et al. 2004, Ho et al. 2006,

Mikhaylichenko et al. 2018). For example, it has been shown that in macrophages, deposition of H3K4me2 histone mark at enhancers is dependent on the act of transcription and not on the resulting eRNA transcripts (Kaikkonen et al. 2013). Currently however, a major obstacle in addressing this issue is the inability to fully uncouple the act of enhancer transcription from the direct roles of eRNAs. Thus developing complementary cell-based and reconstitution systems that would allow for dissecting the role of eRNAs independently of transcriptional events that precede their production is critical. Lastly, studies with focus on examining the consequences of eRNA length, sequence, and structure are needed to better understand the intrinsic contributions of these noncoding transcripts to gene regulation.

References

Adorno, M., M. Cordenonsi, M. Montagner, S. Dupont, C. Wong, B. Hann, A. Solari, S. Bobisse, M. B. Rondina, V. Guzzardo, A. R. Parenti, A. Rosato, S. Bicciato, A. Balmain & S. Piccolo (2009) A Mutant-p53/Smad complex opposes p63 to empower TGFbeta-induced metastasis. *Cell,* 137**,** 87-98.

Aguilera, A. & T. García-Muse (2012) R loops: from transcription byproducts to threats to genome stability. *Mol Cell,* 46**,** 115-24.

Akhtar, A., D. Zink & P. B. Becker (2000) Chromodomains are protein-RNA interaction modules. *Nature,* 407**,** 405-9.

Akhtar-Zaidi, B., R. Cowper-Sal-lari, O. Corradin, A. Saiakhova, C. F. Bartels, D. Balasubramanian, L. Myeroff, J. Lutterbaugh, A. Jarrar, M. F. Kalady, J. Willis, J. H. Moore, P. J. Tesar, T. Laframboise, S. Markowitz, M. Lupien & P. C. Scacheri (2012) Epigenomic enhancer profiling defines a signature of colon cancer. *Science,* 336**,** 736-9.

Amaral, P. P., M. E. Dinger, T. R. Mercer & J. S. Mattick (2008) The eukaryotic genome as an RNA machine. *Science,* 319**,** 1787-9.

Andersson, R., C. Gebhard, I. Miguel-Escalada, I. Hoof, J. Bornholdt, M. Boyd, Y. Chen, X. Zhao, C. Schmidl, T. Suzuki, E. Ntini, E. Arner, E. Valen, K. Li, L. Schwarzfischer, D. Glatz, J. Raithel, B. Lilje, N. Rapin, F. O. Bagger, M. Jørgensen, P. R. Andersen, N. Bertin, O. Rackham, A. M. Burroughs, J. K. Baillie, Y. Ishizu, Y. Shimizu, E. Furuhata, S. Maeda, Y. Negishi, C. J. Mungall, T. F. Meehan, T. Lassmann, M. Itoh, H. Kawaji, N. Kondo, J. Kawai, A. Lennartsson, C. O. Daub, P. Heutink, D. A. Hume, T. H. Jensen, H. Suzuki, Y. Hayashizaki, F. Müller, A. R. R. Forrest, P. Carninci, M. Rehli & A. Sandelin (2014) An atlas of active enhancers across human cell types and tissues. *Nature,* 507**,** 455-461.

Aran, D. & A. Hellman (2013) DNA methylation of transcriptional enhancers and cancer predisposition. *Cell,* 154**,** 11-3.

Aran, D., S. Sabato & A. Hellman (2013) DNA methylation of distal regulatory sites characterizes dysregulation of cancer genes. *Genome Biol,* 14**,** R21.

Arner, E., C. O. Daub, K. Vitting-Seerup, R. Andersson, B. Lilje, F. Drablos, A. Lennartsson, M. Ronnerblad, O. Hrydziuszko, M. Vitezic, T. C. Freeman, A. M. Alhendi, P. Arner, R. Axton, J. K. Baillie, A. Beckhouse, B. Bodega, J. Briggs, F. Brombacher, M. Davis, M. Detmar, A. Ehrlund, M. Endoh, A. Eslami, M. Fagiolini, L. Fairbairn, G. J. Faulkner, C. Ferrai, M. E. Fisher, L. Forrester, D. Goldowitz, R. Guler, T. Ha, M. Hara, M. Herlyn, T.

Ikawa, C. Kai, H. Kawamoto, L. M. Khachigian, S. P. Klinken, S. Kojima, H. Koseki, S. Klein, N. Mejhert, K. Miyaguchi, Y. Mizuno, M. Morimoto, K. J. Morris, C. Mummery, Y. Nakachi, S. Ogishima, M. Okada-Hatakeyama, Y. Okazaki, V. Orlando, D. Ovchinnikov, R. Passier, M. Patrikakis, A. Pombo, X. Y. Qin, S. Roy, H. Sato, S. Savvi, A. Saxena, A. Schwegmann, D. Sugiyama, R. Swoboda, H. Tanaka, A. Tomoiu, L. N. Winteringham, E. Wolvetang, C. Yanagi-Mizuochi, M. Yoneda, S. Zabierowski, P. Zhang, I. Abugessaisa, N. Bertin, A. D. Diehl, S. Fukuda, M. Furuno, J. Harshbarger, A. Hasegawa, F. Hori, S. Ishikawa-Kato, Y. Ishizu, M. Itoh, T. Kawashima, M. Kojima, N. Kondo, M. Lizio, T. F. Meehan, C. J. Mungall, M. Murata, H. Nishiyori-Sueki, S. Sahin, S. Nagao-Sato, J. Severin, M. J. de Hoon, J. Kawai, T. Kasukawa, T. Lassmann, H. Suzuki, H. Kawaji, K. M. Summers, C. Wells, FANTOM Consortium, D. A. Hume, A. R. R. Forrest, A. Sandelin, P. Carninci, Y. Hayashizaki (2015) Transcribed enhancers lead waves of coordinated transcription in transitioning mammalian cells. *Science,* 347**,** 1010-4.

Bachmann, I. M., O. J. Halvorsen, K. Collett, I. M. Stefansson, O. Straume, S. A. Haukaas, H. B. Salvesen, A. P. Otte & L. A. Akslen (2006) EZH2 expression is associated with high proliferation rate and aggressive tumor subgroups in cutaneous melanoma and cancers of the endometrium, prostate, and breast. *J Clin Oncol,* 24**,** 268-73.

Baltz, A. G., M. Munschauer, B. Schwanhäusser, A. Vasile, Y. Murakawa, M. Schueler, N. Youngs, D. Penfold-Brown, K. Drew, M. Milek, E. Wyler, R. Bonneau, M. Selbach, C. Dieterich & M. Landthaler (2012) The mRNA-bound proteome and its global occupancy profile on protein-coding transcripts. *Mol Cell,* 46**,** 674-90.

Bansal, K., H. Yoshida, C. Benoist & D. Mathis (2017) The transcriptional regulator Aire binds to and activates super-enhancers. *Nat Immunol,* 18**,** 263-273.

Baranello, L., D. Wojtowicz, K. Cui, B. N. Devaiah, H. J. Chung, K. Y. Chan-Salis, R. Guha, K. Wilson, X. Zhang, H. Zhang, J. Piotrowski, C. J. Thomas, D. S. Singer, B. F. Pugh, Y. Pommier, T. M. Przytycka, F. Kouzine, B. A. Lewis, K. Zhao & D. Levens (2016) RNA Polymerase II Regulates Topoisomerase 1 Activity to Favor Efficient Transcription. *Cell,* 165**,** 357-71.

Barish, G. D., R. T. Yu, M. Karunasiri, C. B. Ocampo, J. Dixon, C. Benner, A. L. Dent, R. K. Tangirala & R. M. Evans (2010) Bcl-6 and NF-kappaB cistromes mediate opposing regulation of the innate immune response. *Genes Dev,* 24**,** 2760-5.

Barnes, P. J. & M. Karin (1997) Nuclear factor-kappaB: a pivotal transcription factor in chronic inflammatory diseases. *N Engl J Med,* 336**,** 1066-71.

Beckerman, R. & C. Prives (2010) Transcriptional regulation by p53. *Cold Spring Harb Perspect Biol, 2***,** a000935.

Ben-Neriah, Y. & M. Karin (2011) Inflammation meets cancer, with NF-κB as the matchmaker. *Nat Immunol,* 12**,** 715-23.

Bernstein, E. & C. D. Allis (2005) RNA meets chromatin. *Genes Dev,* 19**,** 1635-55.

Biddie, S. C., S. John, P. J. Sabo, R. E. Thurman, T. A. Johnson, R. L. Schiltz, T. B. Miranda, M. H. Sung, S. Trump, S. L. Lightman, C. Vinson, J. A. Stamatoyannopoulos & G. L. Hager (2011) Transcription factor AP1 potentiates chromatin accessibility and glucocorticoid receptor binding. *Mol Cell,* 43**,** 145-55.

Bonizzi, G. & M. Karin (2004) The two NF-kappaB activation pathways and their role in innate and adaptive immunity. *Trends Immunol,* 25**,** 280-8.

Bonn, S., R. P. Zinzen, C. Girardot, E. H. Gustafson, A. Perez-Gonzalez, N. Delhomme, Y. Ghavi-Helm, B. Wilczynski, A. Riddell & E. E. Furlong (2012) Tissue-specific analysis of chromatin state identifies temporal signatures of enhancer activity during embryonic development. *Nat Genet,* 44**,** 148-56.

Borodina, T., J. Adjaye & M. Sultan (2011) A strand-specific library preparation protocol for RNA sequencing. *Methods Enzymol,* 500**,** 79-98.

Bose, D. A., G. Donahue, D. Reinberg, R. Shiekhattar, R. Bonasio & S. L. Berger (2017) RNA Binding to CBP Stimulates Histone Acetylation and Transcription. *Cell,* 168**,** 135-149.e22.

Bougeard, G., R. Sesboüé, S. Baert-Desurmont, S. Vasseur, C. Martin, J. Tinat, L. Brugières, A. Chompret, B. B. de Paillerets, D. Stoppa-Lyonnet, C. Bonaïti-Pellié, T. Frébourg & F. L. w. group (2008) Molecular basis of the Li-Fraumeni syndrome: an update from the French LFS families. *J Med Genet,* 45**,** 535-8.

Boulon, S., B. J. Westman, S. Hutten, F. M. Boisvert & A. I. Lamond (2010) The nucleolus under stress. *Mol Cell,* 40**,** 216-27.

Bowen, C., A. Stuart, J. H. Ju, J. Tuan, J. Blonder, T. P. Conrads, T. D. Veenstra & E. P. Gelmann (2007) NKX3.1 homeodomain protein binds to topoisomerase I and enhances its activity. *Cancer Res,* 67**,** 455-64.

Brill, S. J., S. DiNardo, K. Voelkel-Meiman & R. Sternglanz (1987) Need for DNA topoisomerase activity as a swivel for DNA replication for transcription of ribosomal RNA. *Nature,* 326**,** 414-6.

Brogna, S., T. A. Sato & M. Rosbash (2002) Ribosome components are associated with sites of transcription. *Mol Cell,* 10**,** 93-104.

Cammas, F., M. Oulad-Abdelghani, J. L. Vonesch, Y. Huss-Garcia, P. Chambon & R. Losson (2002) Cell differentiation induces TIF1beta association with centromeric heterochromatin via an HP1 interaction. *J Cell Sci,* 115**,** 3439-48.

Cassiday, L. A. & L. J. Maher (2002) Having it both ways: transcription factors that bind DNA and RNA. *Nucleic Acids Res,* 30**,** 4118-26.

Castello, A., B. Fischer, K. Eichelbaum, R. Horos, B. M. Beckmann, C. Strein, N. E. Davey, D. T. Humphreys, T. Preiss, L. M. Steinmetz, J. Krijgsveld & M. W. Hentze (2012) Insights into RNA biology from an atlas of mammalian mRNA-binding proteins. *Cell,* 149**,** 1393-406.

Caudron-Herger, M., S. F. Rusin, M. E. Adamo, J. Seiler, V. K. Schmid, E. Barreau, A. N. Kettenbach & S. Diederichs (2019) R-DeeP: Proteome-wide and Quantitative Identification of RNA-Dependent Proteins by Density Gradient Ultracentrifugation. *Mol Cell,* 75**,** 184-199.e10.

Champoux, J. J. (2001) DNA topoisomerases: structure, function, and mechanism. *Annu Rev Biochem,* 70**,** 369-413.

Chepelev, I., G. Wei, D. Wangsa, Q. Tang & K. Zhao (2012) Characterization of genome-wide enhancer-promoter interactions reveals co-expression of interacting genes and modes of higher order chromatin organization. *Cell Res,* 22**,** 490-503.

Cho, Y., S. Gorina, P. D. Jeffrey & N. P. Pavletich (1994) Crystal structure of a p53 tumor suppressor-DNA complex: understanding tumorigenic mutations. *Science,* 265**,** 346-55.

Ciavarra, R. P., C. Goldman, K. K. Wen, B. Tedeschi & F. J. Castora (1994) Heat stress induces hsc70/nuclear topoisomerase I complex formation in vivo: evidence for hsc70-mediated, ATP-independent reactivation in vitro. *Proc Natl Acad Sci U S A,* 91**,** 1751-5.

Cooks, T., I. S. Pateras, L. M. Jenkins, K. M. Patel, A. I. Robles, J. Morris, T. Forshew, E. Appella, V. G. Gorgoulis & C. C. Harris (2018) Mutant p53 cancers reprogram macrophages to tumor supporting macrophages via exosomal miR-1246. *Nat Commun,* 9**,** 771.

Cooks, T., I. S. Pateras, O. Tarcic, H. Solomon, A. J. Schetter, S. Wilder, G. Lozano, E. Pikarsky, T. Forshew, N. Rosenfeld, N. Rozenfeld, N. Harpaz, S. Itzkowitz, C. C. Harris, V. Rotter, V. G. Gorgoulis & M. Oren (2013) Mutant p53 prolongs NF-κB activation and promotes chronic inflammation and inflammation-associated colorectal cancer. *Cancer Cell,* 23**,** 634-46.

Core, L. J., J. J. Waterfall & J. T. Lis (2008) Nascent RNA sequencing reveals widespread pausing and divergent initiation at human promoters. *Science,* 322**,** 1845-8.

Creyghton, M. P., A. W. Cheng, G. G. Welstead, T. Kooistra, B. W. Carey, E. J. Steine, J. Hanna, M. A. Lodato, G. M. Frampton, P. A. Sharp, L. A. Boyer, R. A. Young & R. Jaenisch (2010) Histone H3K27ac separates active from poised enhancers and predicts developmental state. *Proc Natl Acad Sci U S A,* 107**,** 21931-6.

Dawson, M. A. & T. Kouzarides (2012) Cancer epigenetics: from mechanism to therapy. *Cell,* 150**,** 12-27.

Dawson, M. A., R. K. Prinjha, A. Dittmann, G. Giotopoulos, M. Bantscheff, W. I. Chan, S. C. Robson, C. W. Chung, C. Hopf, M. M. Savitski, C. Huthmacher, E. Gudgin, D. Lugo, S. Beinke, T. D. Chapman, E. J. Roberts, P. E. Soden, K. R. Auger, O. Mirguet, K. Doehner, R. Delwel, A. K. Burnett, P. Jeffrey, G. Drewes, K. Lee, B. J. Huntly & T. Kouzarides (2011) Inhibition of BET recruitment to chromatin as an effective treatment for MLL-fusion leukaemia. *Nature,* 478**,** 529-33.

De, S., A. L. Wurster, P. Precht, W. H. Wood, K. G. Becker & M. J. Pazin (2011) Dynamic BRG1 recruitment during T helper differentiation and activation reveals distal regulatory elements. *Mol Cell Biol,* 31**,** 1512-27.

De Santa, F., I. Barozzi, F. Mietton, S. Ghisletti, S. Polletti, B. K. Tusi, H. Muller, J. Ragoussis, C. L. Wei & G. Natoli (2010) A large fraction of extragenic RNA pol II transcription sites overlap enhancers. *PLoS Biol,* 8**,** e1000384.

Delmore, J. E., G. C. Issa, M. E. Lemieux, P. B. Rahl, J. Shi, H. M. Jacobs, E. Kastritis, T. Gilpatrick, R. M. Paranal, J. Qi, M. Chesi, A. C. Schinzel, M. R. McKeown, T. P. Heffernan, C. R. Vakoc, P. L. Bergsagel, I. M. Ghobrial, P. G. Richardson, R. A. Young, W. C. Hahn, K. C. Anderson, A. L. Kung, J. E. Bradner & C. S. Mitsiades (2011) BET bromodomain inhibition as a therapeutic strategy to target c-Myc. *Cell,* 146**,** 904-17.

Demaria, S., E. Pikarsky, M. Karin, L. M. Coussens, Y. C. Chen, E. M. El-Omar, G. Trinchieri, S. M. Dubinett, J. T. Mao, E. Szabo, A. Krieg, G. J. Weiner, B. A. Fox, G. Coukos, E. Wang, R. T. Abraham, M. Carbone & M. T. Lotze (2010) Cancer and inflammation: promise for biologic therapy. *J Immunother,* 33**,** 335-51.

DeNardo, D. G., P. Andreu & L. M. Coussens (2010) Interactions between lymphocytes and myeloid cells regulate pro- versus anti-tumor immunity. *Cancer Metastasis Rev,* 29**,** 309-16.

Devaiah, B. N., C. Case-Borden, A. Gegonne, C. H. Hsu, Q. Chen, D. Meerzaman, A. Dey, K. Ozato & D. S. Singer (2016) BRD4 is a histone acetyltransferase that evicts nucleosomes from chromatin. *Nat Struct Mol Biol,* 23**,** 540-8.

Devaiah, B. N., B. A. Lewis, N. Cherman, M. C. Hewitt, B. K. Albrecht, P. G. Robey, K. Ozato, R. J. Sims & D. S. Singer (2012) BRD4 is an atypical kinase that phosphorylates serine2 of the RNA polymerase II carboxy-terminal domain. *Proc Natl Acad Sci U S A,* 109**,** 6927-32.

Di Agostino, S., S. Strano, V. Emiliozzi, V. Zerbini, M. Mottolese, A. Sacchi, G. Blandino & G. Piaggio (2006) Gain of function of mutant p53: the mutant p53/NF-Y protein complex reveals an aberrant transcriptional mechanism of cell cycle regulation. *Cancer Cell,* 10**,** 191-202.

Di Minin, G., A. Bellazzo, M. Dal Ferro, G. Chiaruttini, S. Nuzzo, S. Bicciato, S. Piazza, D. Rami, R. Bulla, R. Sommaggio, A. Rosato, G. Del Sal & L. Collavin (2014) Mutant p53 reprograms TNF signaling in cancer cells through interaction with the tumor suppressor DAB2IP. *Mol Cell,* 56**,** 617-29.

Dittmer, D., S. Pati, G. Zambetti, S. Chu, A. K. Teresky, M. Moore, C. Finlay & A. J. Levine (1993) Gain of function mutations in p53. *Nat Genet,* 4**,** 42-6.

Djebali, S., C. A. Davis, A. Merkel, A. Dobin, T. Lassmann, A. Mortazavi, A. Tanzer, J. Lagarde, W. Lin, F. Schlesinger, C. Xue, G. K. Marinov, J. Khatun, B. A. Williams, C. Zaleski, J. Rozowsky, M. Röder, F. Kokocinski, R. F. Abdelhamid, T. Alioto, I. Antoshechkin, M. T. Baer, N. S. Bar, P. Batut, K. Bell, I. Bell, S. Chakrabortty, X. Chen, J. Chrast, J. Curado, T. Derrien, J. Drenkow, E. Dumais, J. Dumais, R. Duttagupta, E. Falconnet, M. Fastuca, K. Fejes-Toth, P. Ferreira, S. Foissac, M. J. Fullwood, H. Gao, D. Gonzalez, A. Gordon, H. Gunawardena, C. Howald, S. Jha, R. Johnson, P. Kapranov, B. King, C. Kingswood, O. J. Luo, E. Park, K. Persaud, J. B. Preall, P. Ribeca, B. Risk, D. Robyr, M. Sammeth, L. Schaffer, L. H. See, A. Shahab, J. Skancke, A. M. Suzuki, H. Takahashi, H. Tilgner, D. Trout, N. Walters, H. Wang, J. Wrobel, Y. Yu, X. Ruan, Y. Hayashizaki, J. Harrow, M. Gerstein, T. Hubbard, A. Reymond, S. E. Antonarakis, G. Hannon, M. C. Giddings, Y. Ruan, B. Wold, P. Carninci, R. Guigó & T. R. Gingeras (2012) Landscape of transcription in human cells. *Nature,* 489**,** 101-8.

Do, P. M., L. Varanasi, S. Fan, C. Li, I. Kubacka, V. Newman, K. Chauhan, S. R. Daniels, M. Boccetta, M. R. Garrett, R. Li & L. A. Martinez (2012) Mutant p53 cooperates with ETS2 to promote etoposide resistance. *Genes Dev,* 26**,** 830-45.

Dobin, A., C. A. Davis, F. Schlesinger, J. Drenkow, C. Zaleski, S. Jha, P. Batut, M. Chaisson & T. R. Gingeras (2013) STAR: ultrafast universal RNA-seq aligner. *Bioinformatics,* 29**,** 15-21.

Doyle, B., J. P. Morton, D. W. Delaney, R. A. Ridgway, J. A. Wilkins & O. J. Sansom (2010) p53 mutation and loss have different effects on tumourigenesis in a novel mouse model of pleomorphic rhabdomyosarcoma. *J Pathol,* 222**,** 129-37.

Durand-Dubief, M., J. Persson, U. Norman, E. Hartsuiker & K. Ekwall (2010) Topoisomerase I regulates open chromatin and controls gene expression in vivo. *EMBO J,* 29**,** 2126-34.

Durand-Dubief, M., J. P. Svensson, J. Persson & K. Ekwall (2011) Topoisomerases, chromatin and transcription termination. *Transcription,* 2**,** 66-70.

El Hage, A., S. L. French, A. L. Beyer & D. Tollervey (2010) Loss of Topoisomerase I leads to R-loop-mediated transcriptional blocks during ribosomal RNA synthesis. *Genes Dev,* 24**,** 1546-58.

Feric, M., N. Vaidya, T. S. Harmon, D. M. Mitrea, L. Zhu, T. M. Richardson, R. W. Kriwacki, R. V. Pappu & C. P. Brangwynne (2016) Coexisting Liquid Phases Underlie Nucleolar Subcompartments. *Cell,* 165**,** 1686-1697.

Ferrè, F., A. Colantoni & M. Helmer-Citterich (2016) Revealing protein-lncRNA interaction. *Brief Bioinform,* 17**,** 106-16.

Filippakopoulos, P., J. Qi, S. Picaud, Y. Shen, W. B. Smith, O. Fedorov, E. M. Morse, T. Keates, T. T. Hickman, I. Felletar, M. Philpott, S. Munro, M. R. McKeown, Y. Wang, A. L. Christie, N. West, M. J. Cameron, B. Schwartz, T. D. Heightman, N. La Thangue, C. A. French, O. Wiest, A. L. Kung, S. Knapp & J. E. Bradner (2010) Selective inhibition of BET bromodomains. *Nature,* 468**,** 1067-73.

Freed-Pastor, W. A. & C. Prives (2012) Mutant p53: one name, many proteins. *Genes Dev,* 26**,** 1268-86.

Frottin, F., F. Schueder, S. Tiwary, R. Gupta, R. Körner, T. Schlichthaerle, J. Cox, R. Jungmann, F. U. Hartl & M. S. Hipp (2019) The nucleolus functions as a phase-separated protein quality control compartment. *Science,* 365**,** 342-347.

Fujisawa, T. & P. Filippakopoulos (2017) Functions of bromodomain-containing proteins and their roles in homeostasis and cancer. *Nat Rev Mol Cell Biol,* 18**,** 246-262.

Gaiddon, C., M. Lokshin, J. Ahn, T. Zhang & C. Prives (2001) A subset of tumor-derived mutant forms of p53 down-regulate p63 and p73 through a direct interaction with the p53 core domain. *Mol Cell Biol,* 21**,** 1874-87.

Giffard, R. G., R. Q. Han, J. F. Emery, M. Duan & J. F. Pittet (2008) Regulation of apoptotic and inflammatory cell signaling in cerebral ischemia: the complex roles of heat shock protein 70. *Anesthesiology,* 109**,** 339-48.

Gilmore, T. D. & M. Herscovitch (2006) Inhibitors of NF-kappaB signaling: 785 and counting. *Oncogene,* 25**,** 6887-99.

Girardini, J. E., M. Napoli, S. Piazza, A. Rustighi, C. Marotta, E. Radaelli, V. Capaci, L. Jordan, P. Quinlan, A. Thompson, M. Mano, A. Rosato, T. Crook, E. Scanziani, A. R. Means, G. Lozano, C. Schneider & G. Del Sal (2011) A Pin1/mutant p53 axis promotes aggressiveness in breast cancer. *Cancer Cell,* 20**,** 79-91.

Goldberg, A. D., C. D. Allis & E. Bernstein (2007) Epigenetics: a landscape takes shape. *Cell,* 128**,** 635-8.

Gonzales, B., D. Henning, R. B. So, J. Dixon, M. J. Dixon & B. C. Valdez (2005) The Treacher Collins syndrome (TCOF1) gene product is involved in pre-rRNA methylation. *Hum Mol Genet,* 14**,** 2035-43.

Goswami, A., S. Qiu, T. S. Dexheimer, P. Ranganathan, R. Burikhanov, Y. Pommier & V. M. Rangnekar (2008) Par-4 binds to topoisomerase 1 and attenuates its DNA relaxation activity. *Cancer Res,* 68**,** 6190-8.

Grisanzio, C. & M. L. Freedman (2010) Chromosome 8q24-Associated Cancers and MYC. *Genes Cancer,* 1**,** 555-9.

Grivennikov, S. I., F. R. Greten & M. Karin (2010) Immunity, inflammation, and cancer. *Cell,* 140**,** 883-99.

Guttman, M., G. N. Betts, H. Barnes, M. Ghassemian, P. van der Geer & E. A. Komives (2009) Interactions of the NPXY microdomains of the low density lipoprotein receptor-related protein 1. *Proteomics,* 9**,** 5016-28.

Hah, N., C. G. Danko, L. Core, J. J. Waterfall, A. Siepel, J. T. Lis & W. L. Kraus (2011) A rapid, extensive, and transient transcriptional response to estrogen signaling in breast cancer cells. *Cell,* 145**,** 622-34.

Hanahan, D. & R. A. Weinberg (2011) Hallmarks of cancer: the next generation. *Cell,* 144**,** 646-74.

Hanel, W., N. Marchenko, S. Xu, S. X. Yu, W. Weng & U. Moll (2013) Two hot spot mutant p53 mouse models display differential gain of function in tumorigenesis. *Cell Death Differ,* 20**,** 898-909.

Hayano, T., M. Yanagida, Y. Yamauchi, T. Shinkawa, T. Isobe & N. Takahashi (2003) Proteomic analysis of human Nop56p-associated pre-ribosomal ribonucleoprotein complexes. Possible link between Nop56p and the nucleolar protein treacle responsible for Treacher Collins syndrome. *J Biol Chem,* 278**,** 34309-19.

He, C., S. Sidoli, R. Warneford-Thomson, D. C. Tatomer, J. E. Wilusz, B. A. Garcia & R. Bonasio (2016) High-Resolution Mapping of RNA-Binding Regions in the Nuclear Proteome of Embryonic Stem Cells. *Mol Cell,* 64**,** 416-430.

Heintzman, N. D., G. C. Hon, R. D. Hawkins, P. Kheradpour, A. Stark, L. F. Harp, Z. Ye, L. K. Lee, R. K. Stuart, C. W. Ching, K. A. Ching, J. E. Antosiewicz-Bourget, H. Liu, X. Zhang, R. D. Green, V. V. Lobanenkov, R. Stewart, J. A. Thomson, G. E. Crawford, M. Kellis & B. Ren (2009) Histone modifications at human enhancers reflect global cell-type-specific gene expression. *Nature,* 459**,** 108-12.

Heintzman, N. D., R. K. Stuart, G. Hon, Y. Fu, C. W. Ching, R. D. Hawkins, L. O. Barrera, S. Van Calcar, C. Qu, K. A. Ching, W. Wang, Z. Weng, R. D. Green, G. E. Crawford & B. Ren (2007) Distinct and predictive chromatin signatures of transcriptional promoters and enhancers in the human genome. *Nat Genet,* 39**,** 311-8.

Heinz, S., C. Benner, N. Spann, E. Bertolino, Y. C. Lin, P. Laslo, J. X. Cheng, C. Murre, H. Singh & C. K. Glass (2010) Simple combinations of lineage-determining transcription factors prime cis-regulatory elements required for macrophage and B cell identities. *Mol Cell,* 38**,** 576-89.

Heinz, S., C. E. Romanoski, C. Benner & C. K. Glass (2015) The selection and function of cell type-specific enhancers. *Nat Rev Mol Cell Biol,* 16**,** 144-54.

Herz, H. M. (2016) Enhancer deregulation in cancer and other diseases. *Bioessays,* 38**,** 1003-15.

Hnisz, D., B. J. Abraham, T. I. Lee, A. Lau, V. Saint-André, A. A. Sigova, H. A. Hoke & R. A. Young (2013) Super-enhancers in the control of cell identity and disease. *Cell,* 155**,** 934-47.

Ho, Y., F. Elefant, S. A. Liebhaber & N. E. Cooke (2006) Locus control region transcription plays an active role in long-range gene activation. *Mol Cell,* 23**,** 365-75.

Hsieh, C. L., T. Fei, Y. Chen, T. Li, Y. Gao, X. Wang, T. Sun, C. J. Sweeney, G. S. Lee, S. Chen, S. P. Balk, X. S. Liu, M. Brown & P. W. Kantoff (2014) Enhancer RNAs participate in androgen receptor-driven looping that selectively enhances gene activation. *Proc Natl Acad Sci U S A,* 111**,** 7319-24.

Huang, Q., T. Whitington, P. Gao, J. F. Lindberg, Y. Yang, J. Sun, M. R. Väisänen, R. Szulkin, M. Annala, J. Yan, L. A. Egevad, K. Zhang, R. Lin, A. Jolma, M. Nykter, A. Manninen, F. Wiklund, M. H. Vaarala, T. Visakorpi, J. Xu, J. Taipale & G. H. Wei (2014) A prostate cancer susceptibility allele at 6q22 increases RFX6 expression by modulating HOXB13 chromatin binding. *Nat Genet,* 46**,** 126-35.

Huang, W. C., T. K. Ju, M. C. Hung & C. C. Chen (2007) Phosphorylation of CBP by IKKalpha promotes cell growth by switching the binding preference of CBP from p53 to NF-kappaB. *Mol Cell,* 26**,** 75-87.

Jeong, K. W., K. Kim, A. J. Situ, T. S. Ulmer, W. An & M. R. Stallcup (2011) Recognition of enhancer element-specific histone methylation by TIP60 in transcriptional activation. *Nat Struct Mol Biol,* 18**,** 1358-65.

John, S., P. J. Sabo, R. E. Thurman, M. H. Sung, S. C. Biddie, T. A. Johnson, G. L. Hager & J. A. Stamatoyannopoulos (2011) Chromatin accessibility pre-determines glucocorticoid receptor binding patterns. *Nat Genet,* 43**,** 264-8.

Kaikkonen, M. U., N. J. Spann, S. Heinz, C. E. Romanoski, K. A. Allison, J. D. Stender, H. B. Chun, D. F. Tough, R. K. Prinjha, C. Benner & C. K. Glass (2013) Remodeling of the enhancer landscape during macrophage activation is coupled to enhancer transcription. *Mol Cell,* 51**,** 310-25.

Kalo, E., I. Kogan-Sakin, H. Solomon, E. Bar-Nathan, M. Shay, Y. Shetzer, E. Dekel, N. Goldfinger, Y. Buganim, P. Stambolsky, I. Goldstein, S. Madar & V. Rotter (2012) Mutant p53R273H attenuates the expression of phase 2 detoxifying enzymes and promotes the survival of cells with high levels of reactive oxygen species. *J Cell Sci,* 125**,** 5578-86.

Kandoth, C., M. D. McLellan, F. Vandin, K. Ye, B. Niu, C. Lu, M. Xie, Q. Zhang, J. F. McMichael, M. A. Wyczalkowski, M. D. M. Leiserson, C. A. Miller, J. S. Welch, M. J. Walter, M. C. Wendl, T. J. Ley, R. K. Wilson, B. J. Raphael & L. Ding (2013) Mutational landscape and significance across 12 major cancer types. *Nature,* 502**,** 333-339.

Karayan, L., J. F. Riou, P. Séité, J. Migeon, A. Cantereau & C. J. Larsen (2001) Human ARF protein interacts with topoisomerase I and stimulates its activity. *Oncogene,* 20**,** 836-48.

Karnoub, A. E. & R. A. Weinberg (2006) Chemokine networks and breast cancer metastasis. *Breast Dis,* 26**,** 75-85.

Kashatus, D., P. Cogswell & A. S. Baldwin (2006) Expression of the Bcl-3 proto-oncogene suppresses p53 activation. *Genes Dev,* 20**,** 225-35.

Kim, D., B. J. Blus, V. Chandra, P. Huang, F. Rastinejad & S. Khorasanizadeh (2010a) Corecognition of DNA and a methylated histone tail by the MSL3 chromodomain. *Nat Struct Mol Biol,* 17**,** 1027-9.

Kim, T. K., M. Hemberg, J. M. Gray, A. M. Costa, D. M. Bear, J. Wu, D. A. Harmin, M. Laptewicz, K. Barbara-Haley, S. Kuersten, E. Markenscoff-Papadimitriou, D. Kuhl, H. Bito, P. F. Worley, G. Kreiman & M. E. Greenberg (2010b) Widespread transcription at neuronal activity-regulated enhancers. *Nature,* 465**,** 182-7.

Knoechel, B., J. E. Roderick, K. E. Williamson, J. Zhu, J. G. Lohr, M. J. Cotton, S. M. Gillespie, D. Fernandez, M. Ku, H. Wang, F. Piccioni, S. J. Silver, M. Jain, D. Pearson, M. J. Kluk, C. J. Ott, L. D. Shultz, M. A. Brehm, D. L. Greiner, A. Gutierrez, K. Stegmaier, A. L. Kung, D. E. Root, J. E. Bradner, J. C. Aster, M. A. Kelliher & B. E. Bernstein (2014) An epigenetic mechanism of resistance to targeted therapy in T cell acute lymphoblastic leukemia. *Nat Genet,* 46**,** 364-70.

Kogo, R., T. Shimamura, K. Mimori, K. Kawahara, S. Imoto, T. Sudo, F. Tanaka, K. Shibata, A. Suzuki, S. Komune, S. Miyano & M. Mori (2011) Long noncoding RNA HOTAIR regulates polycomb-dependent chromatin modification and is associated with poor prognosis in colorectal cancers. *Cancer Res,* 71**,** 6320-6.

Kouzarides, T. (2007) Chromatin modifications and their function. *Cell,* 128**,** 693-705.

Kouzine, F., A. Gupta, L. Baranello, D. Wojtowicz, K. Ben-Aissa, J. Liu, T. M. Przytycka & D. Levens (2013) Transcription-dependent dynamic supercoiling is a short-range genomic force. *Nat Struct Mol Biol,* 20**,** 396-403.

Kretzschmar, M., M. Meisterernst & R. G. Roeder (1993) Identification of human DNA topoisomerase I as a cofactor for activator-dependent transcription by RNA polymerase II. *Proc Natl Acad Sci U S A,* 90**,** 11508-12.

Krogan, N. J., M. Kim, S. H. Ahn, G. Zhong, M. S. Kobor, G. Cagney, A. Emili, A. Shilatifard, S. Buratowski & J. F. Greenblatt (2002) RNA polymerase II elongation factors of Saccharomyces cerevisiae: a targeted proteomics approach. *Mol Cell Biol,* 22**,** 6979-92.

Lafontaine, D. & D. Tollervey (1995) Trans-acting factors in yeast pre-rRNA and pre-snoRNA processing. *Biochem Cell Biol,* 73**,** 803-12.

Lam, Y. W., L. Trinkle-Mulcahy & A. I. Lamond (2005) The nucleolus. *J Cell Sci,* 118**,** 1335-7.

Lang, G. A., T. Iwakuma, Y. A. Suh, G. Liu, V. A. Rao, J. M. Parant, Y. A. Valentin-Vega, T. Terzian, L. C. Caldwell, L. C. Strong, A. K. El-Naggar & G. Lozano (2004) Gain of function of a p53 hot spot mutation in a mouse model of Li-Fraumeni syndrome. *Cell,* 119**,** 861-72.

Langmead, B. & S. L. Salzberg (2012) Fast gapped-read alignment with Bowtie 2. *Nat Methods,* 9**,** 357-9.

Lanza, A., S. Tornaletti, C. Rodolfo, M. C. Scanavini & A. M. Pedrini (1996) Human DNA topoisomerase I-mediated cleavages stimulated by ultraviolet light-induced DNA damage. *J Biol Chem,* 271**,** 6978-86.

Lauberth, S. M., A. C. Bilyeu, B. A. Firulli, K. L. Kroll & M. Rauchman (2007) A phosphomimetic mutation in the Sall1 repression motif disrupts recruitment of the nucleosome remodeling and deacetylase complex and repression of Gbx2. *J Biol Chem,* 282**,** 34858-68.

Lee, D. H. & A. L. Goldberg (1998) Proteasome inhibitors: valuable new tools for cell biologists. *Trends Cell Biol,* 8**,** 397-403.

Lee, J. S., E. Smith & A. Shilatifard (2010) The language of histone crosstalk. *Cell,* 142**,** 682-5.

Lefterova, M. I., D. J. Steger, D. Zhuo, M. Qatanani, S. E. Mullican, G. Tuteja, E. Manduchi, G. R. Grant & M. A. Lazar (2010) Cell-specific determinants of peroxisome proliferator-activated receptor gamma function in adipocytes and macrophages. *Mol Cell Biol,* 30**,** 2078-89.

Leroy, B., J. L. Fournier, C. Ishioka, P. Monti, A. Inga, G. Fronza & T. Soussi (2013) The TP53 website: an integrative resource centre for the TP53 mutation database and TP53 mutant analysis. *Nucleic Acids Res,* 41**,** D962-9.

Li, M., S. Pokharel, J. T. Wang, X. Xu & Y. Liu (2015a) RECQ5-dependent SUMOylation of DNA topoisomerase I prevents transcription-associated genome instability. *Nat Commun,* 6**,** 6720.

Li, W., D. Notani, Q. Ma, B. Tanasa, E. Nunez, A. Y. Chen, D. Merkurjev, J. Zhang, K. Ohgi, X. Song, S. Oh, H. S. Kim, C. K. Glass & M. G. Rosenfeld (2013) Functional roles of enhancer RNAs for oestrogen-dependent transcriptional activation. *Nature,* 498**,** 516-20.

Li, W., D. Notani & M. G. Rosenfeld (2016) Enhancers as non-coding RNA transcription units: recent insights and future perspectives. *Nat Rev Genet,* 17**,** 207-23.

Li, X., W. Wang, J. Wang, A. Malovannaya, Y. Xi, W. Li, R. Guerra, D. H. Hawke, J. Qin & J. Chen (2015b) Proteomic analyses reveal distinct chromatin-associated and soluble transcription factor complexes. *Mol Syst Biol,* 11**,** 775.

Li, X. Y., S. Thomas, P. J. Sabo, M. B. Eisen, J. A. Stamatoyannopoulos & M. D. Biggin (2011) The role of chromatin accessibility in directing the widespread, overlapping patterns of Drosophila transcription factor binding. *Genome Biol,* 12**,** R34.

Liccardi, G., J. A. Hartley & D. Hochhauser (2014) Importance of EGFR/ERCC1 interaction following radiation-induced DNA damage. *Clin Cancer Res,* 20**,** 3496-506.

Lin, Y., D. S. Protter, M. K. Rosen & R. Parker (2015) Formation and Maturation of Phase-Separated Liquid Droplets by RNA-Binding Proteins. *Mol Cell,* 60**,** 208-19.

Lindström, M. S. (2011) NPM1/B23: A Multifunctional Chaperone in Ribosome Biogenesis and Chromatin Remodeling. *Biochem Res Int,* 2011**,** 195209.

Ling, J., L. Ainol, L. Zhang, X. Yu, W. Pi & D. Tuan (2004) HS2 enhancer function is blocked by a transcriptional terminator inserted between the enhancer and the promoter. *J Biol Chem,* 279**,** 51704-13.

Liu, L. F. & J. C. Wang (1987) Supercoiling of the DNA template during transcription. *Proc Natl Acad Sci U S A,* 84**,** 7024-7.

Livak, K. J. & T. D. Schmittgen (2001) Analysis of relative gene expression data using real-time quantitative PCR and the 2(-Delta Delta C(T)) Method. *Methods,* 25**,** 402-8.

Luger, K., A. W. Mäder, R. K. Richmond, D. F. Sargent & T. J. Richmond (1997) Crystal structure of the nucleosome core particle at 2.8 A resolution. *Nature,* 389**,** 251-60.

Ma, J., L. Bai & M. D. Wang (2013) Transcription under torsion. *Science,* 340**,** 1580-3.

Magnani, L., A. Stoeck, X. Zhang, A. Lánczky, A. C. Mirabella, T. L. Wang, B. Gyorffy & M. Lupien (2013) Genome-wide reprogramming of the chromatin landscape underlies endocrine therapy resistance in breast cancer. *Proc Natl Acad Sci U S A,* 110**,** E1490-9.

Mahat, D. B., H. Kwak, G. T. Booth, I. H. Jonkers, C. G. Danko, R. K. Patel, C. T. Waters, K. Munson, L. J. Core & J. T. Lis (2016) Base-pair-resolution genome-wide mapping of active RNA polymerases using precision nuclear run-on (PRO-seq). *Nat Protoc,* 11**,** 1455-76.

Malovannaya, A., R. B. Lanz, S. Y. Jung, Y. Bulynko, N. T. Le, D. W. Chan, C. Ding, Y. Shi, N. Yucer, G. Krenciute, B. J. Kim, C. Li, R. Chen, W. Li, Y. Wang, B. W. O'Malley & J. Qin (2011) Analysis of the human endogenous coregulator complexome. *Cell,* 145**,** 787-99.

Mao, Y., S. Okada, L. S. Chang & M. T. Muller (2000) p53 dependence of topoisomerase I recruitment in vivo. *Cancer Res,* 60**,** 4538-43.

McCormack, A. L., D. M. Schieltz, B. Goode, S. Yang, G. Barnes, D. Drubin & J. R. Yates (1997) Direct analysis and identification of proteins in mixtures by LC/MS/MS and database searching at the low-femtomole level. *Anal Chem,* 69**,** 767-76.

Melgar, M. F., F. S. Collins & P. Sethupathy (2011) Discovery of active enhancers through bidirectional expression of short transcripts. *Genome Biol,* 12**,** R113.

Merino, A., K. R. Madden, W. S. Lane, J. J. Champoux & D. Reinberg (1993) DNA topoisomerase I is involved in both repression and activation of transcription. *Nature,* 365**,** 227-32.

Mikhaylichenko, O., V. Bondarenko, D. Harnett, I. E. Schor, M. Males, R. R. Viales & E. E. M. Furlong (2018) The degree of enhancer or promoter activity is reflected by the levels and directionality of eRNA transcription. *Genes Dev,* 32**,** 42-57.

Miller, T. C., B. Simon, V. Rybin, H. Grotsch, S. Curtet, S. Khochbin, T. Carlomagno & C. W. Muller (2016) A bromodomain-DNA interaction facilitates acetylation-dependent bivalent nucleosome recognition by the BET protein BRDT. *Nat Commun,* 7**,** 13855.

Mitrea, D. M., J. A. Cika, C. B. Stanley, A. Nourse, P. L. Onuchic, P. R. Banerjee, A. H. Phillips, C. G. Park, A. A. Deniz & R. W. Kriwacki (2018) Self-interaction of NPM1 modulates multiple mechanisms of liquid-liquid phase separation. *Nat Commun,* 9**,** 842.

Molliex, A., J. Temirov, J. Lee, M. Coughlin, A. P. Kanagaraj, H. J. Kim, T. Mittag & J. P. Taylor (2015) Phase separation by low complexity domains promotes stress granule assembly and drives pathological fibrillization. *Cell,* 163**,** 123-33.

Morin, R. D., M. Mendez-Lago, A. J. Mungall, R. Goya, K. L. Mungall, R. D. Corbett, N. A. Johnson, T. M. Severson, R. Chiu, M. Field, S. Jackman, M. Krzywinski, D. W. Scott, D. L. Trinh, J. Tamura-Wells, S. Li, M. R. Firme, S. Rogic, M. Griffith, S. Chan, O. Yakovenko, I. M. Meyer, E. Y. Zhao, D. Smailus, M. Moksa, S. Chittaranjan, L. Rimsza, A. Brooks-Wilson, J. J. Spinelli, S. Ben-Neriah, B. Meissner, B. Woolcock, M. Boyle, H. McDonald, A. Tam, Y. Zhao, A. Delaney, T. Zeng, K. Tse, Y. Butterfield, I. Birol, R. Holt, J. Schein, D. E. Horsman, R. Moore, S. J. Jones, J. M. Connors, M. Hirst, R. D. Gascoyne & M. A. Marra (2011) Frequent mutation of histone-modifying genes in non-Hodgkin lymphoma. *Nature,* 476**,** 298-303.

Morrison, E. A., J. C. Sanchez, J. L. Ronan, D. P. Farrell, K. Varzavand, J. K. Johnson, B. X. Gu, G. R. Crabtree & C. A. Musselman (2017) DNA binding drives the association of BRG1/hBRM bromodomains with nucleosomes. *Nat Commun,* 8**,** 16080.

Mousavi, K., H. Zare, S. Dell'orso, L. Grontved, G. Gutierrez-Cruz, A. Derfoul, G. L. Hager & V. Sartorelli (2013) eRNAs promote transcription by establishing chromatin accessibility at defined genomic loci. *Mol Cell,* 51**,** 606-17.

Mullen, A. C., D. A. Orlando, J. J. Newman, J. Lovén, R. M. Kumar, S. Bilodeau, J. Reddy, M. G. Guenther, R. P. DeKoter & R. A. Young (2011) Master transcription factors determine cell-type-specific responses to TGF-β signaling. *Cell,* 147**,** 565-76.

Muller, P. A., A. G. Trinidad, P. Timpson, J. P. Morton, S. Zanivan, P. V. van den Berghe, C. Nixon, S. A. Karim, P. T. Caswell, J. E. Noll, C. R. Coffill, D. P. Lane, O. J. Sansom, P. M. Neilsen, J. C. Norman & K. H. Vousden (2013) Mutant p53 enhances MET trafficking and signalling to drive cell scattering and invasion. *Oncogene,* 32**,** 1252-65.

Muller, P. A. & K. H. Vousden (2014) Mutant p53 in cancer: new functions and therapeutic opportunities. *Cancer Cell,* 25**,** 304-17.

Munschauer, M., C. T. Nguyen, K. Sirokman, C. R. Hartigan, L. Hogstrom, J. M. Engreitz, J. C. Ulirsch, C. P. Fulco, V. Subramanian, J. Chen, M. Schenone, M. Guttman, S. A. Carr & E. S. Lander (2018) The NORAD lncRNA assembles a topoisomerase complex critical for genome stability. *Nature,* 561**,** 132-136.

Murano, K., M. Okuwaki, M. Hisaoka & K. Nagata (2008) Transcription regulation of the rRNA gene by a multifunctional nucleolar protein, B23/nucleophosmin, through its histone chaperone activity. *Mol Cell Biol,* 28**,** 3114-26.

Nair, S. J., L. Yang, D. Meluzzi, S. Oh, F. Yang, M. J. Friedman, S. Wang, T. Suter, I. Alshareedah, A. Gamliel, Q. Ma, J. Zhang, Y. Hu, Y. Tan, K. A. Ohgi, R. S. Jayani, P. R. Banerjee, A. K. Aggarwal & M. G. Rosenfeld (2019) Phase separation of ligand-activated enhancers licenses cooperative chromosomal enhancer assembly. *Nat Struct Mol Biol,* 26**,** 193-203.

Natoli, G. (2012) NF-κB and chromatin: ten years on the path from basic mechanisms to candidate drugs. *Immunol Rev,* 246**,** 183-92.

Newman, D. R., J. F. Kuhn, G. M. Shanab & E. S. Maxwell (2000) Box C/D snoRNA-associated proteins: two pairs of evolutionarily ancient proteins and possible links to replication and transcription. *RNA,* 6**,** 861-79.

Nielsen, R., T. A. Pedersen, D. Hagenbeek, P. Moulos, R. Siersbaek, E. Megens, S. Denissov, M. Børgesen, K. J. Francoijs, S. Mandrup & H. G. Stunnenberg (2008) Genome-wide profiling of PPARgamma:RXR and RNA polymerase II occupancy reveals temporal activation of distinct metabolic pathways and changes in RXR dimer composition during adipogenesis. *Genes Dev,* 22**,** 2953-67.

Oldridge, D. A., A. C. Wood, N. Weichert-Leahey, I. Crimmins, R. Sussman, C. Winter, L. D. McDaniel, M. Diamond, L. S. Hart, S. Zhu, A. D. Durbin, B. J. Abraham, L. Anders, L. Tian, S. Zhang, J. S. Wei, J. Khan, K. Bramlett, N. Rahman, M. Capasso, A. Iolascon, D. S. Gerhard, J. M. Guidry Auvil, R. A. Young, H. Hakonarson, S. J. Diskin, A. T. Look & J. M. Maris (2015) Genetic predisposition to neuroblastoma mediated by a LMO1 super-enhancer polymorphism. *Nature,* 528**,** 418-21.

Olive, K. P., D. A. Tuveson, Z. C. Ruhe, B. Yin, N. A. Willis, R. T. Bronson, D. Crowley & T. Jacks (2004) Mutant p53 gain of function in two mouse models of Li-Fraumeni syndrome. *Cell,* 119**,** 847-60.

Olivier, M., R. Eeles, M. Hollstein, M. A. Khan, C. C. Harris & P. Hainaut (2002) The IARC TP53 database: new online mutation analysis and recommendations to users. *Hum Mutat,* 19**,** 607-14.

Pedersen, J. M., J. Fredsoe, M. Roedgaard, L. Andreasen, K. Mundbjerg, M. Kruhøffer, M. Brinch, M. H. Schierup, L. Bjergbaek & A. H. Andersen (2012) DNA Topoisomerases maintain promoters in a state competent for transcriptional activation in Saccharomyces cerevisiae. *PLoS Genet,* 8**,** e1003128.

Perkins, N. D. (2007) Integrating cell-signalling pathways with NF-kappaB and IKK function. *Nat Rev Mol Cell Biol,* 8**,** 49-62.

Pfister, A. S. (2019) Emerging Role of the Nucleolar Stress Response in Autophagy. *Front Cell Neurosci,* 13**,** 156.

Pietras, K. & A. Ostman (2010) Hallmarks of cancer: interactions with the tumor stroma. *Exp Cell Res,* 316**,** 1324-31.

Pommier, Y. (2013) Drugging topoisomerases: lessons and challenges. *ACS Chem Biol,* 8**,** 82-95.

Pommier, Y., Y. Sun, S. N. Huang & J. L. Nitiss (2016) Roles of eukaryotic topoisomerases in transcription, replication and genomic stability. *Nat Rev Mol Cell Biol,* 17**,** 703-721.

Ponting, C. P., P. L. Oliver & W. Reik (2009) Evolution and functions of long noncoding RNAs. *Cell,* 136**,** 629-41.

Puc, J., P. Kozbial, W. Li, Y. Tan, Z. Liu, T. Suter, K. A. Ohgi, J. Zhang, A. K. Aggarwal & M. G. Rosenfeld (2015) Ligand-dependent enhancer activation regulated by topoisomerase-I activity. *Cell,* 160**,** 367-80.

Qian, B. Z. & J. W. Pollard (2010) Macrophage diversity enhances tumor progression and metastasis. *Cell,* 141**,** 39-51.

Rada-Iglesias, A., R. Bajpai, T. Swigut, S. A. Brugmann, R. A. Flynn & J. Wysocka (2011) A unique chromatin signature uncovers early developmental enhancers in humans. *Nature,* 470**,** 279-83.

Rahnamoun, H., J. Lee, Z. Sun, H. Lu, K. M. Ramsey, E. A. Komives & S. M. Lauberth (2018) RNAs interact with BRD4 to promote enhanced chromatin engagement and transcription activation. *Nat Struct Mol Biol,* 2**5,** 687-697.

Rahnamoun, H., H. Lu, S. H. Duttke, C. Benner, C. K. Glass & S. M. Lauberth (2017) Mutant p53 shapes the enhancer landscape of cancer cells in response to chronic immune signaling. *Nat Commun,* 8**,** 754.

Ramírez, F., D. P. Ryan, B. Grüning, V. Bhardwaj, F. Kilpert, A. S. Richter, S. Heyne, F. Dündar & T. Manke (2016) deepTools2: a next generation web server for deep-sequencing data analysis. *Nucleic Acids Res,* 44**,** W160-5.

Ravi, R., B. Mookerjee, Y. van Hensbergen, G. C. Bedi, A. Giordano, W. S. El-Deiry, E. J. Fuchs & A. Bedi (1998) p53-mediated repression of nuclear factor-kappaB RelA via the transcriptional integrator p300. *Cancer Res,* 58**,** 4531-6.

Rinn, J. L., M. Kertesz, J. K. Wang, S. L. Squazzo, X. Xu, S. A. Brugmann, L. H. Goodnough, J. A. Helms, P. J. Farnham, E. Segal & H. Y. Chang (2007) Functional demarcation of active and silent chromatin domains in human HOX loci by noncoding RNAs. *Cell,* 129**,** 1311-23.

Robinson, M. D., D. J. McCarthy & G. K. Smyth (2010) edgeR: a Bioconductor package for differential expression analysis of digital gene expression data. *Bioinformatics,* 26**,** 139-40.

Roca, J. (2011) Transcriptional inhibition by DNA torsional stress. *Transcription,* 2**,** 82-85.

Rothe, M., V. Sarma, V. M. Dixit & D. V. Goeddel (1995) TRAF2-mediated activation of NF-kappa B by TNF receptor 2 and CD40. *Science,* 269**,** 1424-7.

Ryan, K. M., M. K. Ernst, N. R. Rice & K. H. Vousden (2000) Role of NF-kappaB in p53-mediated programmed cell death. *Nature,* 404**,** 892-7.

Sabari, B. R., A. Dall'Agnese, A. Boija, I. A. Klein, E. L. Coffey, K. Shrinivas, B. J. Abraham, N. M. Hannett, A. V. Zamudio, J. C. Manteiga, C. H. Li, Y. E. Guo, D. S. Day, J. Schuijers, E. Vasile, S. Malik, D. Hnisz, T. I. Lee, I. I. Cisse, R. G. Roeder, P. A. Sharp, A. K. Chakraborty & R. A. Young (2018) Coactivator condensation at super-enhancers links phase separation and gene control. *Science,* 361.

Sanyal, A., B. R. Lajoie, G. Jain & J. Dekker (2012) The long-range interaction landscape of gene promoters. *Nature,* 489**,** 109-13.

Schaukowitch, K., J. Y. Joo, X. Liu, J. K. Watts, C. Martinez & T. K. Kim (2014) Enhancer RNA facilitates NELF release from immediate early genes. *Mol Cell,* 56**,** 29-42.

Schetter, A. J., N. H. Heegaard & C. C. Harris (2010) Inflammation and cancer: interweaving microRNA, free radical, cytokine and p53 pathways. *Carcinogenesis,* 31**,** 37-49.

Schneider, G., A. Henrich, G. Greiner, V. Wolf, A. Lovas, M. Wieczorek, T. Wagner, S. Reichardt, A. von Werder, R. M. Schmid, F. Weih, T. Heinzel, D. Saur & O. H. Krämer (2010) Cross talk between stimulated NF-kappaB and the tumor suppressor p53. *Oncogene,* 29**,** 2795-806.

Schultz, M. C., S. J. Brill, Q. Ju, R. Sternglanz & R. H. Reeder (1992) Topoisomerases and yeast rRNA transcription: negative supercoiling stimulates initiation and topoisomerase activity is required for elongation. *Genes Dev,* 6**,** 1332-41.

Scian, M. J., K. E. Stagliano, M. A. Anderson, S. Hassan, M. Bowman, M. F. Miles, S. P. Deb & S. Deb (2005) Tumor-derived p53 mutants induce NF-kappaB2 gene expression. *Mol Cell Biol,* 25**,** 10097-110.

Shen, W., H. Sun, C. L. De Hoyos, J. K. Bailey, X. H. Liang & S. T. Crooke (2017) Dynamic nucleoplasmic and nucleolar localization of mammalian RNase H1 in response to RNAP I transcriptional R-loops. *Nucleic Acids Res,* 45**,** 10672-10692.

Shi, J., W. A. Whyte, C. J. Zepeda-Mendoza, J. P. Milazzo, C. Shen, J. S. Roe, J. L. Minder, F. Mercan, E. Wang, M. A. Eckersley-Maslin, A. E. Campbell, S. Kawaoka, S. Shareef, Z. Zhu, J. Kendall, M. Muhar, C. Haslinger, M. Yu, R. G. Roeder, M. H. Wigler, G. A. Blobel, J. Zuber, D. L. Spector, R. A. Young & C. R. Vakoc (2013) Role of SWI/SNF in acute leukemia maintenance and enhancer-mediated Myc regulation. *Genes Dev,* 27**,** 2648-62.

Shlyueva, D., G. Stampfel & A. Stark (2014) Transcriptional enhancers: from properties to genome-wide predictions. *Nat Rev Genet,* 15**,** 272-86.

Shykind, B. M., J. Kim, L. Stewart, J. J. Champoux & P. A. Sharp (1997) Topoisomerase I enhances TFIID-TFIIA complex assembly during activation of transcription. *Genes Dev,* 11**,** 397-407.

Silke, J. & P. Meier (2013) Inhibitor of apoptosis (IAP) proteins-modulators of cell death and inflammation. *Cold Spring Harb Perspect Biol,* 5.

Song, H., M. Hollstein & Y. Xu (2007) p53 gain-of-function cancer mutants induce genetic instability by inactivating ATM. *Nat Cell Biol,* 9**,** 573-80.

Song, L., Z. Zhang, L. L. Grasfeder, A. P. Boyle, P. G. Giresi, B. K. Lee, N. C. Sheffield, S. Gräf, M. Huss, D. Keefe, Z. Liu, D. London, R. M. McDaniell, Y. Shibata, K. A. Showers, J. M. Simon, T. Vales, T. Wang, D. Winter, N. D. Clarke, E. Birney, V. R. Iyer, G. E. Crawford, J. D. Lieb & T. S. Furey (2011) Open chromatin defined by DNaseI and FAIRE identifies regulatory elements that shape cell-type identity. *Genome Res,* 21**,** 1757-67.

Spitz, F. & E. E. Furlong (2012) Transcription factors: from enhancer binding to developmental control. *Nat Rev Genet,* 13**,** 613-26.

Stewart, A. F. & G. Schütz (1987) Camptothecin-induced in vivo topoisomerase I cleavages in the transcriptionally active tyrosine aminotransferase gene. *Cell,* 50**,** 1109-17.

Strano, S., G. Fontemaggi, A. Costanzo, M. G. Rizzo, O. Monti, A. Baccarini, G. Del Sal, M. Levrero, A. Sacchi, M. Oren & G. Blandino (2002) Physical interaction with human tumor-derived p53 mutants inhibits p63 activities. *J Biol Chem,* 277**,** 18817-26.

Szklarczyk, D., A. Franceschini, S. Wyder, K. Forslund, D. Heller, J. Huerta-Cepas, M. Simonovic, A. Roth, A. Santos, K. P. Tsafou, M. Kuhn, P. Bork, L. J. Jensen & C. von Mering (2015) STRING v10: protein-protein interaction networks, integrated over the tree of life. *Nucleic Acids Res,* 43**,** D447-52.

Taberlay, P. C., A. L. Statham, T. K. Kelly, S. J. Clark & P. A. Jones (2014) Reconfiguration of nucleosome-depleted regions at distal regulatory elements accompanies DNA methylation of enhancers and insulators in cancer. *Genome Res,* 24**,** 1421-32.

Tafforeau, L., C. Zorbas, J. L. Langhendries, S. T. Mullineux, V. Stamatopoulou, R. Mullier, L. Wacheul & D. L. Lafontaine (2013) The complexity of human ribosome biogenesis revealed by systematic nucleolar screening of Pre-rRNA processing factors. *Mol Cell,* 51**,** 539-51.

Tallant, C., E. Valentini, O. Fedorov, L. Overvoorde, F. M. Ferguson, P. Filippakopoulos, D. I. Svergun, S. Knapp & A. Ciulli (2015) Molecular basis of histone tail recognition by human TIP5 PHD finger and bromodomain of the chromatin remodeling complex NoRC. *Structure,* 23**,** 80-92.

Tergaonkar, V., M. Pando, O. Vafa, G. Wahl & I. Verma (2002) p53 stabilization is decreased upon NFkappaB activation: a role for NFkappaB in acquisition of resistance to chemotherapy. *Cancer Cell,* 1**,** 493-503.

Tollervey, D. (1996) Trans-acting factors in ribosome synthesis. *Exp Cell Res,* 229**,** 226-32.

Tripathi, S., M. O. Pohl, Y. Zhou, A. Rodriguez-Frandsen, G. Wang, D. A. Stein, H. M. Moulton, P. DeJesus, J. Che, L. C. Mulder, E. Yángüez, D. Andenmatten, L. Pache, B. Manicassamy, R. A. Albrecht, M. G. Gonzalez, Q. Nguyen, A. Brass, S. Elledge, M. White, S. Shapira, N. Hacohen, A. Karlas, T. F. Meyer, M. Shales, A. Gatorano, J. R. Johnson, G. Jang, T. Johnson, E. Verschueren, D. Sanders, N. Krogan, M. Shaw, R. König, S. Stertz, A. García-Sastre & S. K. Chanda (2015) Meta- and Orthogonal Integration of Influenza "OMICs" Data Defines a Role for UBR4 in Virus Budding. *Cell Host Microbe,* 18**,** 723-35.

Trompouki, E., T. V. Bowman, L. N. Lawton, Z. P. Fan, D. C. Wu, A. DiBiase, C. S. Martin, J. N. Cech, A. K. Sessa, J. L. Leblanc, P. Li, E. M. Durand, C. Mosimann, G. C. Heffner, G. Q. Daley, R. F. Paulson, R. A. Young & L. I. Zon (2011) Lineage regulators direct BMP and Wnt pathways to cell-specific programs during differentiation and regeneration. *Cell,* 147**,** 577-89.

Tsai, M. C., O. Manor, Y. Wan, N. Mosammaparast, J. K. Wang, F. Lan, Y. Shi, E. Segal & H. Y. Chang (2010a) Long noncoding RNA as modular scaffold of histone modification complexes. *Science,* 329**,** 689-93.

Tsai, W. W., Z. Wang, T. T. Yiu, K. C. Akdemir, W. Xia, S. Winter, C. Y. Tsai, X. Shi, D. Schwarzer, W. Plunkett, B. Aronow, O. Gozani, W. Fischle, M. C. Hung, D. J. Patel & M. C. Barton (2010b) TRIM24 links a non-canonical histone signature to breast cancer. *Nature,* 468**,** 927-32.

Valdez, B. C., D. Henning, R. B. So, J. Dixon & M. J. Dixon (2004) The Treacher Collins syndrome (TCOF1) gene product is involved in ribosomal DNA gene transcription by interacting with upstream binding factor. *Proc Natl Acad Sci U S A,* 101**,** 10709-14.

van Haaften, G., G. L. Dalgliesh, H. Davies, L. Chen, G. Bignell, C. Greenman, S. Edkins, C. Hardy, S. O'Meara, J. Teague, A. Butler, J. Hinton, C. Latimer, J. Andrews, S. Barthorpe, D. Beare, G. Buck, P. J. Campbell, J. Cole, S. Forbes, M. Jia, D. Jones, C. Y. Kok, C. Leroy, M. L. Lin, D. J. McBride, M. Maddison, S. Maquire, K. McLay, A. Menzies, T. Mironenko, L. Mulderrig, L. Mudie, E. Pleasance, R. Shepherd, R. Smith, L. Stebbings, P. Stephens, G. Tang, P. S. Tarpey, R. Turner, K. Turrell, J. Varian, S. West, S. Widaa, P. Wray, V. P. Collins, K. Ichimura, S. Law, J. Wong, S. T. Yuen, S. Y. Leung, G. Tonon, R. A. DePinho, Y. T. Tai, K. C. Anderson, R. J. Kahnoski, A. Massie, S. K. Khoo, B. T. Teh, M. R. Stratton & P. A. Futreal (2009) Somatic mutations of the histone H3K27 demethylase gene UTX in human cancer. *Nat Genet,* 41**,** 521-3.

Van Nostrand, E. L., T. B. Nguyen, C. Gelboin-Burkhart, R. Wang, S. M. Blue, G. A. Pratt, A. L. Louie & G. W. Yeo (2017) Robust, Cost-Effective Profiling of RNA Binding Protein Targets with Single-end Enhanced Crosslinking and Immunoprecipitation (seCLIP). *Methods Mol Biol,* 1648**,** 177-200.

Wadgaonkar, R., K. M. Phelps, Z. Haque, A. J. Williams, E. S. Silverman & T. Collins (1999) CREB-binding protein is a nuclear integrator of nuclear factor-kappaB and p53 signaling. *J Biol Chem,* 274**,** 1879-82.

Wang, D., A. Baumann, A. Szebeni & M. O. Olson (1994) The nucleic acid binding activity of nucleolar protein B23.1 resides in its carboxyl-terminal end. *J Biol Chem,* 269**,** 30994-8.

Wang, D., I. Garcia-Bassets, C. Benner, W. Li, X. Su, Y. Zhou, J. Qiu, W. Liu, M. U. Kaikkonen, K. A. Ohgi, C. K. Glass, M. G. Rosenfeld & X. D. Fu (2011a) Reprogramming transcription by distinct classes of enhancers functionally defined by eRNA. *Nature,* 474**,** 390-4.

Wang, K. C. & H. Y. Chang (2011) Molecular mechanisms of long noncoding RNAs. *Mol Cell,* 43**,** 904-14.

Wang, K. C., Y. W. Yang, B. Liu, A. Sanyal, R. Corces-Zimmerman, Y. Chen, B. R. Lajoie, A. Protacio, R. A. Flynn, R. A. Gupta, J. Wysocka, M. Lei, J. Dekker, J. A. Helms & H. Y. Chang (2011b) A long noncoding RNA maintains active chromatin to coordinate homeotic gene expression. *Nature,* 472**,** 120-4.

Wang, X., S. Arai, X. Song, D. Reichart, K. Du, G. Pascual, P. Tempst, M. G. Rosenfeld, C. K. Glass & R. Kurokawa (2008) Induced ncRNAs allosterically modify RNA-binding proteins in cis to inhibit transcription. *Nature,* 454**,** 126-30.

Wang, Y., Y. A. Suh, M. Y. Fuller, J. G. Jackson, S. Xiong, T. Terzian, A. Quintás-Cardama, J. A. Bankson, A. K. El-Naggar & G. Lozano (2011c) Restoring expression of wild-type p53 suppresses tumor growth but does not cause tumor regression in mice with a p53 missense mutation. *J Clin Invest,* 121**,** 893-904.

Weaver, T. M., E. A. Morrison & C. A. Musselman (2018) Reading More than Histones: The Prevalence of Nucleic Acid Binding among Reader Domains. *Molecules,* 23.

Webster, G. A. & N. D. Perkins (1999) Transcriptional cross talk between NF-kappaB and p53. *Mol Cell Biol,* 19**,** 3485-95.

Weisz, L., A. Damalas, M. Liontos, P. Karakaidos, G. Fontemaggi, R. Maor-Aloni, M. Kalis, M. Levrero, S. Strano, V. G. Gorgoulis, V. Rotter, G. Blandino & M. Oren (2007a) Mutant p53 enhances nuclear factor kappaB activation by tumor necrosis factor alpha in cancer cells. *Cancer Res,* 67**,** 2396-401.

Weisz, L., M. Oren & V. Rotter (2007b) Transcription regulation by mutant p53. *Oncogene,* 26**,** 2202-11.

Whyte, W. A., D. A. Orlando, D. Hnisz, B. J. Abraham, C. Y. Lin, M. H. Kagey, P. B. Rahl, T. I. Lee & R. A. Young (2013) Master transcription factors and mediator establish super-enhancers at key cell identity genes. *Cell,* 153**,** 307-19.

Xu, J., J. Wang, Y. Hu, J. Qian, B. Xu, H. Chen, W. Zou & J. Y. Fang (2014) Unequal prognostic potentials of p53 gain-of-function mutations in human cancers associate with drug-metabolizing activity. *Cell Death Dis,* 5**,** e1108.

Yap, K. L., S. Li, A. M. Muñoz-Cabello, S. Raguz, L. Zeng, S. Mujtaba, J. Gil, M. J. Walsh & M. M. Zhou (2010) Molecular interplay of the noncoding RNA ANRIL and methylated histone H3 lysine 27 by polycomb CBX7 in transcriptional silencing of INK4a. *Mol Cell,* 38**,** 662-74.

Yeager, M., N. Orr, R. B. Hayes, K. B. Jacobs, P. Kraft, S. Wacholder, M. J. Minichiello, P. Fearnhead, K. Yu, N. Chatterjee, Z. Wang, R. Welch, B. J. Staats, E. E. Calle, H. S. Feigelson, M. J. Thun, C. Rodriguez, D. Albanes, J. Virtamo, S. Weinstein, F. R. Schumacher, E. Giovannucci, W. C. Willett, G. Cancel-Tassin, O. Cussenot, A. Valeri, G. L. Andriole, E. P. Gelmann, M. Tucker, D. S. Gerhard, J. F. Fraumeni, R. Hoover, D. J. Hunter, S. J. Chanock & G. Thomas (2007) Genome-wide association study of prostate cancer identifies a second risk locus at 8q24. *Nat Genet,* 39**,** 645-9.

Zentner, G. E., P. J. Tesar & P. C. Scacheri (2011) Epigenetic signatures distinguish multiple classes of enhancers with distinct cellular functions. *Genome Res,* 21**,** 1273-83.

Zerdoumi, Y., J. Aury-Landas, C. Bonaïti-Pellié, C. Derambure, R. Sesboüé, M. Renaux-Petel, T. Frebourg, G. Bougeard & J. M. Flaman (2013) Drastic effect of germline TP53 missense mutations in Li-Fraumeni patients. *Hum Mutat,* 34**,** 453-61.

Zhou, Y., B. Zhou, L. Pache, M. Chang, A. H. Khodabakhshi, O. Tanaseichuk, C. Benner & S. K. Chanda (2019) Metascape provides a biologist-oriented resource for the analysis of systems-level datasets. *Nat Commun,* 10**,** 1523.

Zhu, J., M. A. Sammons, G. Donahue, Z. Dou, M. Vedadi, M. Getlik, D. Barsyte-Lovejoy, R. Al-awar, B. W. Katona, A. Shilatifard, J. Huang, X. Hua, C. H. Arrowsmith & S. L. Berger (2015) Gain-of-function p53 mutants co-opt chromatin pathways to drive cancer growth. *Nature,* 525**,** 206-11.

Zhu, Y., L. Sun, Z. Chen, J. W. Whitaker, T. Wang & W. Wang (2013) Predicting enhancer transcription and activity from chromatin modifications. *Nucleic Acids Res,* 41**,** 10032-43.

Zuber, J., J. Shi, E. Wang, A. R. Rappaport, H. Herrmann, E. A. Sison, D. Magoon, J. Qi, K. Blatt, M. Wunderlich, M. J. Taylor, C. Johns, A. Chicas, J. C. Mulloy, S. C. Kogan, P. Brown, P. Valent, J. E. Bradner, S. W. Lowe & C. R. Vakoc (2011) RNAi screen identifies Brd4 as a therapeutic target in acute myeloid leukaemia. *Nature,* 478**,** 524-8.